UNIVERSITY OF CALIFORNIA,
IRVINE

# Glial cells promote calyceal maturation in the developing auditory brainstem

DISSERTATION

submitted in partial satisfaction of the requirements
for the degree of

DOCTOR OF PHILOSOPHY

in Biological Sciences

by

Minhan Lynn Dinh

Dissertation Committee:
Professor Karina S. Cramer, Chair
Professor Jorge Busciglio
Associate Professor Kim Green

2016

**DEDICATION**

To

my family and Matthew

for their unconditional love and support

Có chí thì nên

## TABLE OF CONTENTS

Page

## LIST OF FIGURES

Page

CHAPTER 1



CHAPTER 2

CHAPTER 3

CHAPTER 4



CHAPTER 5

## ACKNOWLEDGEMENTS

This work would not be possible if not for the mentorship and immense patience of my advisor, Dr. Karina S. Cramer, who has served as my role model for how to be a critical scientist and scientific educator.

I would like to thank the Cramer lab for their immense help and support during my time at UCI. I have been fortunate to have received guidance from Drs. Candace Hsieh, Sonia Marshak, and Paul Nakamura for their technical support. I would like to thank Drs. Matthew Korn, Michelle Allen-Sharpley, Mariam Abdul-Latif, and Sarah Rotschafer for their helpful discussions and comments on my manuscript and scientific talks. Additionally, I would like to thank the undergrads who have all been integral in helping me with data collection and analysis, and have helped me discover the joys of mentoring. I would like to thank Scott Koppel for his work in the initial studies looking at glial markers during mouse development. I would especially like to thank Veronica Veksler for her long-standing commitment and enthusiasm for research during my time at UCI.

This dissertation has culminated and grown through the support of my advancement and thesis committee. I would like to thank Drs. Jorge Busciglio, Kim Green, Dritan Agaliu, and Katumi Sumikawa for their critical feedback. I would like to extend my appreciation for the Green lab, with special thanks to Allison Haskell and Dr. Monica Elmore for their support in confocal imaging and *Cx3cr1* colony maintenance. Lastly, the STORM imaging experiments and analysis program would not be possible without the help of Dr. Ian Smith and Brett Settle, respectively.

Lastly, I would like to thank my family for their unfaltering support and believing in me always. And to Matthew – who has endured this journey with me, and been my continuing source of strength and patience.

These studies were supported by the following grants: NIHT32 DC010775, NIH R01DC010796, and DOE GAANN P200A120165

Permission to use copyrighted material contained in Chapter 1 was granted by the Nature Publishing Group, Elsevier, Wiley Interscience, and the American Association for the Advancement of Science. Chapter 2 and the Appendix are reprints of the material as it appears in *Neuroscience* and *Neural Development*, respectively. The co-authors listed in this publication directed and supervised research which forms the basis for the dissertation. Permission to use material not formally published has been granted from the Principal Investigator Dr. Karina S. Cramer, who directed and supervised the proposed research project (Chapters 3 and 4).

# CURRICULUM VITAE

Minhan Dinh

mldinh@uci.edu

## EDUCATION

09/10 – 06/16 University of California, Irvine (Irvine, CA)
Doctor of Philosophy in Neurobiology and Behavior
Thesis advisor: Karina S. Cramer, PhD

- Advanced to Ph.D. candidacy in May 2014
- Title of dissertation: Glial cells promote calyceal maturation in the developing auditory brainstem

09/10 – 12/15 University of California, Irvine (Irvine, CA)
Master's Degree in Neurobiology and Behavior
Thesis advisor: Karina S. Cramer, PhD

- Advanced to candidacy in June 2015

09/05 – 06/09 University of California, Davis (Davis, CA)
Bachelor of Science in Neurobiology, Physiology, and Behavior
Thesis advisor: Nobuko Hagiwara, PhD

## RESEARCH EXPERIENCE

03/11 – 06/16 Graduate Student Researcher, UC Irvine Department of Neurobiology and Behavior
Advisor: Karina S. Cramer, Ph.D.

- Importance of glia in mediating neural development of the chick and mouse auditory brainstem using cellular and molecular biology techniques
- Performed developmental experiments using various molecular biology techniques (organotypic and whole embryo culture, microsurgery, glial culture, RNA/DNA extraction, quantitative real time-PCR, western blot, vibratome sectioning, cryostat sectioning, gel electrophoresis to assess DNA/protein, fluorescent axon tracing, immunohistochemistry, mouse colony maintenance)
- Mentored undergraduates
- Analyzed and presented primary literature

Publications:

- Abdul-Latif ML, Salazar JA, Marshak S, **Dinh ML**, Cramer KS. Ephrin-A2 and ephrin-A5 guide contralateral targeting but not topographic mapping of ventral cochlear nucleus axons. *Neural Development*, 2015 Dec 15; 10:27.
- **Dinh ML**, Koppel SJ, Korn MJ, Cramer KS. Distribution of glial cells in the auditory brainstem: normal development and effects of unilateral lesion. *Neuroscience*, 2014 Oct 10;278:237-52.
- Benoit, ME, Hernandez, MX., **Dinh ML**., Benavente, F., Vasquez, O., Tenner, AJ. C1q-induced LRP1B and GPR6, expressed early in AD mouse models, are essential for the C1q-mediated protection against Amyloid-β neurotoxicity. *Journal of Biological Chemistry*, 2013 Jan 4;288(1):654-65.

Abstracts:

- Cramer KS, **Dinh ML**, Rotschafer SR. Microglia Promote Synaptic Maturation in the Auditory Brainstem. 39th Annual Association of Research in Otolaryngology MidWinter Meeting, San Diego, California, 2016.
- **Dinh ML**, Rotschafer SE, Cramer KS. Microglia refine auditory brainstem pathways. 9th Annual UC Riverside Center for Glial and Neuronal Interactions Symposium, Riverside, California, 2016.
- Cramer KS and **Dinh ML**. Glial cells in auditory brainstem development and plasticity. Auditory System Gordon Research Conference at Bates College, Lewiston, Maine, 2014.
- **Dinh ML**, Koppel SJ, Korn MK, Cramer KS. Glial cell types in auditory brainstem development and lesion-induced plasticity. Society for Neuroscience 43rd Annual Meeting at San Diego Convention Center, San Diego, California, 2013.

09/07 - 07/10 Junior Specialist, UC Davis Department of Cardiology
Advisor: Nobuko Hagiwara, Ph.D.

- Studied the role of transcription factor Sox6 in muscle fiber differentiation
- Performed molecular biology techniques (western blot, immunohistochemistry, immunoprecipitation, quantitative PCR, cloning, culture work, mouse husbandry)
- Read and presented primary literature in journal club

Abstracts:

- **Dinh ML**, Dong Y., Furlow JD, Hagiwara, N. Evolutionary conservation of the role of Sox6 in terminal differentiation of skeletal muscle. Society of Developmental Biology 69th Annual Meeting at the Albuquerque Convention Center, Albuquerque, New Mexico, 2010.

## RELEVANT COURSEWORK

Graduate studies (UC Irvine)
University Studies (Pedagogy program), Scientific Communication, Auditory Neuroscience, Molecular Neurobiology, Behavioral Neuroscience, Molecular Neuroscience, Cellular Neuroscience, Systems Neuroscience I and II, Systems Neuroscience, Molecular Neuroscience
Undergraduate studies (UC Davis)
Systemic Physiology, Advanced Systemic Physiology, General Chemistry, Organic Chemistry, General Biology, Biochemistry, Bioenergetics, Neurobiology, Neuroscience, Neurobiology of Speech, Mammalian Vision, Animal Behavior, Regulation of Gene Function, Physics, Genetics, Ethics in Biotechnology and associated labs.

## TEACHING EXPERIENCE

02/16 – 05/16 Instructor, Cellular and Molecular Biology (BIO180L), Orange Coast College

- Class enrollment: 30
- Instruct and lead students in molecular biology techniques
- Prepare lectures for laboratory component of course
- Timely record keeping of student enrollment, attendance and progress
- Applied new pedagogical techniques (online tools) to further student understanding
- Formulate course objectives and assess student learning outcomes through grading laboratory reports
- Integrate current cell and molecular biology practices into curriculum for students
- Incorporate primary research to foster undergraduate interest in STEM
- Maintained informal office hours after class to accommodate diverse student schedules
- Collaborate with instructors on maintaining curriculum

01/16 Endocrinology guest instructor, Endocrinology, CSU Long Beach

- Class enrollment: 30
- Guest-lectured twice on introduction to endocrinology

10/14-12/14;
09/15-12/15 Teaching Assistant, Developmental Neurobiology (N152), UC Irvine

- Class enrollment: 110
- Guest lectured four times prior to midterm and final examinations
- Maintained formal office hours and performed group tutoring to help students prepare for quizzes and exams
- Prepared lectures, quizzes, and exams
- Proctored exams and updated student records

03/12 – 06/13;
03/13-06/13 Lab Instructor, Neurobiology Lab Course (N113L), UC Irvine

- Class enrollment: 24
- Instructed undergraduates to perform neurobiological experiments in a controlled laboratory setting during Spring and Winter quarter
- Attended preparation sections and created independent curricula such as creating lecture content, anatomy practicals, quizzes, and exams
- Proctored examinations and graded student lab assignments and reports
- Held regular tutoring sessions

09/13 – 12/13 Head Teaching Assistant (head TA), DNA to Organisms (BI093), UC Irvine

- Class enrollment: 32
- Collaborated with TAs to help teach discussion sections for a class of 900 undergraduates
- Provided weekly lesson plans to teach introductory biology to 30 undergraduates within a discussion section
- Designed active learning techniques such as worksheets, homework assignments, and group activities for use in discussion sections
- Lead TAs and helped prepare TAs for upcoming content by presenting weekly lesson plan ideas during training session
- Held regular office hours to assist students seeking additional help on subject matter
- Serve as liaison for TA communication with course instructors

## CAREER DEVELOPMENT

03/15 – 03/16 University Studies 390ABC, Center for Engaged Instruction, UC Irvine

- Assist in providing guidance and instruction in pedagogical practices to incoming graduate students through campus wide orientation called TA Professional Development Program (TAPDP)
- Stay current in discipline, advanced pedagogy and learning techniques and academic job preparation
- Learn and apply new technologies in advances to enhance student retention

09/13 – 06/16 Science, Technology, Engineering and Mathematics Education (STEM Ed), Molecular Biology and Biochemistry, UC Irvine, 09/13 – present

- Read and discuss implementation of pedagogical techniques into STEM classes
- Synthesize primary research on STEM education

04/14 – 05/15 Center for Engaged Instruction Workshops, UC Irvine

- Designing Better Test Questions to Assess Student Learning
- Strategies for Effective Lesson Planning
- Course Design Certification Program

10/14 – 11/14 Mentoring Excellence Series, Graduate Resource Center, UC Irvine

- Professional development on expanding mentorship strategies and skills

09/13 – 12/13 Howard Hughes Medical Institute (HHMI) Teaching Fellows Program, School of Biological Sciences, UC Irvine

- Receive weekly pedagogical instruction on teaching biology to freshman students

## HONORS AND AWARDS

2015 Graduate Assistance in Areas of National Need (GAANN) Award
2015 Pedagogical Fellow for the UCI Center for Engaged Instruction
2014 Center for Hearing Research Trainee Award
2014 Edward Steinhaus Teaching Award
2014 Roger W. Russell Scholar's Award in the Neurobiology of Learning and Memory
2013 Graduate Fellow Award, HHMI-UCI Teaching Fellows Program

## EDUCATIONAL OUTREACH AND SERVICE

09/14 –09/15 Pedagogical Instructor for TA Professional Development Program (TAPDP), Center for Engaged Instruction, UC Irvine

- Prepared incoming TAs on pedagogy and teaching strategies by designing and leading a 1.5-day workshop

02/15 – 06/16 Science Olympiad Event Supervisor and Judge, Orange County Department of Education, Irvine, CA

- Write BioProcess event for division B (middle school students)
- Proctor event

02/15 Volunteer neuroscientist, Los Angeles Brain Bee. UC Irvine

05/12-09/14 Science Outreach Volunteer, Center for the Neurobiology of Learning and Memory, UC Irvine

- Attended outreach events to promote neuroscience education to the general public
- Served as docent for CNLM tours for K-12 students in giving presentations on fundamentals of neuroscience.

04/14 Judge, Intel International Science and Engineering Fair. UC Irvine

03/13-09/13 Graduate Representative for NB&B Search Committee, UC Irvine

- Reviewed applicant files for Systems Biology UCI NB&B faculty position
- Collected and presented graduate student opinion on prospective faculty to NB&B faculty meeting

08/13 TechTrek lab docent, Neurobiology and Behavior, UC Irvine

- Provided lab tours to participants of TechTrek, an AAUW (American Association of University Women) sponsored event providing young women from underprivileged communities the opportunity to get hands-on experience of pursuing a career in the STEM field
- Led students around the lab and showcased different research techniques such as tissue preparation, immunohistology, and gross dissection.

01/08 – 06/09 Instructor, Adventures in Science, UC Davis

- Researched scientific topics to present to elementary and middle school students that fall under K12 curriculum
- Collaborated within groups to create interactive presentations for students to garner interest in studying biology.

**SKILLS**

- Blackboard and EEE platform
- Microsoft Office (Excel, Word, and Powerpoint)
- Keynote
- Adobe Photoshop and Illustrator
- Effective scientific communication and delivery of material for diverse audience
- Biology curriculum generation and formation
- Synthesis of scientific literature
- Effective communication to a multi-ethnic environment with students of different learning modalities and abilities
- Lesson plan development based on course objectives and student learning outcomes
- Knowledge of best practices of effective teaching and assessment
- Experience teaching students from diverse ethnic and cultural backgrounds
- Syllabus and course design

**MENTORING UNDERGRADUATES (mentees listed below)**

- Veronica Veksler (2013 – 2016)
- Thao Pham (2015 – 2016)
- Hongnhi Nguyen (2013-2014)
- Kimberly Martinez (2014-2015)
- Michelle Tjia (2011-2013)

## ABSTRACT OF THE DISSERTATION

**Glial cells promote calyceal maturation in the developing auditory brainstem**

By

Minhan Lynn Dinh

Doctor of Philosophy in Biological Sciences

University of California, Irvine, 2016

Professor Karina S. Cramer, Chair

The formation and maturation of precise synapses are a central question in the field of developmental neuroscience. This dissertation focuses on investigating the mechanisms underlying appropriate synapse growth within the mammalian brainstem. This region is comprised of several precisely wired connections that allows an organism to process auditory stimuli and to perform sound localization. This dissertation investigates glial mechanisms important for mediating development of the pathway from the ventral cochlear nucleus (VCN) to the medial nucleus of the trapezoid body (MNTB), a contralateral projection that terminates in the calyx of Held. Glial mechanisms are considered both in normal developmental and in lesion-induced plasticity.

In Chapter 2, we found that several glial markers are present in the auditory brainstem regions of VCN and MNTB during early postnatal development. In particular, astrocytes and microglia were found in direct apposition to the developing calyx. Following cochlear removal, in which ectopic calyces form from the intact VCN, microglia and astrocytes can be found within close proximity of the new calyces.

The subsequent chapters further investigate the role of microglia in shaping the VCN-MNTB circuitry during normal development (Chapter 3). Here, two microglial mutant mouse lines (*Cx3cr1* and *Csf1R*) were used. Both mutant mice exhibited a decreased calyx size, decreased MNTB area, in addition to pruning deficits. High-resolution imaging demonstrated that mutant Cx3cr1 mice had decreased levels of VGLUT1/2, suggesting that microglia may mediate overall amount of synaptic proteins. Additionally, we observed that activation of microglia activity, through LPS injections, resulted in an increase in VGLUT1/2 levels, further supporting our data.

Finally, we tested the role of microglia in lesion-induced synaptic plasticity in the brainstem (Chapter 4). Following unilateral cochlear removal, we observed that microglia were associated with newly formed calyces that formed following injury. In addition, mutant *Cx3cr1* mice exhibited decreased plasticity compared to their littermate controls.

Collectively, these results point to the importance of non-neuronal mechanisms that help form and maintain synapses within the brainstem and support the overarching hypothesis that both astrocytes and microglia are important for mediating development of the VCN-MNTB pathway in development and in lesion-induced plasticity.

# CHAPTER 1: GENERAL INTRODUCTION

The nervous system is comprised of an intricate network of neural connections that enables an organism to process and experience its environment. These complex synapses are precisely wired together early in development and can potentially be modified through experience over the course of an animal's life span. Establishing the appropriate connections as well as refining the number and strength of functioning synapses are essential steps for proper nervous system function.

An understanding of the coordinated signals that lead to the formation of precise and functional neural networks is a central focus of developmental neurobiology. Further, determining the processes and molecular signals needed for proper synapse formation will significantly aid our understanding of neurodevelopmental disorders and their potential treatments, and will contribute to identification of strategies for improving nervous system recovery following injury. This dissertation focuses on neural pathway formation and lesion-induced plasticity in regions of the auditory brainstem that use highly precise and specialized connections to compute information about sound source locations. Taking advantage of selective molecular and genetic tools accessible within the mouse, my dissertation focuses on mouse lines with impaired microglial signaling. I report on studies that critically test the roles of microglia and their signaling pathways on circuit formation and maturation in the auditory brainstem.

## 1.1 THE MAMMALIAN AUDITORY BRAINSTEM

### *1.1.1 Overview*

Our ability to perform sound localization is dependent upon the precise and highly specialized circuitry within the auditory brainstem. As described in this

Introduction, the auditory brainstem provides an elegant model system in which to study mechanisms of circuit formation and maturation, including target selection and innervation, synaptic competition, and synapse elimination. As these connections ultimately come together to help an organism compute and react to complex sounds in their environment, the formation of synapses within this system must be properly wired together. Anatomical and physiological observations of this circuitry have demonstrated specialized pathways and synapses that provide high fidelity synaptic transmission. The mechanisms underlying circuit formation during development remain an active area of research.

The sensory epithelium in the cochlea displays an orderly progression of best frequencies, with high frequencies detected in the base and low frequencies in the apex. Like many pathways, the projections from the cochlea are topographic, so that neighboring regions of the cochlea project to neighboring regions of the target nucleus. This topography preserves a map of frequency representation, or tonotopy. Thus while other sensory epithelia primarily map space, the cochlea maps frequency. Auditory space information is extracted through circuitry at early processing stages in the brainstem. Sound localization relies primarily on interaural time differences (ITD) and interaural level differences (ILD) (reviewed in (Grothe et al., 2010, Ashida and Carr, 2011). In mammals, four main brainstem nuclei form circuits to compute cues for sound localization: the cochlear nucleus (CN), medial nucleus of the trapezoid body (MNTB), lateral superior olive (LSO), and medial superior olive (MSO) (Kandler et al., 2009). After sound enters the ear, sound information is transduced by inner hair cells, which synapse onto spiral ganglion cells. The central processes of these ganglion cells enter

the brainstem through the VIIIth cranial nerve and form synapses centrally onto cells of the cochlear nucleus. The cochlear nucleus is comprised of the dorsal cochlear nucleus (DCN) and ventral cochlear nucleus (VCN) (Fekete et al., 1984). Axons from VCN globular bushy cells provide glutamatergic innervation to the contralateral MNTB (Banks and Smith, 1992). These terminations are highly specialized and are considered the largest axon terminations in the mammalian brain (Morest, 1968, Friauf and Ostwald, 1988, Spirou et al., 1990, Kuwabara et al., 1991, Kuwabara and Zook, 1991, Kandler and Friauf, 1993, Kil et al., 1995). My dissertation focuses on this synaptic termination, known as the calyx of Held, and the mechanisms that guide its formation and its lesion-induced plasticity. MNTB neurons provide a major source of glycinergic inhibition to the ipsilateral LSO, where the balance of excitation and inhibition is used for determining ILDs. (Cant, 1984, Smith et al., 1998, Grothe et al., 2010). Along with neurons from the lateral nucleus of the trapezoid body (LNTB), MNTB also provides inhibitory input to MSO, the major nucleus used to compute ITDs in mammals (Spangler et al., 1985, Banks and Smith, 1992). A schematic illustration of the mammalian auditory brainstem is shown in Figure 1.1.

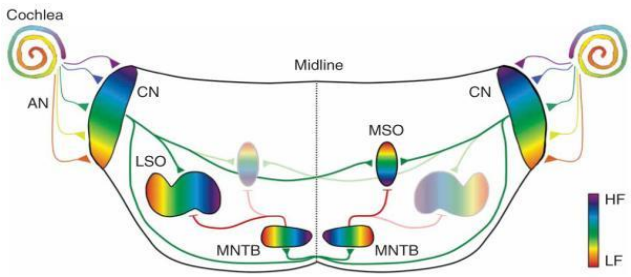


**Figure 1.1. Schematic of mammalian auditory brainstem.** Tonotopy is preserved from the cochlea, auditory nerve (AN), and throughout the brainstem nuclei, ranging from high frequency (HF) to low frequency (LF) regions. Excitatory pathways are labeled in green; inhibitory pathways are labeled in red. From Kandler et al., 2009.

### *1.1.2 VCN-MNTB circuitry*

The development of the VCN-MNTB pathway spans from embryonic day 13 (E13) to postnatal (P) day 21 (P21) (Nakamura and Cramer, 2011, Borst and Soria van Hoeve, 2012). A schematic illustration of the key developmental events is shown in Figure 1.2.

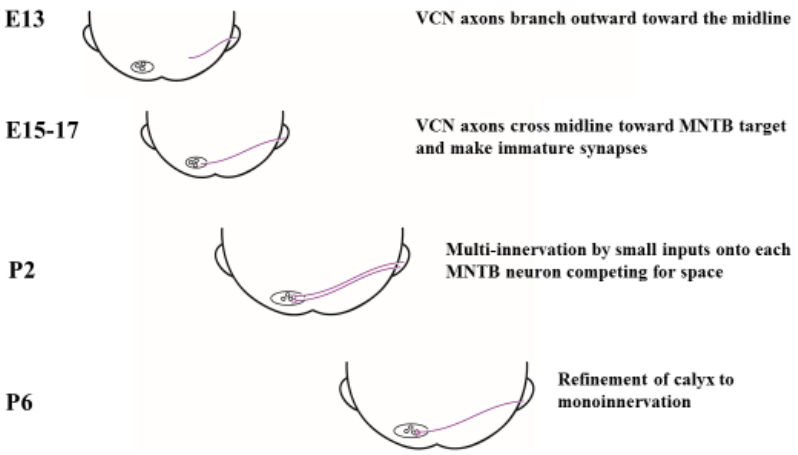


**Figure 1.2. VCN axons innervate contralateral MNTB neurons during normal development.** Axons begin to grow towards their respective targets during embryonic age. Pruning of synapses occurs postnatally such that every MNTB neuron receives synaptic input from a single calyx.

During embryogenesis, VCN axons grow towards the contralateral MNTB and cross the midline by E15 (Howell et al., 2007). Multiple axons provide immature connections and terminate onto a single MNTB (Borst and Soria van Hoeve, 2012). By the first postnatal week, many changes occur in the calyces during maturation of the MNTB (Saliu et al., 2014). At P0, rudimentary calyces are seen with several inputs on each MNTB neuron. At P2-4, a protocalyx appears as a cup-shaped presynaptic termination onto the MNTB neuron. By P4, the immature calyx is functional with AMPA- and NMDA-mediated neurotransmission (Hoffpauir et al., 2006). At this age, several

collateral branches are actively competing to become the dominant input onto an MNTB neuron. By P6, most MNTB neurons have a single dominant input. Bone morphogenetic protein (BMP) signaling has been shown to influence overall calyx growth, as conditional deletion of BMPR1a and BMPR1b results in impaired synaptic morphology of the calyx (Xiao et al., 2013). By hearing onset, the VCN collaterals are refined and a mature calyx provides a single excitatory input onto an MNTB neuron (Hoffpauir et al., 2006, Rodriguez-Contreras et al., 2006, Rodriguez-Contreras et al., 2008, Holcomb et al., 2013). After the first postnatal week, the calyx also assumes a complex reticulated structure, with numerous fingerlike processes encapsulating the postsynaptic cell. Fenestration in the mature calyx is associated with astrocytic fiber inclusions and develops along the tonotopic axis, with the medial high frequency region first affected, followed by the lateral, low frequency region (Ford et al., 2009). Once mature, the calyx can provide high fidelity synaptic transmission due to the numerous synaptic contacts made by each calyx (Figure 1.3).

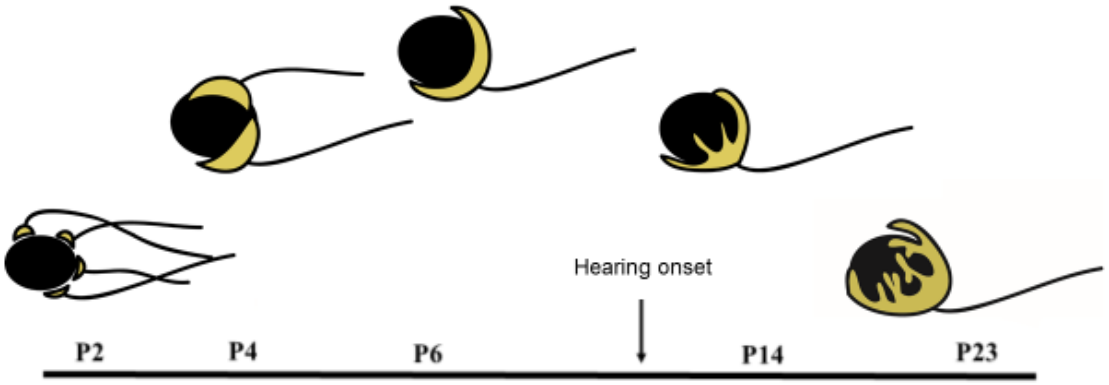


**Figure 1.3. Postnatal calyceal development in mouse.** Beginning at P2, MNTB neurons receive many inputs actively competing to be the dominant input. Pruning and refinement of the calyx occurs by hearing onset, with a shift in calyx morphology from spoon shaped to highly fenestrated with multiple processes encapsulating the postsynaptic cell.

Several properties enable the calyx to provide high fidelity synaptic transmission to the postsynaptic cell such as an increased vesicular pool size, exocytotic efficiency, and number of active release zones (Taschenberger et al., 2002). Glial cells have also been proposed to contribute to the fast neurotransmission by collecting excess glutamate at the synaptic cleft (Ford et al., 2009). While the calyx terminates solely onto the contralateral MNTB target, this circuitry can be reorganized during critical periods of lesion-induced plasticity.

### *1.1.3 Alterations in circuitry following lesion-induced plasticity*

Following early postnatal unilateral cochlear removal, the deafferented cochlear nucleus undergoes extensive cell death, leading to a massive reduction in VCN size and neuron number in turn resulting in significant denervation of the contralateral MNTB (Figure 1.4, (Trune, 1982, Hashisaki and Rubel, 1989, Mostafapour et al., 2000, Hsieh and Cramer, 2006).

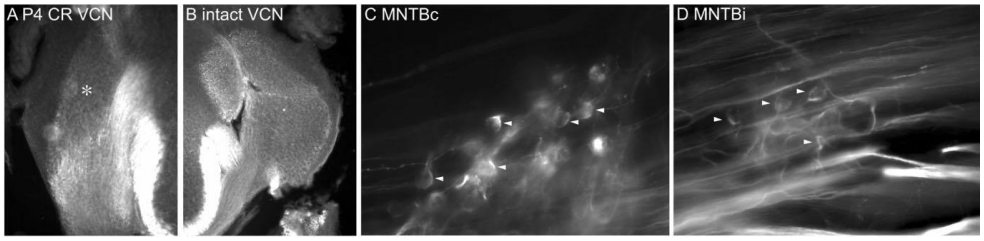


**Figure 1.4. Cochlear removal prior to hearing onset leads to ectopic projections onto ipsilateral MNTB.** A) VCN on the lesioned side undergoes cell death after early cochlear removal. B) VCN on the unoperated side appears normal. C and D) Calyces form normally on the ipsilateral side in addition to normally developing calyces on the contralateral side. CR: cochlea removal; VCN: ventral cochlear nucleus; c: contralateral; i: ipsilateral. From Hsieh and Cramer, 2006.

Axons from the intact VCN subsequently branch and form new calyceal connections, so that they innervate the denervated ipsilateral MNTB in addition to their normal contralateral target. (Moore and Kowalchuk, 1988, Kitzes et al., 1995, Russell

and Moore, 1995, Hsieh and Cramer, 2006, Hsieh et al., 2007). Despite their inappropriate location in ipsilateral MNTB, the newly formed calyces have normal synaptic properties and are sustained through adulthood (Hsieh et al., 2010). Ipsilateral projections are only induced if the cochlea is removed within the first postnatal week in mice, or later if the cochlear nucleus is removed directly (Hsieh and Cramer, 2006, Nakamura and Cramer, 2013).

### *1.1.4 Role of axon guidance molecules in development of VCN-MNTB pathway*

Several axon guidance molecules have been implicated in determining proper VCN-MNTB circuitry formation. For instance, EphB/ephrin-B signaling was shown to be important for preventing ipsilateral projections during development and following unilateral cochlear removal (Hsieh et al., 2007, Hsieh et al., 2010, Nakamura et al., 2012, Nakamura and Cramer, 2013). More recently, ephrin-A2 and ephrin-A5 have been shown to contribute towards the development of contralateral VCN axon targeting (Abdul-Latif et al., 2015). Other axon guidance molecules such as Robo/Slit and Netrin/DCC are also needed for normal VCN-MNTB development (Figure 1.5).

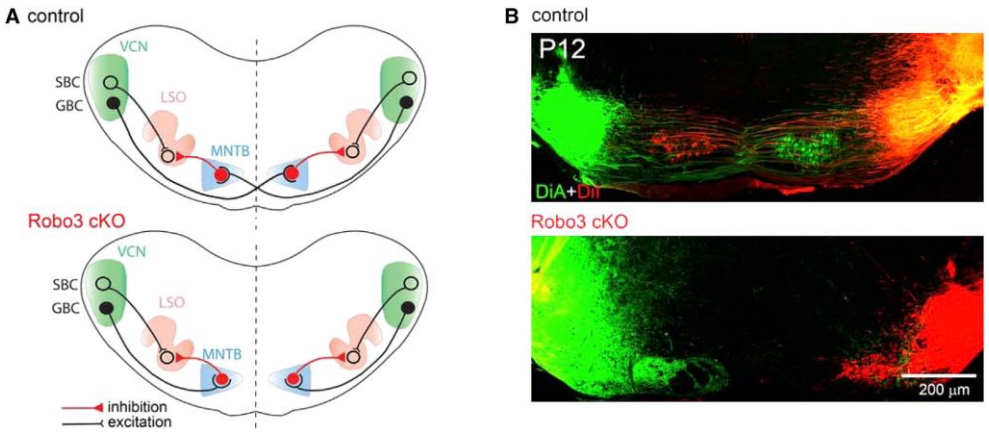


**Figure 1.5. Robo mutant VCN axons terminate onto ipsilateral, not contralateral targets of MNTB.** A) Schematic comparing brainstem circuitry in control versus Robo mutant mice – instead of terminating onto contralateral MNTB targets, VCN axons synapse onto ipsilateral MNTB. B) Coronal sections of DiI or DiA labelled samples – dye was placed into cochlear nucleus. From Michalski et al., 2013.

*Robo3* deficient mutant mice have VCN axons that fail to cross the midline and synapse only onto the ipsilateral MNTB. These mice also exhibit impaired synaptic transmission, suggesting the calyx has not matured (Figure 1.5, (Michalski et al., 2013)). In *DCC* knockout mice, VCN axons fail to reach any target and lack axonal outgrowth (Howell et al., 2007). The literature suggests that the interplay between many axon guidance molecules governs normal VCN-MNTB circuitry. Orchestrating proper synapse development of this pathway however, likely depends on various molecules that can originate in a number of cell sources. Notably, glial cells may contribute cues that would affect normal development and lesion-induced plasticity (Nakamura et al., 2012, Nakamura and Cramer, 2013).

## 1.2 GLIAL INFLUENCES ON SYNAPSE FUNCTION

### *1.2.1 Overview of glial cell types*

Synapse formation and pruning have been shown to involve several forms of cell-cell communication (Chung and Barres, 2012). Glial cells, non-neuronal cells that make up the majority of the brain, have been implicated in synapse formation and synaptic refinement both in development and following injury (Ullian et al., 2001, Stellwagen and Malenka, 2006, Barres, 2008, Chung and Barres, 2012, Karimi-Abdolrezaee and Billakanti, 2012, Schafer et al., 2012, Wake et al., 2013). One of the earliest studies showing how glial cells could influence synaptic activity was done in retinal ganglion cell cultures (RGCs; Figure 1.6). RGCs cultured together with glia

showed a large increase in synaptic activity demonstrating the synaptogenic potential of these glial cells (Pfrieger and Barres, 1997).

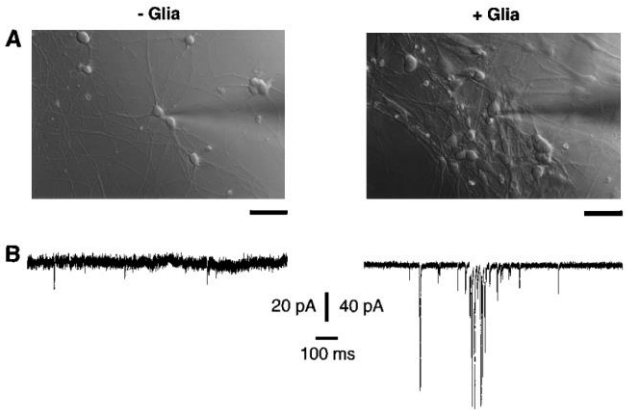


**Figure 1.6. Spontaneous activity observed in RGC culture upon treatment with glia.** A) RGCs were cultured in the absence (left panel) or presence (right panel) of glia. B) Whole-cell patch-clamp recordings were performed to assess synaptic activity - spontaneous activity was only generated in cells cultured with glia. Scale bar for micrographs of RGCs is 50 μm. From Pfrieger and Barres, 1997.

Three main glial cell types are found in the nervous system: 1) astrocytes, known to provide metabolic support to neurons and secrete neurotrophic factors, 2) microglia, known to be recruited in response to injury, and 3) oligodendrocytes, cells that serve as the primary myelin source (reviewed in (Bacci et al., 1999, Barres, 2008). As this dissertation focuses primarily on the role of astrocytes and microglia in shaping postnatal circuits in the auditory brainstem, the latter portion of this introduction describes the influences of astrocytes and microglia on synapse maturation.

### *1.2.2 Astrocytes*

Astrocytes are derived from radial glia or neuronal precursor cells. Radial glia give rise to both neurons as well as astrocytes and oligodendrocytes. Astrogenesis normally occurs postnatally and is initiated through the JAK/STAT pathway, a pathway repressed during neurogenesis (Freeman, 2010). Originally thought to play purely a

supporting role in the nervous system, astrocytes are localized near active synapses and are highly mobile, often surveying the environment, transiently extending their filopodia (Hirrlinger et al., 2004). Astrocytes occupy distinct domains – it is estimated that a single astrocyte may make up to 600 contacts onto dendrites (Bushong et al., 2002, Halassa et al., 2007). The function of astrocytes in synaptogenesis seems to be conserved across many vertebrate species, ranging from *Drosophila* to mice. In Drosophila, glia are important for clearance of axonal debris following injury (Ziegenfuss et al., 2012). Astrocytes are also known to secrete neurotrophic factors and neurotransmitters that are important for synapse maturation. One of the earliest studies identifying astrocytic influences on neuronal cultures showed that neurons co-cultured with neuroglia led to fewer synaptic transmission failures and increased amplitude of spontaneous postsynaptic currents (Pfrieger and Barres, 1997). Following this seminal study, various astrocyte-secreted factors such as thrombospondin, brain-derived neurotrophic factor, and SPARC have been implicated as being important for establishing synapse number, structure, and function in both excitatory and inhibitory synapses in normal development (Mauch et al., 2001, Christopherson et al., 2005, Elmariah et al., 2005, Garcia et al., 2010, Hughes et al., 2010, Korn et al., 2011, Kucukdereli et al., 2011, Allen et al., 2012, Korn et al., 2012, Zhu et al., 2016). For example, Allen and colleagues found an astrocyte-secreted factor, Glypican-4, to be sufficient for promoting synapse strengthening and recruitment of surface AMPA receptors (Allen et al., 2012). Astrocyte-derived signals can also dictate the neuronal phenotype in several neurodevelopmental disease models. Deficiency in MeCP2, the gene mutated in Rett syndrome, is associated with severe neuronal abnormalities. In

one study, co-cultures of MeCP2-null astrocytes with wildtype neurons exhibited several deficiencies in dendrite outgrowth and secretion of growth factors, and demonstrated a non-cell autonomous mechanism (Maezawa et al., 2009). In addition to synapse formation, astrocytes are also important for synaptic pruning, an event critical for proper nervous system circuit maturation (Chung et al., 2013). In a study performed by Hakim and colleagues, mushroom body pruning in Drosophila was found to be dictated solely by astrocytes through the apoptotic cell engulfment receptor Draper (Hakim et al., 2014). While much literature has pointed to astrocytes influencing synapse formation, microglia have recently emerged as another glial population that can mediate synaptic pruning and affect overall network connectivity (Chung and Barres, 2012, Zhan et al., 2014).

### *1.2.3 Microglia*

In contrast to astrocytes and oligodendrocytes, microglia share a common lineage with macrophages and come from the myeloid lineage. Microglia originate from the yolk sac, and migrate to the brain and proliferate within the first two postnatal weeks (Alliot et al., 1999, Kettenmann et al., 2011). These glial cells were first identified in 1932 by Del Rio-Hortega and are known as highly motile, dynamically scanning the microenvironment for injury, often making several contacts with synapses (Nimmerjahn et al., 2005, Tremblay et al., 2010, Kettenmann et al., 2011). Microglial development is dependent on Pu.1, Irf8 and colony stimulating factor 1 receptor (*Csf1R*), and communicate with neurons via fractalkine signaling (Kierdorf et al., 2013, Elmore et al., 2014, Pagani et al., 2015). As active surveyors or their environments, microglia are able to detect and gather at sites of neuronal insult (Rappert et al., 2004). Microglial

activity also is linked to neuronal activity, as studies in the visual cortex have shown that microglial movement is reduced following binocular enucleation (Wake et al., 2009).

### *1.2.4 Microglial role in synaptic pruning*

More recently, microglia have been shown to be important for synaptic pruning, constantly scanning their environment and phagocytosing synaptic material. Three molecular mechanisms have been shown to mediate synaptic pruning by microglia (Paolicelli et al., 2011, Schafer et al., 2012, Preissler et al., 2015). One potential mechanism is through the fractalkine pathway. Fractalkine, the chemokine Cx3Cl, is released from neurons and binds to the CX3C chemokine receptor 1 (*Cx3cr1*). Genetic deletion of *Cx3cr1* in mice results in increased synaptic puncta and higher spine density (Paolicelli et al., 2011). Follow-up studies have shown that *Cx3cr1*$^{-/-}$ mice have fewer microglia during postnatal development, show persistent synaptic connectivity problems, possess reduced brain connectivity, and display deficits in social behavior paralleling the phenotype of various autism like spectrum disorders (Zhan et al., 2014). Fractalkine signaling also affects normal physiological properties of the microglia – *Cx3cr1*$^{-/-}$ mice have decreased voltage-gated K-currents and also have reduced processes (Pagani et al., 2015). Microglia can also engulf synapses through complement-mediated pathways (Rappert et al., 2004). In the study conducted by Schafer and colleagues, microglia engulfment of excitatory presynaptic terminals was observed at its highest level during the peak synaptic pruning age in the dorsolateral geniculate nucleus (Figure 1.7).

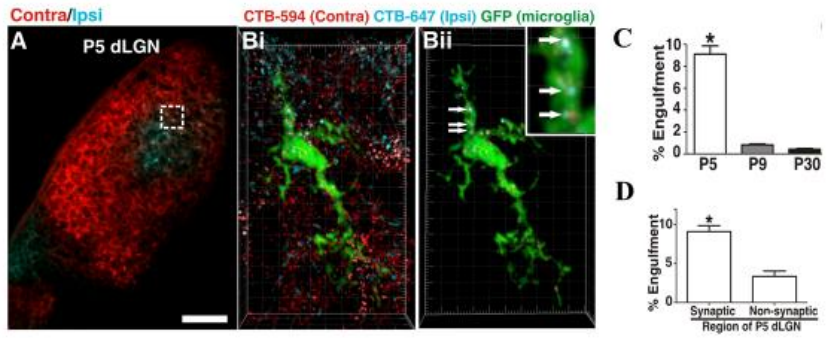


**Figure 1.7. Microglia engulf synaptic inputs during peak pruning period in dLGN.** A) Immunostain of P5 dLGN featuring ipsilateral (blue) and contralateral inputs (red). Bi-ii) Microglia (green) stained for synaptic input shows synaptic inputs inside cell. C) Across postnatal ages, highest synaptic engulfment by microglia is observed at P5. D) Microglia engulf predominantly synaptic inputs. Scale bar 100 μm. From Schafer et al., 2012.

Engulfment is decreased in complement receptor 3 (*CR3*) knockout mice and these mutant mice had higher synaptic density (Schafer et al., 2012). Expression of a Gi/o protein-coupled receptor (GPR34) has also been implicated as essential for microglial phagocytosis (Preissler et al., 2015).

### *1.2.5 Microglial role in synaptic plasticity*

Microglia have also been implicated in synaptic plasticity in different neural regions (reviewed in (Schafer and Stevens, 2015). Similar to astrocytes, microglia can secrete neurotrophic factors important for neuronal survival. Microglia extracted from MeCP2 null mice have increased glutamate synthesis, which produces excitotoxicity in neurons. Furthermore, neurons cultured with *MeCP2*-null microglia exhibit stunted dendritic morphology and have a beaded appearance compared to controls (Maezawa and Jin, 2010). More recently, a 2013 study conducted by Parkhurst and colleagues found that *Cx3cr1*$^{-/-}$ mice have decreased spine formation, impaired performance in a rotarod motor task as well as reduced learning in other behavioral tasks including an

auditory cued fear conditioning paradigm by impairments in microglial-BDNF signaling (Parkhurst et al., 2013). Within the barrel cortex, Cx3cr1 signaling has been shown to be important for the maturation of thalamocortical excitatory synapses. In normal development, maturation of excitatory synapses occurs with a gradual increase in AMPA receptors by the first postnatal week, in addition to a shift in NMDAR subtype. In this study, researchers found that the mutants had a reduced ratio of AMPA/NMDA expression and had a greater presence of the immature GluN2B synapses (Hoshiko et al., 2012).

In addition to fractalkine signaling, other microglial receptors have been shown to regulate plasticity. The purinergic receptor P2Y12 was identified as an important factor in ocular dominance plasticity – mutant mice lacking this key receptor exhibited microglia with fewer processes and, significantly, did not display shifts in their visual preference following monodeprivation (Sipe et al., 2016).

In addition to their neuroprotective roles in development, microglia are also able to shift to a reactive state in which these cells can secrete excitotoxic substances and incur extensive damage to the injured brain (Kettenmann et al., 2011). While reactive microglia are usually associated with negative consequences on synapse function, some studies have shown that LPS activation of microglia leads to enhanced food aversive learning through secretion of ATP (Delpech et al., 2015).

Given the importance of astrocytes and microglia in synapse formation, my dissertation research sought to identify potential glial cell populations that affect auditory brainstem development. Despite the wealth of knowledge known on the auditory brainstem circuitry, the mechanisms that dictate proper synapse formation and

maintenance remain an active question in auditory neuroscience. The high degree of precision and the specialized synapses seen in the auditory brainstem pose a need for highly regulated and coordinated molecular signals. Glial cells have the potential to serve these developmental functions. In the following three chapters, I provide data to support my overarching hypothesis that glia are important for refinement and maturation of the Calyx of Held synapse. In Chapter 2 I present data that demonstrate the presence of different classes of glial cells during key developmental time points during maturation of the Calyx of Held. In this project, I found two classes of astrocytes expressed at different time points in calyceal development. Oligodendrocytes were seen throughout the ages examined. Microglia were also present in the brainstem, and shifted from an ameboid immature morphology to highly ramified processes by hearing onset. We also investigated glial markers during calyx formation and following lesion-induced plasticity, and found that both astrocytes and microglia are directly apposed to the newly developing calyces. In Chapter 3, I examined synapse formation in *Cx3cr1* mutant mice that have impaired microglial signaling. My data suggest that impaired microglial communication results in an overall immature calyx phenotype in which the calyx is smaller in size, the MNTB neuron is decreased in size, and there are pruning deficits. Interestingly, *Csf1R* mutant mice also exhibited similar phenotype with smaller calyx area and pruning deficits. We performed high resolution imaging and found that *Cx3cr1* mutants exhibited decreased levels of VGLUT1/2 compared to controls. Additionally, we found that enhanced microglial signaling by LPS administration resulted in increased levels of VGLUT1/2. In Chapter 4 I examined the effects of microglia and their signaling pathways on synapse formation during plastic events and provide

evidence that following cochlear removal, animals with impairments in microglial signaling exhibited decreased plasticity with less ectopic projections compared to their control littermates. Lastly, Chapter 5 provides overall conclusions from these studies and outlines potential future studies that will address some of the new questions raised by my results. Collectively, this dissertation provides a framework suggesting that within the brainstem, microglia primarily act to sculpt and refine various parameters necessary for efficient synaptogenesis such as synapse size, cell size, and synapse maturation.

## CHAPTER 2: Distribution of glial cells in the auditory brainstem: Normal development and effects of unilateral lesion

*This work has been published in Neuroscience 278:237-252, October 10, 2014*

### 2.1 SUMMARY

Auditory brainstem networks facilitate sound source localization through binaural integration. A key component is the projection from the ventral cochlear nucleus (VCN) to the medial nucleus of the trapezoid body (MNTB), a relay nucleus that provides inhibition to the superior olivary complex. This strictly contralateral VCN projection terminates in the large calyx of Held synapse. The formation of this pathway requires spatiotemporal coordination of cues that promote cell maturation, axon growth, and synaptogenesis. Here we have examined the emergence of distinct classes of glial cells, which are known to function in development and in response to injury. Immunofluorescence for several astrocyte markers revealed unique expression patterns. ALDH1L1 was expressed earliest in both nuclei, followed by S100ß, during the first postnatal week. GFAP expression was seen in the second postnatal week. GFAP-positive cell bodies remained outside the boundaries of VCN and MNTB, with a limited number of labeled fibers penetrating into the margins of the nuclei. OLIG3 expression revealed the presence of oligodendrocytes in VCN and MNTB from birth until after hearing onset. In addition, IBA1-positive microglia were observed after the first postnatal week. Following hearing onset, all glial populations were found in MNTB. We then determined the distribution of glial cells following early (P2) unilateral cochlear removal, which results in formation of ectopic projections from the intact VCN to

ipsilateral MNTB. We found that following perturbation, astrocytic and microglial markers showed expression near the ectopic ipsilateral calyx. Taken together, the developmental expression patterns are consistent with a role for glial cells in the maturation of the calyx of Held and suggest that these cells may have a similar role in maturation of lesion-induced connections.

## 2.2 INTRODUCTION

Precise neural circuits in the auditory brainstem compute binaural timing and intensity disparities that are used to localize sound sources. In mammals, auditory information is carried by the VIIIth cranial nerve into the central nervous system (CNS), where branches of VIIIth nerve fibers terminate onto targets in the ventral cochlear nucleus (VCN). VCN globular bushy cells project to the contralateral medial nucleus of the trapezoid body (MNTB) where their large reticulated terminations, the calyces of Held, synapse onto principle neurons (Kuwabara et al., 1991, Kuwabara and Zook, 1991, Kandler and Friauf, 1993, Kil et al., 1995). MNTB neurons in turn provide glycinergic inhibition to the medial superior olive (MSO) and the lateral superior olive (LSO), which integrate excitation and inhibition to compute interaural time differences and interaural level differences, respectively.

This unique projection matures over a protracted period of development (Nakamura and Cramer, 2011). Axons reach the target and form immature connections by embryonic day (E) 17 (Borst and Soria van Hoeve, 2012). At postnatal day (P) 0, rudimentary calyces are seen with several inputs on each MNTB neuron. As the terminations expand, the number of VCN inputs is reduced until a single input

encapsulates each MNTB neuron by P4 (Hoffpauir et al., 2006, Holcomb et al., 2013). Synapse formation and pruning have been shown to involve several forms of cell-cell communication. Notably, glial-secreted factors play a role in synaptic maturation (Mauch et al., 2001, Christopherson et al., 2005, Garcia et al., 2010, Hughes et al., 2010, Kucukdereli et al., 2011, Allen et al., 2012, Korn et al., 2012). In addition, several types of glial cells have been shown to be important for synaptic refinement both in development and in response to injury (Chung and Barres, 2012, Karimi-Abdolrezaee and Billakanti, 2012, Schafer et al., 2012, Wake et al., 2013).

While the contribution of glial cells to the maturation of the central auditory circuitry is not known, recent studies have reported that astrocytes contact both the pre- and postsynaptic membranes of the calyx of Held (Elezgarai et al., 2001). These astrocytes elicit slow inward currents in the postsynaptic MNTB neuron via gliotransmission in the mature animal (Reyes-Haro et al., 2010). The close apposition of astrocytes to the calyx suggests a potential role for astrocytes in the development and function of this pathway.

To explore the role(s) of glial cells in the maturation of auditory circuits, we characterized the spatiotemporal emergence of glial subtypes in the VCN and MNTB. We used several markers to identify multiple astrocyte-specific proteins, including the intermediate filament glial fibrillary acidic protein (GFAP), the calcium binding protein S100β, and aldehyde dehydrogenase 1 family member L1 (ALDH1L1) (Cahoy et al., 2008). Oligodendrocytes were identified by expression of oligodendrocyte transcription factor 3 (OLIG3). Microglia development was assessed by expression of the ionized calcium binding adaptor molecule 1 (IBA1).

Additional clues to mechanisms of neural circuit formation may be obtained from experimentally induced reorganization of synapses. Following early postnatal unilateral cochlear removal, the cochlear nucleus on the deafferented side undergoes substantial cell death (Trune, 1982, Hashisaki and Rubel, 1989, Mostafapour et al., 2000). Axons from the intact VCN subsequently branch and contact the ipsilateral, denervated MNTB, in addition to their normal contralateral target (Moore and Kowalchuk, 1988, Kitzes et al., 1995, Hsieh and Cramer, 2006, Hsieh et al., 2007). Here we examined the expression of glial markers in denervated and intact MNTB after cochlear removal.

During normal development we found a diversity of patterns for development of glial cell types in VCN and MNTB from birth to the time of hearing onset. We found that expression of astrocyte and oligodendrocyte markers following cochlear removal was similar to the distribution of these glial markers during normal development. In addition, glial cells and their processes were seen in close proximity to the emerging ipsilateral calyx; as in normal development, these populations were primarily astrocytes and microglia. Taken together with our developmental expression data, we posit that glial cells may be important for the development and early plasticity of the mammalian auditory circuit, and that different glial cell types may serve distinct functions in this pathway.

## 2.3 MATERIALS AND METHODS

### 2.3.1 *Animals*

All procedures were approved by the University of California, Irvine Institutional Animal Care and Use Committee. Wild-type mice on CD-1 background were used for

these studies. Expression studies included animals at several developmental ages, including postnatal day (P)0, P6, P14, and P23. Cochlear removal (CR) was performed at P2 and animals survived until P4 or P9.

### 2.3.2 *Immunohistochemistry*

Pups were euthanized with isoflurane and perfused with 0.9% saline in phosphate buffer saline (PBS, 137mM NaCl, 2.7mM KCl, 10mM $Na_2HPO_4$, and1.8mM $KH_2PO_4$) followed by 4% paraformaldehyde (PFA). Brainstems were fixed for 2 hours in PFA and cryoprotected in 30% sucrose in PBS overnight at 4° C. Tissue was sectioned coronally on a cryostat (Leica Microsystems) at 18-20 µm thickness onto chrome-alum coated slides. Sections were outlined in PAP pen (Binding Site) to provide a hydrophobic layer and heated on a slide warmer at 37°C for 30 minutes. Slides were rinsed in PBS and blocked with 4% bovine serum albumin (BSA) in 0.1% Triton-X100 in PBS for 1 hour at room temperature. Slides were incubated in primary antibodies diluted in blocking solution overnight at room temperature in a humid chamber. The following day, slides were rinsed with PBS and incubated with secondary antibody that was either goat anti-rabbit, goat anti-mouse, or donkey anti-chicken (1:300, Alexa Fluor, Invitrogen) at room temperature for 1 hour. Slides were then rinsed with PBS and cover slipped with Prolong Gold Anti-Fade reagent with DAPI mounting medium (Invitrogen).

For immunofluorescence we used primary antibodies to identify five different glial markers for astrocytes, oligodendrocytes and microglia. For astrocytes, we used three antibodies: S100β, GFAP, and ALDH1L1. Rabbit S100β (1:500, Abcam) is a monoclonal antibody generated from a synthetic peptide corresponding to C-terminus human S100β. S100β is an 11 kDa calcium binding protein found in mature CNS

astrocytes. Anti-GFAP chicken polyclonal antibody (1:1000, Abcam) was generated against the full length native bovine protein (50 kDa). GFAP antibody was purified from a Triton-X100 extract of myelin associated material, and purified by centrifugation and ion exchange chromatography. The GFAP antibody stains for both reactive and resting state astrocytes. Anti-ALDH1L1 rabbit polyclonal antibody (1:500, Abcam) was generated from a synthetic peptide conjugated to KLH derived from a peptide sequence within amino acid residues 300-400 of mouse ALDH1L1. Anti-Olig3 was used as an oligodendrocyte-specific marker (1:100, Millipore). The polyclonal rabbit antibody was generated against a linear peptide corresponding to amino acids 32-45 of human Olig3 (MMGKMSGESLSRAG). Microglia specific populations were stained using rabbit anti-Iba1 polyclonal antibody (1:1000, Wako). The antibody was generated from a synthetic peptide (PTGPPAKKAISELP) corresponding to the C-terminus fraction of the protein and purified by antigen affinity chromatography from rabbit antisera.

### 2.3.3 *Cochlear removal*

Unilateral cochlear removal (CR) was performed at P2 using previously published methods (Hsieh and Cramer, 2006, Hsieh et al., 2007, Nakamura et al., 2012, Nakamura and Cramer, 2013). Animals were anesthetized with hypothermia and a small incision was made ventral to the pinna to expose the tympanic membrane. A sterile glass pipette was used to aspirate out the cochlea. In sham-operated animals, all procedures were performed except the aspiration. Surgery was performed under a stereomicroscope with heat-sterilized instruments (Germinator 500, Cell Point Scientific). After surgery, pups were returned to their mother and allowed to recover two or seven days before perfusion. Flunixin, a local analgesic, was administered at 2.5

mg/kg for two days, beginning with the day of surgery. Pups were used for neuroanatomical labeling of VCN-MNTB projections and expression of glial markers following lesion. Cochlear removal efficiency was evaluated by a decrease in size of deafferented VCN together with neuronal tracing to visualize ipsilateral VCN-MNTB projections.

### 2.3.4 *Neuroanatomical labeling*

Axonal projections from VCN to MNTB were visualized using rhodamine dextran amine (RDA, MW: 3000, Invitrogen) dye injections. The injection solution included 6.35% RDA with 0.4% Triton-X100 in PBS. Brainstems were isolated and submerged in artificial cerebrospinal fluid (aCSF; 130mM NaCl, 3mM KCl, 1.2mM $KH_2PO_4$, 20mM $NaHCO_3$, 3mM HEPES, 10mM glucose, 2mM $CaCl_2$, 1.3mM $MgSO_4$ perfused with 95% $O_2$ and 5% $CO_2$). A pulled glass micropipette was filled with RDA and pulses of RDA were injected medial to the cochlear nucleus using a Picospritzer at 25 ms. The region surrounding the injection site was electroporated at a rate of 5 pulses per second (pps) at 40 volts (V) for 50 milliseconds (ms). The tissue was immersed in aCSF for 2 hours under continuous oxygenation to allow labeling of axonal projections, and then prepared for histological staining by fixation for two hours in PFA, rinsing, and incubation in 30% sucrose overnight.

### 2.3.5 *Imaging*

All images were examined and analyzed using the Zeiss Axioskop microscope, Axiocam camera, and Axiovision software. Images were imported into Adobe Photoshop to adjust brightness and contrast of the image collectively, and subsequently

uploaded into Adobe Illustrator for further editing. We used DAPI nuclear labeling to assist in the identification of the cochlear nucleus and MNTB.

### 2.3.6 *Image Analysis*

Relative levels of expression of astrocyte and microglia markers on the two sides of the brain were analyzed using optical density measurements or cell counts, respectively. All analyses were performed blind to treatment group. MNTB was outlined using Zeiss Axioskop imaging software and optical density measurements were taken with average optical density subtracted by background intensity. For all animals, at least 3 sections per side were analyzed and values were averaged. To assess effects of unilateral cochlear removal, we obtained measurements from the MNTB contralateral to the lesion (the denervated MNTB) and from the MNTB ipsilateral to the lesion (the innervated MNTB). A ratio of these measurements, the D/I ratio, was compared between cochlear removal animals and sham operated controls. For IBA1, microglial cell density was determined by counting the number of immunopositive cells within MNTB and a D/I ratio similar to optical density measurements was used for comparisons. We quantified GFAP-positive processes using confocal images analyzed using a filament tracing program on the Imaris Software. Statistical comparisons were made with a nonparametric one-way ANOVA. Values reported in text were denoted as mean ± standard error of the mean (SEM).

To determine the extent to which glial cells surround or appose developing calyceal terminations, we analyzed images of RDA-labeled projections in CR animals. All of the labeled ipsilateral calyces were evaluated for immunofluorescent label in proximity to the calyx. We expressed a percentage of these calyces that had glial

marker expression nearby. In each section examined, we also selected at least five labeled calyces on the normal, contralateral side using the red channel alone, then ascertained the percent of these calyces with apposing glial marker expression.

## 2.4 RESULTS

### 2.4.1 *Expression of glial markers during the first postnatal week*

As early as P0, glial markers were evident within the VCN, with notable variability in the expression of astrocyte proteins. GFAP at this age was sparse, limited to the ventral portion and in the central projection of the auditory nerve (Fig. 2.1A). ALDH1L1 (Fig. 2.1B) levels were abundant in VCN, with less expression in the dorsal cochlear nucleus (DCN). S100β displayed a pattern similar to that seen with GFAP (Fig. 2.1C). The oligodendrocyte marker OLIG3 was expressed throughout VCN and in the auditory nerve (Fig. 2.1D). IBA1 immunofluorescence revealed sparsely distributed microglial cells in the VCN (Fig. 2.1E). These microglia were amoeboid in shape and exhibited few short processes consistent with active microglia (Fig. 2.1E').

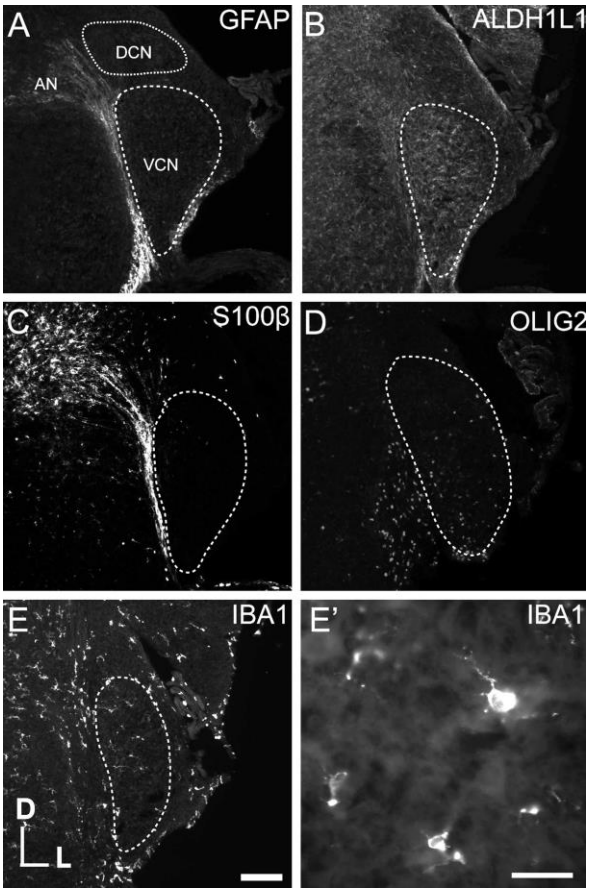


**Figure 2.1. Expression of glial markers in VCN at P0.** (A) At P0, GFAP showed minimal expression in VCN but was evident in the adjacent central projection from the auditory nerve. (B) ALDH1L1 is expressed throughout VCN with less expression in DCN. (C) Similar to GFAP, S100β was expressed in the auditory nerve but excluded from VCN. (D) OLIG2 expression revealed limited cells along the ventral aspect of VCN and in the auditory nerve. (E and E′) IBA1 was expressed in a small number of cells in VCN that were mostly amoeboid in shape with few processes (panel E′ another representative section). Scale bar in E: 100 μm, applies to Panels A–E. Scale bar in E′: 50 μm. N = 6.

All astrocyte markers were expressed in the mouse auditory brainstem except GFAP, which was sparsely distributed along the ventral border of the brainstem, but was not found in MNTB (Fig. 2.2A). S100β was expressed in MNTB fibers to a limited extent, and did not share the ventral expression patterns seen with the other astrocyte markers (Fig. 2.2B). ALDH1L1 was distributed throughout the auditory level of the brainstem with strong expression at the ventral border with many fibrous processes labeled within MNTB (Figure 2.2C – C′). The oligodendrocyte marker OLIG2 was

sparsely along the ventral aspect of the brainstem with few cells inside MNTB (Fig. 2.2D). Staining for the microglial marker IBA1 showed characteristic microglial morphology with thin radial processes in a sparse distribution spread throughout the auditory level of the brainstem. While labeling in MNTB was minimal, the brainstem border ventral to MNTB showed high levels of expression of IBA1 (Fig. 2.2E).

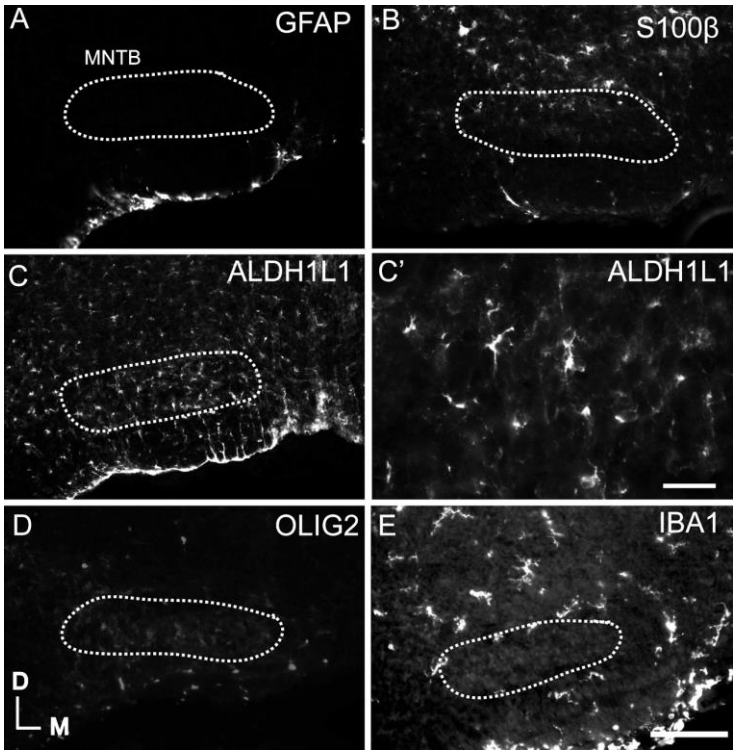


**Figure 2.2**. **Expression of glial markers in MNTB at P0**. **(**A) GFAP expression was limited to the ventral portion of the brainstem outside MNTB. (B) S100β expression was minimal and limited to the dorsal region of MNTB. (C) ALDH1L1 was expressed by fibers surrounding MNTB principal neurons, and more generally throughout the brainstem. ALDH1L1 cells had several processes (C′). (D) OLIG2-positive cells were seen along the ventral brainstem. (E) IBA1- positive cells were found in brainstem, but not found in MNTB. Scale bar in E: 100 μm, applies to all panels except panel C′ (scale bar: 50 μm). N = 6.

By the end of the first postnatal week (P6), GFAP expression remained evident in the auditory nerve and low in VCN (Fig. 2.3A). ALDH1L1 and S100β showed similar expression patterns with fibrous processes in VCN. ALDH1L1 showed more limited expression in the auditory nerve compared to the other astrocyte markers (Fig. 2.3B

and C). Compared to P0, there were many S100β-positive cells found surrounding globular bushy cells (Fig. 2.3C′). OLIG2-positive cells were observed in VCN, but few IBA1-positive cells were seen at this age (Fig. 2.3D–E). In comparison to P0, microglia at P6 had many complex processes with several radiating processes.

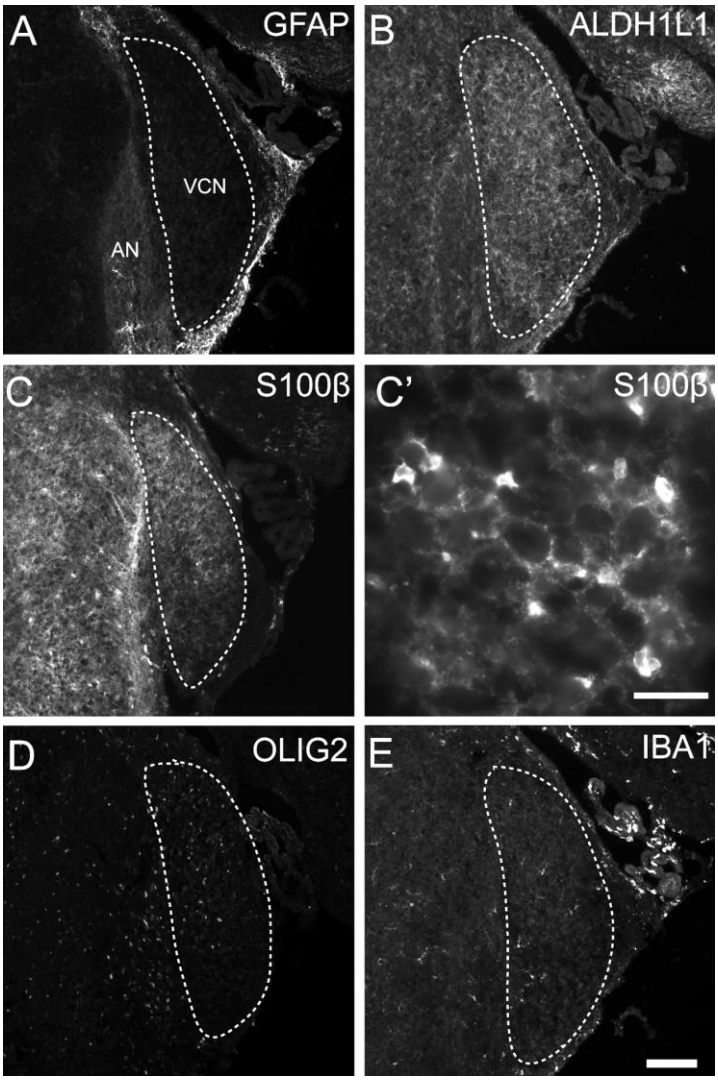


**Figure 2.3**. **Expression of glial markers in VCN at P6.** (A) Similar to P0, GFAP expression is limited to the auditory nerve. (B–C) ALDH1L1 and S100β have similar expression patterns in VCN, including the presence of immunopositive fibrous processes. S100β-positive cells are seen in auditory nerve and in VCN encapsulating the globular bushy cells (C′). (D)OLIG2-positive cells were seen throughout VCN. (E) Few IBA1-positive cells could be observed throughout the VCN. Scale bar in F: 100μm, applies to all panels except C′ (scale bar: 50 μm). N = 9.

GFAP-positive fibers were present in the brainstem at P6, with significantly more processes within MNTB than at P0 ($p=0.03$, Fig. 2.4A). ALDH1L1 and S100β-positive astrocytes were found throughout the MNTB nucleus (Fig. 2.4B–C), in contrast to the limited expression of GFAP. OLIG2 and IBA1 expression patterns showed more cells inside MNTB than at P0 (Fig. 2.4D–E). At this age, microglia had smaller cell bodies with more intricate processes (Fig. 2.4E′).

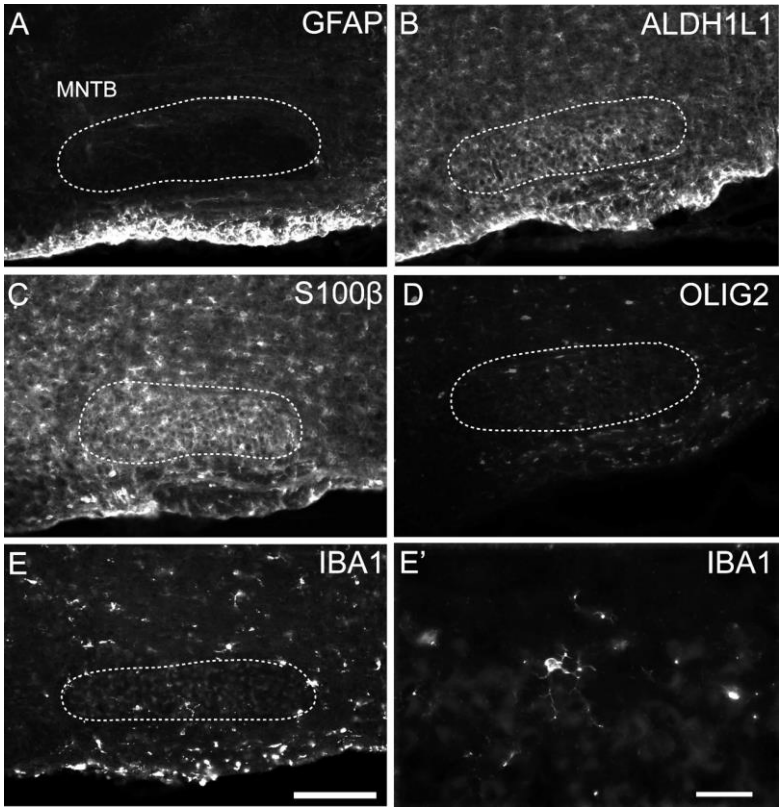


**Figure 2.4**. **Expression of glial markers in MNTB at P6**. (A) While all other astrocytic markers were present throughout brainstem, GFAP expression was limited to fibers in the ventral region of brainstem with more processes in MNTB than at younger age (GFAP at P6 was 595.54 ± 70.14 was significantly higher than GFAP at P0 (143.12 ± 68.79, $p = 0.03$). (B–C) Expression of ALDH1L1 and S100β revealed processes throughout MNTB. (D) OLIG2 immunofluorescence was seen in spherical cells within MNTB. (E)IBA1-positive cells were found throughout the brainstem, particularly at the ventral margin. IBA1-positive cells in MNTB mostly had small cell bodies with elongated processes (E′). Scale bar in F: 100 μm, applies to panels A–E. Scale bar in E′ is 50 μm. N = 9.

### 2.4.2 *Expression of glial markers during the second and third postnatal weeks*

We examined expression patterns of glial markers at P14, after hearing onset. By P14, all glial markers were expressed in VCN (Fig. 2.5).

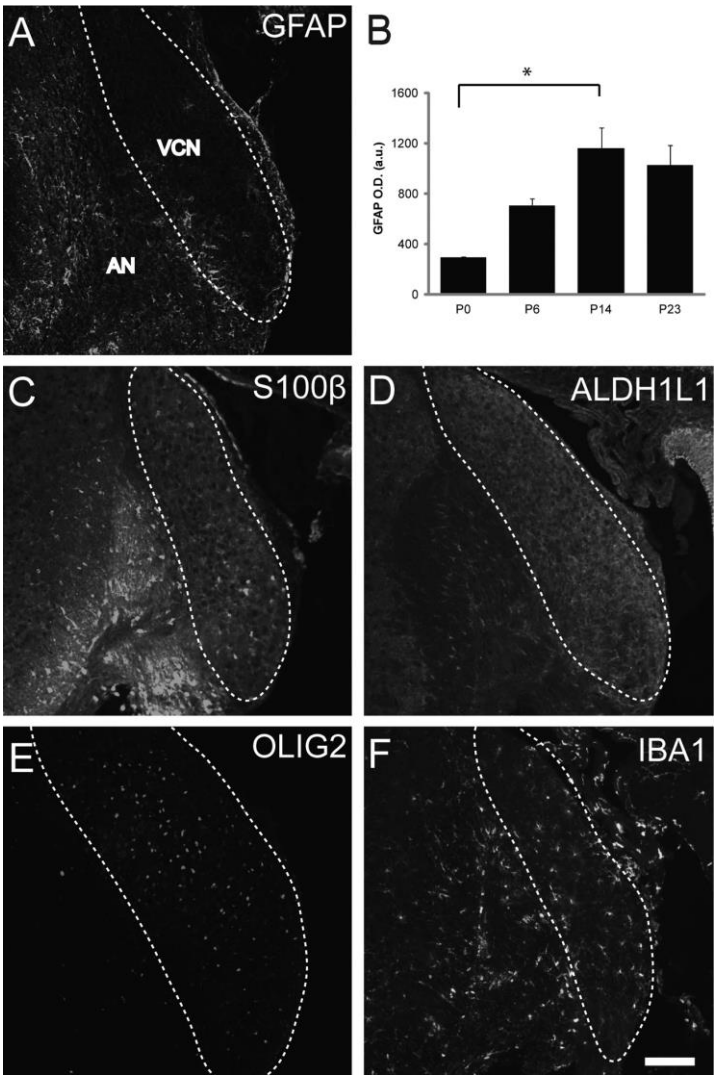


**Figure 2.5**. **Expression of glial markers in VCN at P14**. (A) At P14, an increase in GFAP-positive fibers was seen in VCN in comparison to earlier ages ($p$=0.05; the GFAP O.D. at P0 was 294.74 ± 3.41 while the GFAP O.D. at P14 was 1158.50 ± 165.08). (B–E) Astrocytic markers, S100β and ALDH1L1 were all expressed in VCN. (E) Cellular OLIG3 expression was seen throughout VCN. (F) Several IBA1 expressing cells could be identified within VCN. Scale bar in F: 100 μm, applies to all panels. N = 10.

There was a significant increase in GFAP-positive fibers in VCN compared to P0 ($p < 0.05$), but in contrast to earlier ages, GFAP labeling was not observed in central auditory nerve fibers (Fig.2.5A). S100β and ALDH1L1 continued to show expression in VCN, with diminished expression in the auditory nerve (Fig. 2.5C–D). Olig2 expression appeared throughout VCN (Fig. 5E). At this age VCN showed substantial expression of IBA1 (Fig. 2.5F). Similar to VCN, MNTB showed an increase in the density of GFAP-positive fibers at P14 compared to P0 ($p < 0.001$, Fig. 2.6A–B). The expression patterns of S100β and ALDH1L1 in MNTB were similar to those observed at earlier ages (Fig. 2.6C–D). OLIG2 cells were found inside MNTB (Fig. 2.6E). At P14 numerous IBA1-positive fibers present within MNTB (Fig. 2.6F). Microglial processes at P14 were the most complex of all the ages analyzed, exhibiting many intricate, complex processes (Fig. 2.6F inset).

We next examined expression of glial markers in the auditory brainstem of animals at P23, when the auditory brainstem pathways are mature. GFAP expression was upregulated at this age compared to prior time points with several cell processes within VCN (Fig. 2.7A–A′).

The expression of ALDH1L1 and S100β within VCN was decreased by P23 (Fig. 2.7B–C). OLIG2-positive cells remained prominent throughout VCN (Fig. 2.7D). IBA1 expression was sparsely distributed at P23 (Fig. 2.7E).

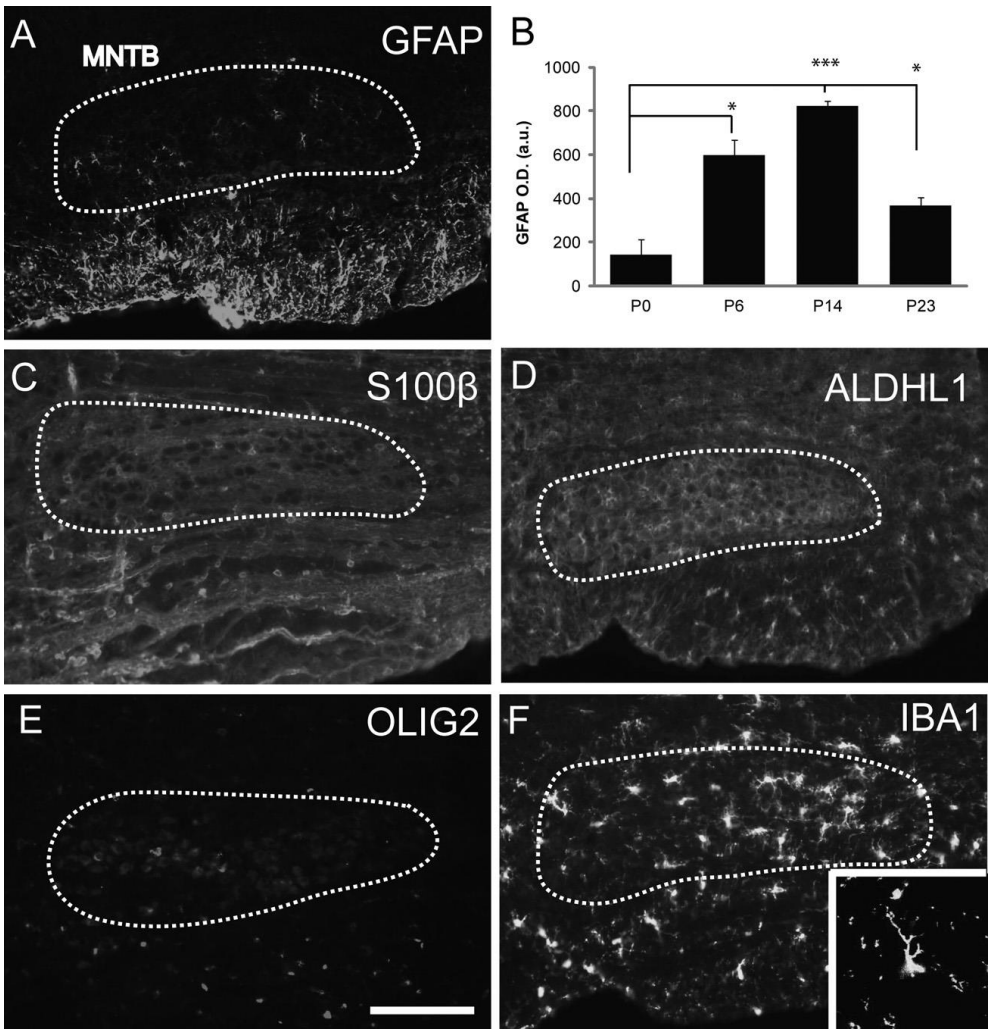


**Figure 2.6**. **Expression of glial markers in MNTB at P14**. (A and B) GFAP-positive fibers were observed penetrating MNTB from the ventral boundary and was significantly increased compared to P0 *(p* = 0.001; GFAP at P14 was 821.08 ± 23.11 compared to GFAP at P0 (143.12 ± 68.79). (C–D) Similar to younger ages, S100β and ALDH1L1 were expressed throughout the brainstem and inside MNTB, surrounding principal neurons. (E) OLIG2 expression showed few cells in MNTB. (F) IBA1 expression had cell bodies penetrating MNTB with many cells possessing intricate processes (inset). Scale bar in F: 100 μm, applies to all panels. N = 10.

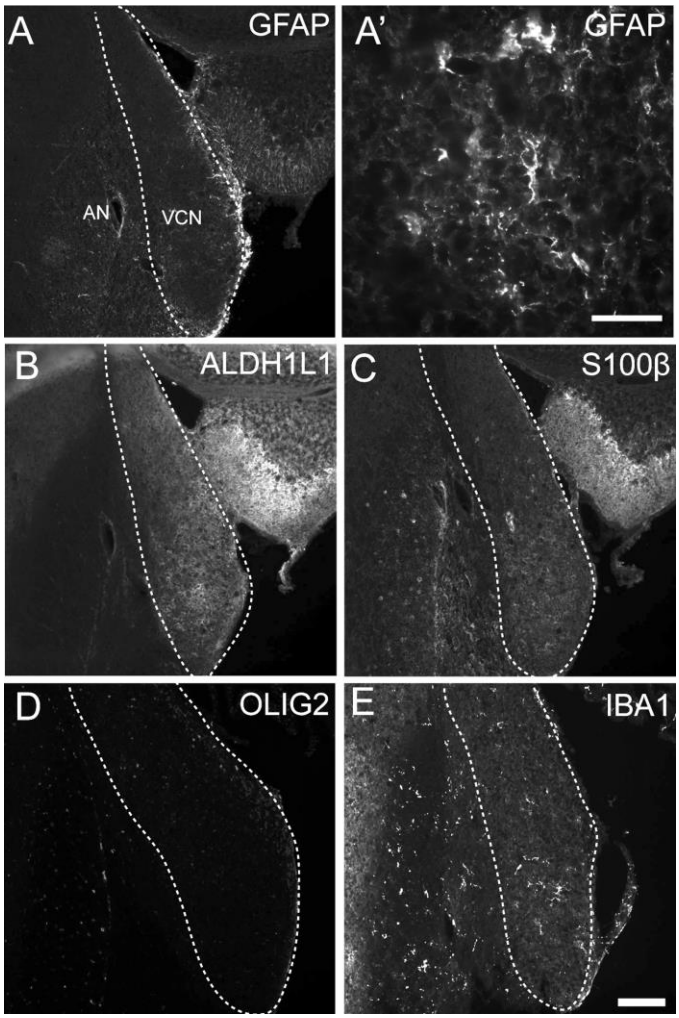


**Figure 2.7**. **Expression of glial markers in VCN at P23**. (A) At P23, an increase in GFAP-positive fibers observed inside VCN with several processes (highlighted in A′ from a representative section). (B–C) Relatively low levels of expression were seen for S100β and ALDH1L1 surrounding VCN neurons. (D) VCN was populated with OLIG2-positive cells, (E) IBA1-positive cells were considerably less numerous than at earlier ages. Scale bar in E: 100 μm, applies to all panels. except for A′, which has a scale bar of 50 μm. N = 7.

GFAP-positive fibers remained numerous in MNTB, albeit expression levels were decreased compared to P14 ($p$ = 0.02, Fig. 2.8A). S100β showed an expression profile similar to earlier time points (Fig. 2.8B).

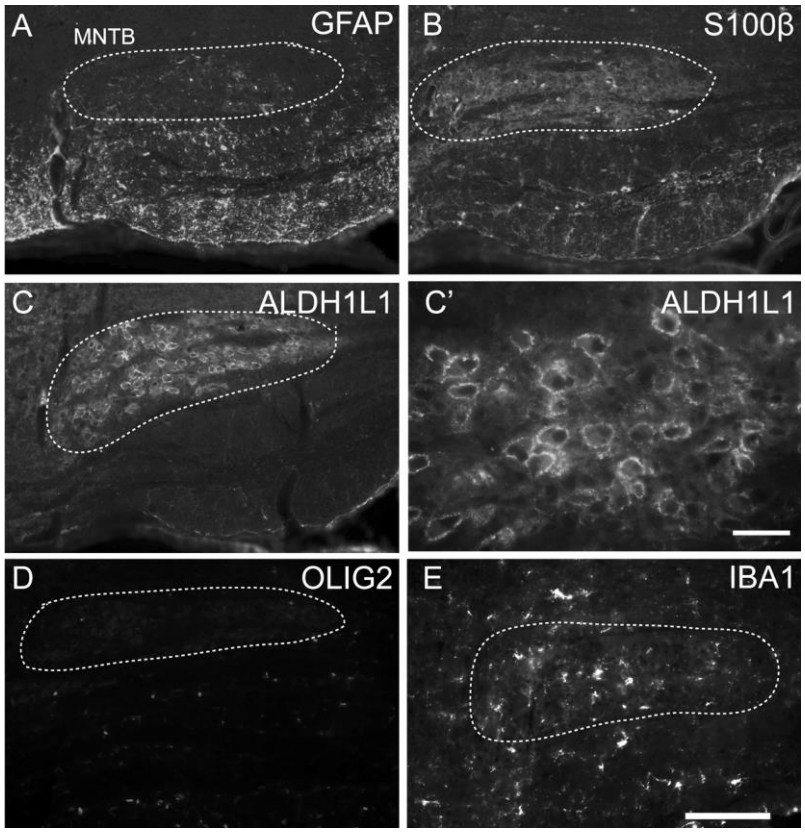


**Figure 2.8. Expression of glial markers in MNTB at P23.** (A) At P23 there was significantly less GFAP-positive processes found in MNTB compared to at P14 ($p$ = 0.02; GFAP at P23 was 368.97 ± 37.02 and GFAP at P14 was 821.08 ± 23.11). (B) S100β had low level of expression in brainstem. In contrast, many ALDH1L1- positive cells were surrounding individual MNTB principal neurons (C–C′). (D) OLIG2 expression was located ventral to MNTB. (E) IBA1-positive microglia were observed in a sparse distribution throughout MNTB. Scale bar in E: 100μm, applies to all panels except panel C′ (scale bar: 50 μm). N = 7.

ALDH1L1 expression was high in MNTB and showed dense labeling around principal neurons rather than the fibrous labeling seen at earlier ages (Fig. 2.8C–C′). OLIG2 expression showed cells predominantly located along the ventral portion of

MNTB (Fig. 2.8D). IBA1 expression remained in MNTB, although it appeared reduced relative to that seen at P14. IBA1-positive cells at P23 were also smaller in size compared to the amoeboid cells observed at P0 (Fig. 2.8E).

### 2.4.3 *Glial subtypes apposed with the developing calyx*

To investigate the extent to which glial cells associate with the developing calyx of Held, we traced VCN-MNTB projections with unilateral RDA injections and stained for glial markers (Fig. 2.9). At P6, the calyx is maturing and elaborating its morphological structure, while additional inputs to MNTB neurons are being eliminated (Holcomb et al., 2013). Both ALDH1L1 and S100β-positive astrocytes were found within the MNTB region in between principal neurons, often adjacent to labeled calyces (Fig. 2.9A–B). No GFAP processes were found adjacent to developing synapses, consistent with the paucity of GFAP-positive fibers at this age (Fig. 2.9C). Microglia were distributed sparsely across MNTB, often nearby developing calyces (Fig. 2.9D). In relation to the calyx, some OLIG2-positive cells were located near the principal neuron, occasionally overlapping with the developing calyx (Fig. 2.9E).

We next examined the association between glial cells in MNTB and the relatively mature calyx after hearing onset at P14 (Fig. 2.9). ALDH1L1-positive astrocytes were closely aligned along the contours of MNTB principal neurons, often situated in apposition to the calyx (Fig. 2.9F), filling in spaces not occupied by the terminal. S100β-positive astrocytes showed an even distribution across MNTB, and were interleaved on the postsynaptic cell not taken up by the calyx (Fig. 2.9G). At this age, GFAP-positive astrocytes were found in MNTB, with astrocytic processes present near calyces (Fig. 2.9H). Microglia were distributed throughout MNTB at this age, with occasional fibers in

the vicinity of calyceal endings (Fig. 2.9I). Oligodendrocyte staining revealed a similar expression pattern to younger ages, with OLIG2-positive cells near the MNTB neurons (Fig. 2.9J).

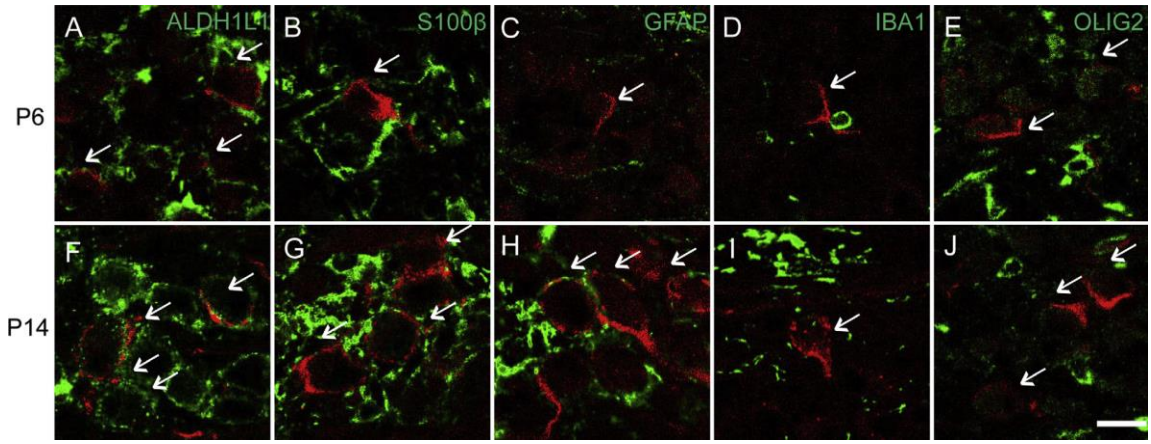


**Figure 2.9**. **Expression of glial markers in relation to the calyx at P6 and P14.** (A–E) Glial cell types near P6 calyx. (A–B) Cells positive for ALDH1L1 and S100β were in close apposition to labeled calyces (calyces indicated with arrows). (C) Few GFAP-positive populations found within MNTB. (D) IBA1-positive cells were found scattered across MNTB, often close to the labeled calyx. (E) Oligodendrocytes fully surround postsynaptic neurons. (F–J) Glial cell types near P14 calyx. (F–G) All astrocytic markers found expressed close to developing calyx. ALDH1L1 and S100β-positive astrocytes were in close proximity to calyx and appeared to align closely to the MNTB neuron. (H) Several GFAP processes extended into MNTB and in some cases were seen in proximity to labeled calyces. (I) IBA1-positive cells were located near calyx and had larger cell bodies compared to younger age. (J) OLIG2-positive staining looked similar to younger age, often near the MNTB neuron. Scale bar in J, 25 μm; applies to all panels.

### 2.4.4 *Expression of Glial Proteins in MNTB Following Unilateral Cochlear Lesion.*

The dynamic expression patterns of astrocyte and microglial cell populations during formation of auditory system connections prompted us to assess how these populations respond during deafferentation-induced formation of new connections. We performed unilateral cochlear ablation to induce ipsilateral sprouting. Tissue was collected at two time points after surgery, P4 and P9, and we performed subsequent

immunofluorescence and dextran dye labeling to assess expression of glial markers during the maturation of the newly formed calyx (Fig. 2.10). We observed ALDH1L1-positive astrocytes positioned closely to the majority of normal, contralateral calyces (95%) and lesion-induced ipsilateral calyces (94%; Fig. 2.10A). Similarly, S100β–positive astrocytes surrounded the new calyx with several processes invading the postsynaptic space (Fig. 4.2B). S100β–positive astrocytes were observed in proximity to 94% of normal contralateral calyces and 96% of induced ipsilateral calyces. In addition, GFAP-positive processes coursed throughout the MNTB, with some processes along the newly formed calyx (74%, Fig. 2.10C). In contrast to the astrocyte labeling, microglial staining showed minimal microglia near the ectopic calyx, in which only half of the calyces had apposition of IBA1-positive expression (Fig. 2.10D). Lastly, staining for oligodendrocytes revealed a similar expression pattern to normal development, in which OLIG2-positive staining were minimally expressed around postsynaptic cells in MNTB – in this case, less than half of the calyces observed had oligodendrocyte apposition (Fig. 2.10E).

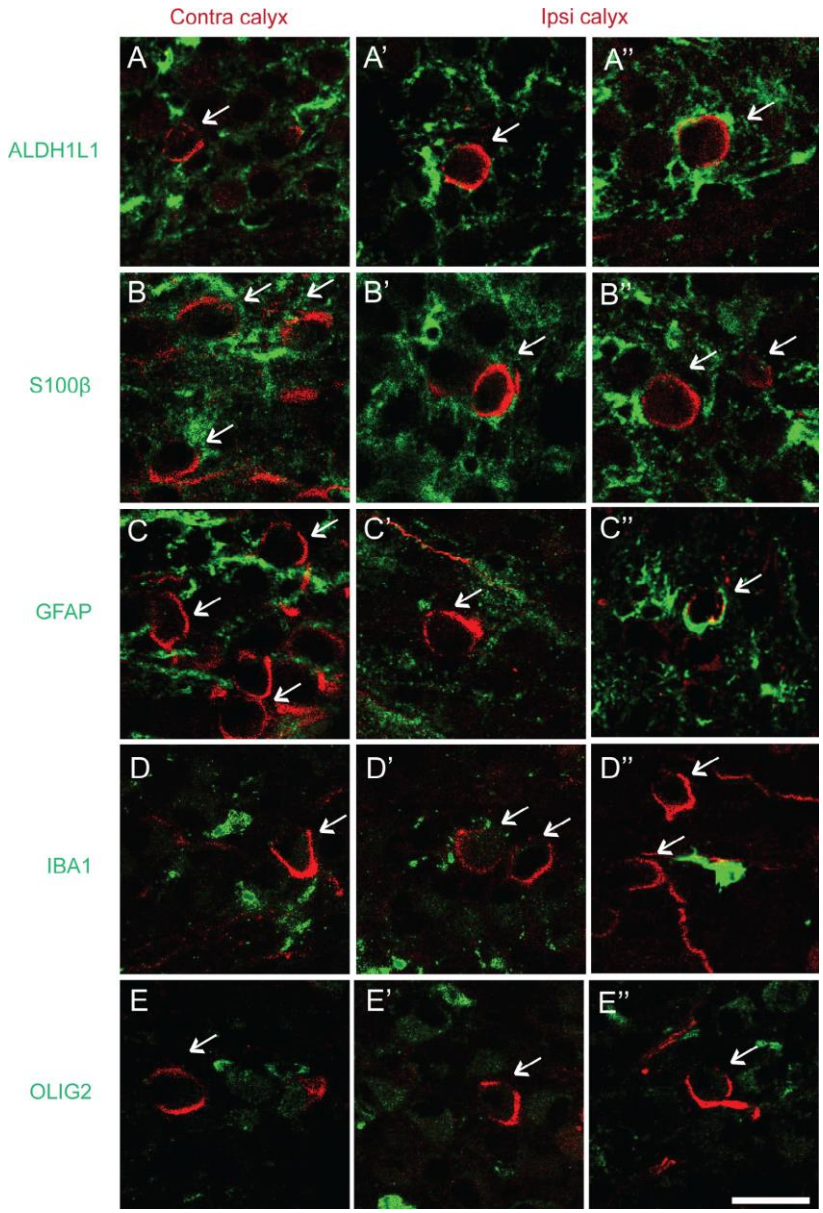


**Figure 2.10**. **Expression of glial markers in relation to ectopic calyx following Cochlea removal**. (A) ALDH1L1-positive astrocytes located along postsynaptic space unoccupied by newly formed calyx, similar to contralateral calyx (calyces indicated with arrows). (B) S100β cells and processes situated around MNTB neurons in both contralateral and ectopic ipsilateral calyx. (C) Several GFAP-positive processes extended into MNTB region, with a majority of cells contacting both contralateral and ectopic calyces (example of close apposition in C″). (D)Unlike astrocytic populations, few microglia found near calyx. (E) Very few OLIG2-positive expression near calyces. Scale bar in E; 25 µm; applies to all panels**.** N = 17 CR and 11 Sham.

We quantitatively assessed the density of glial cells using optical density for all markers except IBA1, for which we used cell counts, and GFAP, for which we measured total process length. For each of the measures we computed a ratio, the D/I ratio, which was compared to similar counts in unilaterally sham-operated animals. Analysis revealed that after a two-day survival period, these ratios were not significantly different (n=9 for both groups; ANOVA, $p$ = 0.23; Fig. 2.11, panel A–E). Similarly, D/I ratios did not differ

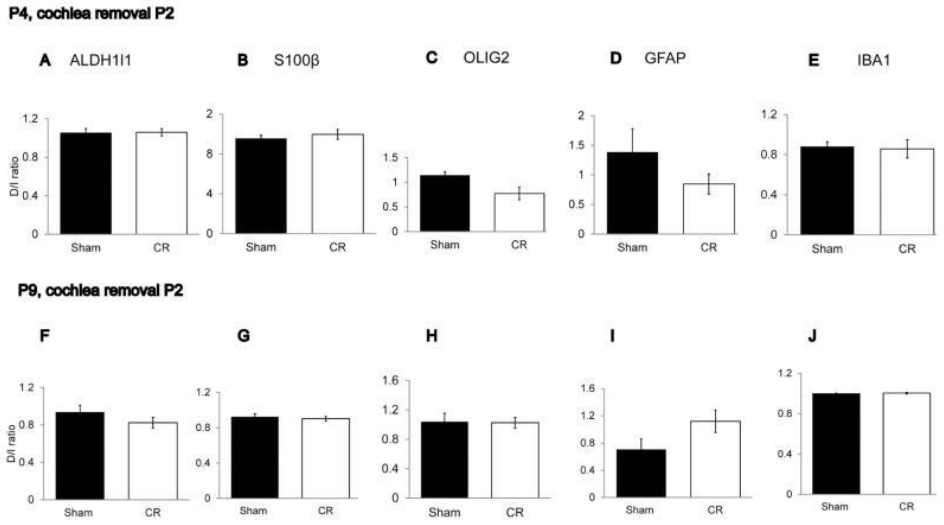


**Figure 2.11**. **Expression of glial markers two days following unilateral Cochlea removal.** (A) No significant difference in expression pattern of glial markers two days after CR (N = 9 CR and 9 Sham; ANOVA, $p$ = 0.23). ALDH1L1 staining in CR animals had a mean D/I ratio of 1.06 ± 0.03 compared to sham animals (1.05 ± 0.05). (B) Expression of S100β cells for CR groups had a D/I ratio of 1.0 ± 0.05 compared to sham group (0.96 ± 0.03). (C) OLIG2 expression had a similar result when comparing CR groups to sham (1.14 ± 0.07 and 0.77 ± 0.13, respectively). (D) Number of GFAP-positive processes was not different - the CR group had a mean D/I ratio of 0.85 ± 0.15 processes compared to sham operated animals, which had a D/I ratio of 1.38 ± 0.41. (E) Number of microglial cells comparing CR animals to sham was not significant (0.86 ± 0.09 compared to 0.88 ± 0.05). (F) One week after CR, no differences in glial marker distribution seen when comparing sham to CR groups (N = 17 CR and 11 Sham; ANOVA, $p$ = 0.13). Staining of ALDH1L1 showed that CR groups had a mean D/I ratio of 0.82 ± 0.06 and were not significantly different compared to the sham group (0.94 ± 0.07). (G) S100β expression between CR and sham was not different (0.9 ± 0.03 and 0.92 ± 0.03, respectively). (H) OLIG2 expression between CR and sham groups was not different with the CR group D/I ratio of 1.03 ± 0.07 and sham group D/I ratio of 1.04 ± 0.12. (I) When comparing GFAP processes, animals subjected to unilateral CR had a D/I ratio of 1.12 ± 0.17, a value greater than sham-operated animals but not significantly different (0.71 ± 0.15). (J) No change in between was seen in IBA1-positive cell density D/I ratio between CR and sham groups (1.0 ± 0.01 and 0.99 ± 0.01). Values are reported as mean ± SEM.

between CR and sham controls after seven days post-operative (n = 17 CR and n = 11 sham; ANOVA, $p = 0.13$; Fig. 2.11, panel F–J).

## 2.5 DISCUSSION

We have characterized the developmental emergence of distinct glial populations in the auditory brainstem, focusing on the projection from VCN to MNTB in relation to the developing calyx of Held. Additionally, we performed similar studies on lesion-induced ipsilateral projections. These studies provide clues to the function of glial cells in auditory synaptogenesis, and suggest that induced calyces share similar glial involvement with normal contralateral calyces.

### 2.5.1 *Glial distribution in brainstem postnatal development – connection to developmental events*

In this study we explored the developmental expression pattern of several glial markers in the mouse auditory brainstem during normal postnatal development and following early unilateral CR. To explore the role of glial cells in the establishment of auditory connections, we examined the expression of glial markers during maturation of the auditory pathway (Borst and Soria van Hoeve, 2012). At P0, VCN axons in MNTB synapse onto multiple postsynaptic targets through collateral branches (Rodriguez-Contreras et al., 2008). We found distinct temporal expression profiles of astrocytes, oligodendrocytes, and microglia. GFAP and S100β expression appeared at low levels beginning at P0 along the ventral border of the brainstem and VCN, with high expression in the auditory nerve. Expression was robust for ALDH1L1 in VCN and MNTB. Like GFAP-positive astrocytes, IBA1-positive microglia were present sparsely in

VCN, but not in MNTB. OLIG2 expression revealed minimal labeling in VCN and MNTB, with many cells located in the auditory nerve. At P6, an early protocalyx has formed and collaterals are extensively pruned so that each MNTB principal neuron receives a single calyceal input (Rodriguez-Contreras et al., 2008). With the exception of GFAP, all astrocytic markers screened were expressed in VCN and MNTB at this age. Few IBA1-positive cells were seen in VCN and MNTB at P6.

We examined glial marker expression at P14, after the period of hearing onset (Mikaelian et al., 1965). Synaptic function and structure change at this stage as the calyx of Held matures. The calyx undergoes a transformation from spoon-shaped to having many finger-like processes; this fenestration is associated with interdigitated astrocytes (Taschenberger et al., 2002, Ford et al., 2009). At this age, we found GFAP-positive fibrous processes that extended into both VCN and MNTB, while the cell bodies of these cells remained outside these auditory nuclei. Other astrocytic markers demonstrated similar staining to earlier ages. In addition, IBA1 staining revealed the presence of numerous microglia in VCN and MNTB. In our survey, GFAP-positive fibers were seen in MNTB only after hearing onset. By P23, while all other glial markers had similar staining patterns to previous ages, ALDH1L1 staining appeared more punctate in MNTB. The change in appearance of ALDH1L1 expression coincides with the developmental age at which all the calyces have undergone a period of fenestration (Ford et al., 2009). In addition, the close apposition of ALDH1L1-positive astrocytes suggests that this particular astrocytic population may be important for the facilitation of glutamate uptake that is necessary for the calyx to have high fidelity synaptic transmission onto the principal neurons.

### 2.5.2 *Oligodendrocytes expressed during brainstem development*

We used an antibody that recognizes OLIG3, a known marker for embryonic, young, and mature oligodendrocytes (Takebayashi et al., 2000), to examine the developmental expression of oligodendrocytes. In all the ages we examined, oligodendrocytes were present throughout VCN and MNTB. Previously published studies using an alternate oligodendrocyte marker, myelin basic protein, have shown a similar expression pattern in rodent brainstem (Delassalle et al., 1981, Foran and Peterson, 1992, Richardson et al., 2006). These observations suggest the presence of oligodendrocytes well in advance of myelination, which occurs in this pathway in rats after P8 (Leao et al., 2005).

### 2.5.3 *Temporally and spatially distinct classes of astrocytes*

Our results suggest the presence of a heterogeneous population of astrocytes. Classically there are considered to be two astrocytic populations: fibrous and protoplasmic astrocytes. While fibrous astrocytes have more elongated processes and are largely located in white matter; protoplasmic astrocytes are more globular with fewer glial processes and are localized to gray matter (Miller and Raff, 1984). In our studies, we found that GFAP-expressing astrocytes appeared later in the brainstem compared to non-GFAP astrocytic markers, suggesting that distinct classes of astrocytes could have differing functions in brainstem development. In our study, GFAP-expressing astrocytes may represent the fibrous astrocytic population, as these astrocytes fit the criteria for having more elaborate processes and are found coursing along the VCN axon tracts to MNTB. In contrast, the morphology of ALDH1L1- and S100β-positive astrocytes was more consistent with protoplasmic astrocytic population; these cells were more rounded

and while not found within the fiber tracts, were localized predominantly to the gray matter, surrounding the principal neurons. The early astrocytes are positioned to play a role in synaptogenesis. GFAP expression at later ages showed astrocytes in close apposition to the calyx of Held as well as localized to the VCN-MNTB fiber tracts, in parallel to studies done in the mature rat brain and cat visual cortex (Ghandour et al., 1980, Hajos and Kalman, 1989, Muller, 1992, Reyes-Haro et al., 2010). While we did not assess astrocyte function within the brainstem, the localization of these cells is consistent with a possible role in regulating neurotransmission and facilitation of glutamatergic clearance (Renden et al., 2005, Reyes-Haro et al., 2010).

### 2.5.4 *Delayed expression of GFAP-positive astrocytes and IBA1-positive microglia in MNTB*

The early expression of the astrocyte markers ALDH1L1 and S100β contrasts with expression of GFAP in MNTB, which was not seen upregulated until after hearing onset. Minimal IBA1 expression was seen inside MNTB at P6. The appearance of GFAP-positive astrocytic fibers and IBA1-positive microglia within the MNTB occurs after formation of the calyx of Held, but during a time of maturation of the calyx (Ford et al., 2009, Borst and Soria van Hoeve, 2012). Our results are consistent with similar findings in chick auditory brainstem development, where GFAP-positive processes were observed entering the *n. laminaris* (NL) cell body layer late in embryonic development, after excitatory inputs to the nucleus have formed (Saunders et al., 1973, Jackson and Parks, 1982, Young and Rubel, 1986, Korn and Cramer, 2008). The delayed expression of GFAP in chick astrocytes coincides with dendritic reorganization of NL neurons and inhibitory synapse maturation. Furthermore, astrocyte-secreted factors

were shown to mediate these developmental events using an *in vitro* preparation (Korn et al., 2011, Korn et al., 2012). While we did not look at astrocyte-secreted factors in the present study, the importance and identity of these factors will be of interest in the study of circuit formation in the mammalian auditory brainstem.

### 2.5.5 *Morphological changes in microglia during postnatal brainstem development*

IBA1 immunofluorescence showed that brainstem microglia undergo morphological changes early in postnatal development. At P0 we observed both amoeboid microglial cells with no processes and cells with few processes emanating from the cell bodies. These microglia appeared more rounded, similar to previously described embryonic forms found in the rat hippocampus (Dalmau et al., 1997). IBA1 microglia observed at older postnatal ages were more dense and exhibited slightly ovoid cell bodies with complex, elongated radial processes, characteristic of the ramified forms observed during the second postnatal week of rat hippocampal development (Dalmau et al., 1998). At three postnatal weeks, microglia were numerous and demonstrated a diversity of types, ranging from only cell bodies to cells with various processes (Lawson et al., 1990).

### 2.5.6 *Distribution of astrocytes and microglia following unilateral CR*

After unilateral CR during the early postnatal period, intact VCN axons branch and make aberrant connections with the denervated ipsilateral MNTB (Kitzes et al., 1995, Russell and Moore, 1995, Hsieh et al., 2007). Similar molecular cues limit ipsilateral projections both during normal development and after CR (Nakamura et al.,

2012, Nakamura and Cramer, 2013). To further explore the similarities of these mechanisms, we examined the extent to which glial distributions in denervated MNTB resemble those seen during normal development. We found that CR was not associated with overall significant increases in glial cell density in MNTB compared to the unlesioned side. Nevertheless, distinct populations of glial cells were closely localized to the newly developing ectopic calyx, similar to those seen in normal development. IBA1-positive microglia were not preferentially located near nascent calyces, either during normal development or after unilateral lesion. The similarity in the spatial distribution of glial cells during developmental and induced synaptogenesis in MNTB is consistent with the view that these processes share molecular and cellular mechanisms.

A number of studies have shown increases in glial reactivity following deafferentation in the adult cochlear nucleus. An increase in astrocytes was found in chick brainstem after CR in *n. magnocellularis*, the avian homolog of the anteroventral cochlear nucleus (Rubel and MacDonald, 1992, Lurie and Rubel, 1994). Prior studies in mammals have also shown that both microglia and astrocytes are upregulated in the cochlear nucleus in response to unilateral inner ear lesions in adult rats (de Waele et al., 1996, Campos Torres et al., 1999, Campos-Torres et al., 2005, Fuentes-Santamaria et al., 2012). These studies showed changes in the cochlear nucleus, the primary target denervated by CR. In our studies, we explored changes in the MNTB, a secondary site of denervation. It is possible that changes in glial cell density are not reflected in this secondary site. Consistent with this possibility, unilateral CR did not alter proliferation in P9 rat MNTB (Saliu et al., 2014). Alternatively, it may be that changes in glial cell density require a longer time to emerge. Because we were

interested in the formation of calyceal terminations, we limited our examination of glial markers to a time window after lesion when the new calyces form (Kitzes et al., 1995; Hsieh et al., 2007). Our findings suggest that glial cell configurations near induced projections are similar to those of normal projections, but that increases in glial number, through proliferation or migration, do not seem to be required for the induction of ipsilateral projections.

### 2.5.7 *Concluding remarks*

Our data show distinct expression profiles of glial markers in the developing mouse brainstem. Specifically, we found that glial cells are found early in development, during synaptogenesis of the VCN-MNTB circuit, and that these populations shift and change overtime. The results are consistent with a role for glial cells and their associated proteins in synapse formation and maturation in the auditory brainstem. Following CR, we found that the expression of glial markers after surgery was largely similar to that of normal development, with astrocytes and microglia surrounding both normal and lesion-induced calyces. These observations support the view that induction of new synapses after lesion relies on the same glial populations needed for normal development.

## 2.6 ACKNOWLEDGEMENTS

We are grateful to H. Nguyen and J. Ayala Salazar for technical support and to Dr. S. Cohen-Cory, Dr. K. Green, and Allison Haskell for assistance with confocal imaging. This work was supported by NIH T32 DC010775.

# CHAPTER 3: Impaired microglial signaling effects on Calyx of Held normal development

## 3.1 SUMMARY

Proper synapse formation requires the orchestration of appropriate cell-cell communication. Abnormalities in synapse development may result in impairments in synaptic connectivity and have been implicated in neurodevelopmental disorders.

In the auditory brainstem, precise circuitry is essential for processing sound localization. The mammalian auditory brainstem provides an excellent model to study various mechanisms of synapse formation such as competition and maturation of synapses. In this study, we focused our work on studying the VCN-MNTB circuit within the mammalian brainstem that provides inhibition to nearby brainstem nuclei. The VCN provides contralateral projections onto MNTB, known as the calyx of Held, and are one of the largest synapses found in the brain (Spirou et al., 1990). While the circuitry has been well characterized, understanding what molecular mechanisms guide proper synapse formation in the brainstem remains a challenge for developmental neuroscience. Here, we investigated what glial influences can affect synapse formation in the auditory brainstem. As glial cells have been documented to promote synapse formation and maturation, we focused on microglial influences. Microglia have been implicated in various aspects of synapse formation and pruning. Initially thought to serve as the immune cells of the nervous system, microglia have emerged as active surveyors of the microenvironment, regulating the number of synapses, and modulating synaptic efficacy.

For this study, we used two mutant mouse lines that have impaired microglial signaling – the *Cx3cr1*$^{-/-}$ and *Csf1R*$^{-/-}$ strains. We examined calyx form and number in P8 mice, at an age when most MNTB neurons have a single dominant input (Holcomb et al., 2013). We measured calyx size, MNTB cell size, and pruning deficits. Our results showed that compared to their wildtype littermates, both *Cx3cr1* and *Csf1R* mutant mice exhibited smaller calyx size, smaller MNTB cell area, and impairment of synaptic pruning. Additionally, we conducted a preliminary assessment that sought to identify a potential mechanism for the immature synapse phenotype observed in the mutant mice. Using super resolution STORM imaging, we observed a reduction in VGLUT1/2 levels in the calyces of mutant *Cx3cr1*$^{-/-}$ mice compared to control mice. Finally, we looked at LPS injected mice and found increased levels of VGLUT1/2 expression.

Overall, our data suggest that impaired microglial signaling influences normal development of the calyx of Held and as a result, influences the target MNTB cell size. These impairments persist through to adulthood and can potentially influence sound localization ability of the animals. Furthermore, we sought to identify what consequences occur due to a reduced calyx size and found that *Cx3cr1*$^{-/-}$ mice have less VGLUT1/2 molecules within the developing calyx compared to controls. Collectively, this data points to microglia serving as an active gatekeeper in mediating key synaptic events in the VCN-MNTB pathway.

## 3.2 INTRODUCTION

Neuronal communication relies on the proper wiring of neural networks. The precision and remarkable connectivity of the central nervous system is first preceded by a wave of exuberant synapses that occurs during early development. Selective pruning, often mediated by neural activity-dependent mechanisms, ensures that weaker synapses are removed and the remaining synapses are stabilized and strengthened. In the mammalian auditory brainstem, connections important for sound localization are similarly pruned (Holcomb et al., 2013). In this pathway, spiral ganglion cells in the cochlea send central projections into the brainstem where they form synapses the ventral cochlear nucleus (VCN). Axons from VCN globular bushy cells provide excitatory, glutamatergic innervation to the contralateral medial nucleus of the trapezoid body (MNTB), the main inhibitory nucleus in the auditory brainstem (Banks and Smith, 1992, Kandler and Friauf, 1993). This VCN-MNTB projection covers each MNTB neuron in a large encapsulating termination known as the calyx of Held (Friauf and Ostwald, 1988, Kuwabara et al., 1991, Kuwabara and Zook, 1991, Kandler and Friauf, 1993). These inputs are specialized synapses that provide fast neurotransmission to the MNTB neuron, which in turn modulates other brainstem nuclei through glycinergic innervation. During early postnatal development, many small calyces terminate onto a single MNTB neuron providing relatively weak synaptic input (Rodriguez-Contreras et al., 2006). Eventually, a dominant input outcompetes weaker synapses by the first postnatal week and the remaining calyx develops into a mature, large reticulated structure (Rodriguez-Contreras et al., 2008, Ford et al., 2009, Holcomb et al., 2013). The mechanisms underlying this progression of developmental events that ensure

proper synaptic pruning remain a significant challenge in developmental auditory research.

Recently, microglia have been shown to mediate many synaptogenic events, including developmental pruning of excess synapses. These glial cells actively survey the microenvironment and make numerous and brief contacts at developing synapses (Nimmerjahn et al., 2005, Wake et al., 2009, Tremblay et al., 2010). In normal development, microglia serve to regulate the appropriate number of synapses through various mechanisms. Evidence for microglial pruning first emerged within the visual system where they were shown to prune synapses terminating in the lateral geniculate nucleus (LGN) through the complement receptor 3 (CR3) and ligand C3 pathway (Schafer et al., 2012).

Impaired microglial signaling through the fractalkine receptor, *Cx3cr1*, also influences synaptogenesis. *Cx3cr1*$^{-/-}$ mice have excess synapses and impaired circuit connectivity (Paolicelli et al., 2011, Zhan et al., 2014). In addition, *Cx3cr1*$^{-/-}$ mice exhibit behavioral abnormalities similar to those seen in animal models of autism (Zhan et al., 2014).

Numerous factors released from microglia have the potential to influence synapse maturation. For example, these cells secrete cytokines such as tumor necrosis factor α (TNF-α), which can influence synaptic strength through the upregulation of glutamate receptors (Beattie et al., 2002). Additionally, microglia secretion of brain derived neurotrophic factor (BDNF) is important for mediating cortical synapse formation required for motor learning (Parkhurst et al., 2013). While microglia can secrete trophic

factors in normal development, impaired or diseased microglia can secrete toxic levels of glutamate that cause dendritic and synaptic damage onto neurons (Maezawa and Jin, 2010).

In this study, we investigated microglial influences on the development of synapses in the VCN-MNTB pathway, focusing on maturation of the Calyx of Held. We examined the effects of mutations in *Cx3cr1*$^{-/-}$ mice, which result in impaired microglial signaling. In addition, we examined effects of mutations in colony stimulating factor 1 receptor (*Csf1R*), in which no microglia develop. We hypothesized that loss of microglia or impaired microglial communication would result in either lack of pruning or a delayed pruning phenotype. Conversely, enhancement of microglial signaling was hypothesized to result in an augmentation of pruning. We found that mutant mice had decreased calyx morphology, decreased MNTB cell size, and pruning deficits. Additionally, we quantified the number of presynaptic excitatory VGLUT1/2 molecules and found an overall decrease in the *Cx3cr1*$^{-/-}$ mice, but an increase in VGLUT1/2 expression in LPS-injected mice. Our results suggest that impaired microglial signaling potentially affects synapse development through an immature calyx that has a decreased release of excitatory synaptic molecules.

## 3.3 MATERIALS AND METHODS

### 3.3.1 *Animals*

All procedures were approved by the University of California, Irvine Institutional Animal Care and Use Committee.

To investigate microglial effects on brainstem synapse formation, two mouse lines were used, both on the C57BL/6 background and obtained from Jackson Laboratory. The first has a null mutation in the Cx3c chemokine receptor 1 (*Cx3cr1*). The Cx3cr1 protein is a receptor expressed in microglia that interacts with a chemokine ligand, fractalkine, which is expressed in neurons. The *Cx3cr1*$^{-/-}$ mouse line thus has impaired neuron-microglia signaling. In addition, these mice have enhanced green fluorescent protein (EGFP) inserted into exon 2, resulting in GFP-positive microglial cells (Jung et al., 2000).

A second mouse line *Csf1r*$^{floxed/floxed}$ have loxP sites flanking exon 5 of the *Csf1r* gene, which encodes colony stimulating factor 1 receptor, a factor essential for microglial survival. These mice were crossed with the B6.FVB-Tg (Zp3-cre)3Mrt/J mouse line that has Cre expressed exclusively in the oocytes to produce Cre-*Csf1R*$^{flox/flox}$ mice. Heterozygotes (*Csf1R*$^{flox/-}$) were generated by crossing Cre-*Csf1R*$^{flox/flox}$ mice with C57BL/6 males. Heterozygotes were bred together in order to generate mutant *Csf1R*$^{-/-}$ mice. In contrast to the *Cx3cr1*$^{-/-}$ mice, the *Csf1r*$^{-/-}$ mice have various physical abnormalities including small body size, lack of teeth, osteoporosis, and premature death by 6 weeks of age (Li et al., 2006, Erblich et al., 2011). It has also been previously shown that *Csf1R* is important for microglia viability, as targeted pharmacological agents inhibiting this receptor result in depletion of microglial populations (Elmore et al., 2014). In additional experiments using wild type *C57bl/6* mice, we induced microglial activation with lipopolysaccharide (LPS) injected intraperitoneally at a dose of 2mg/ml from P2-P7. Mice were perfused at P8.

Studies investigating calyx formation, cell size, and synaptic function were performed on both pups aged postnatal day 7-9 (P7-9). Adult mice were used for calculations of MNTB neuron size was (2 months).

Brainstem tissue was extracted after mice were transcardially perfused with 0.5% saline followed by 4% PFA as outlined in Chapter 2. Tissue was fixed in 4% PFA for 2 hours at 4ºC and dehydrated in 30% sucrose overnight. Tissue was placed in OCT and coronally sectioned at 18-micron thickness onto chrom-alum subbed slides for immunohistochemistry.

### 3.3.2 *Immunohistochemistry and STORM VGLUT labeling*

Slides were rinsed and treated with an antigen retrieval step in 0.1% SDS in 1X phosphate buffer saline (PBS, 137mM NaCl, 2.7mM KCl, 10mM $Na_2HPO_4$, and1.8mM $KH_2PO_4$) for 5 minutes. Slides were then rinsed in PBS solution 3 times at 10 minutes each. Slides were blocked with 4% bovine serum albumin (BSA) in 0.1% triton-x-100 PBS solution for 1 hour at room temperature, followed by primary antibody incubation overnight at room temperature. The following day, slides were rinsed with PBS and incubated in secondary antibody (Alexa Fluor, Invitrogen) for 1 hour at room temperature before rinsing in PBS and were coverslipped with Glycergel (Dako).

Presynaptic excitatory synapses were stained using the VGLUT1/2 antibody (anti-guinea pig, Millipore) at a 1:2500 dilution. The NeuN antibody was used to visualize neuronal cell bodies (anti-mouse, Millipore) at a 1:500 dilution. AlexaFluor secondary antibodies were used at a dilution of 1:500.

For STORM imaging experiments, slides were first cleared in Sca/e buffer for a minimum of 3 days at 4ºC to reduce background autofluorescence. Sca/e2 clearing buffer was prepared with 4M urea, 10% glycerol and 0.01% triton-x-100 as previously published (Hama et al., 2011). Slides were then incubated in sodium borohydride (1mg/ml in PBS) for 5 minutes at room temperature, followed by performing the standard immunolabeling for VGLUT1/2 as described above. Slides were incubated in STORM imaging buffer detailed in the protocol below.

### 3.3.3 *Neuroanatomical labeling*

Rhodamine dextran amine (RDA) dye injections were used to visualize calyces. The RDA (MW: 3000, Invitrogen) dye injection solution included 6.35% RDA with 0.4% Triton-X100 in PBS. Brainstems were extracted and placed in artificial cerebrospinal fluid (aCSF; 130mM NaCl, 3mM KCl, 1.2mM $KH_2PO_4$, 20mM $NaHCO_3$, 3mM HEPES, 10mM glucose, 2mM $CaCl_2$, 1.3mM $MgSO_4$ perfused with 95% $O_2$ and 5% $CO_2$). A pulled glass micropipette was filled with RDA and short pulses of dye were injected using a Picospritzer at 25 ms along the medial extent of the ventral brainstem in order to visualize projections terminating onto both MNTB regions. The region surrounding the injection site was electroporated at a rate of 5 pulses per second (pps) at 40 volts (V) for 50 milliseconds (ms). The brainstem was dissected out and immersed in aCSF for 2 hours under continuous oxygenation and fixed for two hours in PFA for histology, rinsed, and incubated in 30% sucrose overnight.

### 3.3.4 *Imaging*

Images were captured using a fluorescent and confocal microscope (Zeiss Axioskop and Leica Confocal microscope, respectively). Adobe Photoshop was used to adjust images for appropriate brightness and contrast and edited using Adobe Illustrator.

To quantify individual VGLUT1/2 molecules, we used super resolution STORM imaging (Rust et al., 2006). By using this technique, individual VGLUT molecules can be selectively activated and quantified. Following immunohistochemistry, slides were placed in freshly prepared STORM imaging buffer (SIB). Three solutions were used in order to create SIB, which consisted of 98% Imaging Buffer Base (10% glucose, 50mM Tris, 10mM NaCl), 2% β-mercaptoethanol (14.3M), and 2% 100x Glox solution (14 mg glucose oxidase, 50 µl catalase, 8mM Tris, 40mM NaCl). ANDOR software was used to acquire calyx images in addition to expression of VGLUT molecules. The total number of VGLUT molecules within a particular section were analyzed using the ANDOR NStorm Analysis panel, and a Python program was developed in order to selectively measure VGLUT molecules within calyceal regions (script created by Brett Settle from the lab of Dr. Ian Parker).

### 3.3.5 *Imaging analysis*

Quantification of calyx size, neuronal size, VGLUT expression levels, and pruning assessments were performed using ImageJ software and Axiovision. All calyces were quantified to ensure sufficient sampling. Calyceal size was determined by

thresholding images to highlight regions of interest. The ImageJ wand tracing tool was used to individually select calyces and area measurements were taken.

Axiovision software was used to measure MNTB cell size and VGLUT1/2 expression levels. Area was measured by using the Outline Spline tool to trace individual cells. Measurements of cell area were taken on 10 randomly selected cells on at least 3 MNTB sections. VGLUT1/2 levels were quantified by performing an optical density analysis that was subtracted to background staining levels on 3 randomly selected MNTB sections.

To quantify pruning effects, we used VGLUT immunolabel as a marker for presynaptic input onto principal neurons together with sparse RDA labeling of calyces. We performed this analysis on all MNTB neurons with an RDA-labeled calyx. Using ImageJ, we measured VGLUT coverage that coincided with the labeled calyces (presynaptic input derived from the labeled calyx, denoted as $VGLUT_{RDA}$) in addition to total VGLUT coverage of the MNTB cell (value representing all presynaptic inputs on MNTB neuron, known as the $VGLUT_{total}$) and calculated a ratio ($VGLUT_{RDA}$ / $VGLUT_{total}$). Values above 0.8 were indicative of complete pruning (i.e., the only presynaptic input onto MNTB was from the labeled calyx), whereas a value closer below 0.8 suggested additional inputs, observable as regions of VGLUT immunolabel not associated with the labeled calyx, and thus associated with other inputs to the MNTB neuron. From the $VGLUT_{RDA}$ / $VGLUT_{total}$ ratio, we quantified the percentage of monoinnervated synapses.

STORM data analysis was performed using ANDOR-STORM software. Images were analyzed for individually activated VGLUT molecules using the ANDOR NStorm Analysis software and a Python script was created to calculate VGLUT molecules within a calyceal region (script written by Brett Settle from Dr. Ian Parker's lab).

For multiple comparisons, ANOVA with post-hoc Tukey analysis was performed. In comparing wildtype groups to mutant mice groups, a student's t-test with a Bonferroni correction was performed for determining significantly different means.

## 3.4 RESULTS

### 3.4.1 *Csf1R*$^{-/-}$ *mice lack microglia in brainstem*

To observe microglial effects on brainstem development, we focused on the VCN-MNTB pathway. Maturation of this pathway entails several morphological changes that affect both the calyx and principal MNTB neuron. By the first postnatal week, multiple calyceal inputs synapse on a single MNTB neuron and actively compete to become the predominant input. In addition, neurogenesis of MNTB cells occurs with MNTB neurons increasing in size (Holcomb et al., 2013). To this extent, we focused on microglial effects on calyx size, MNTB cell size, and pruning. Two mouse models were used in order to investigate microglial mechanisms within the brainstem – the *Cx3cr1* and *Csf1R* mouse lines. While it was previously shown that *Csf1R* $^{-/-}$ mice have complete elimination of microglia within the cortex, we first determined if microglia were also eliminated in the brainstem. Compared to littermate controls, *Csf1R* $^{-/-}$ mice have no microglia (Figure 3.1).

### 3.4.2 *Cx3cr1*$^{-/-}$ *and Csf1r*$^{-/-}$ *mice exhibit immature calyx morphology and defects in MNTB cell size*

We then looked at calyx size by measuring overall calyx area. We performed sparse RDA midline injections along the ventral brainstem in order to visualize calyces terminating onto both MNTB regions (Figure 3.2).

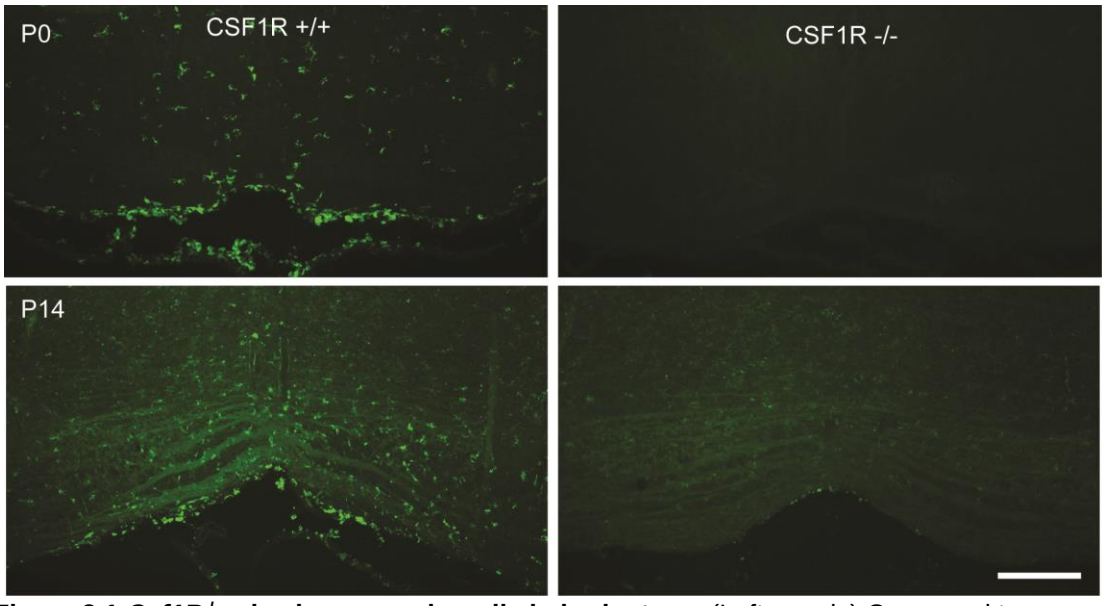


**Figure 3.1 *Csf1R*$^{-/-}$ mice have no microglia in brainstem.** (Left panels) Compared to wildtype mice, *Csf1R*$^{-/-}$ mice (right panels) have no microglia, as documented in Erblich et al., 2011. Scale bar represents 100µm.

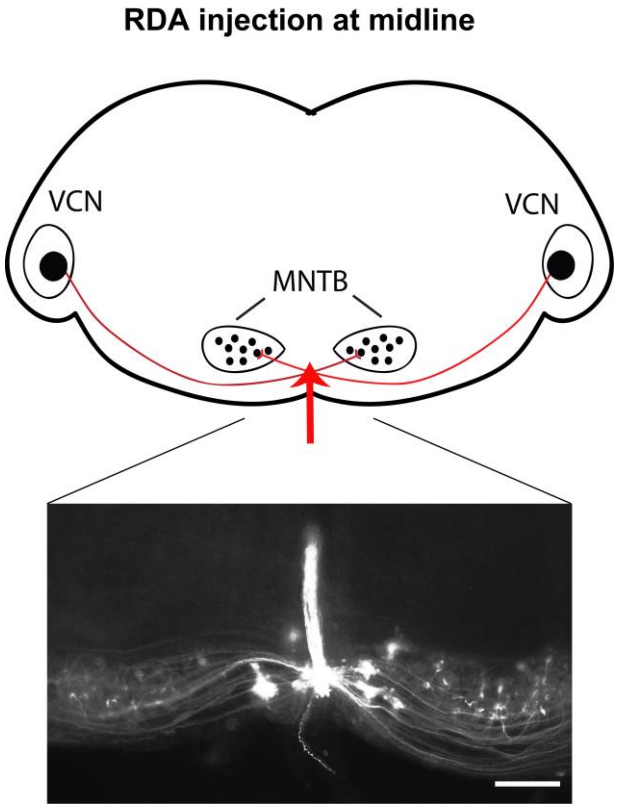


**Figure 3.2 Illustration of sparse labeling technique.** Top, Schematic diagram shows location of dye injections. Small volumes of RDA dye were injected into the midline of the ventral brainstem. Bottom, inset shows calyceal labeling from both MNTB regions. Scale bar, 100µm.

The mean calyx size of wildtype mice was 50.05 ± 3.92 µm$^2$ (n = 13, Figure 3.3A), which was significantly larger than the mean calyx size *Cx3cr1*$^{-/-}$ mice (Figure 3.3B; 37.09 ± 2.44 µm$^2$; n = 9, $p$=0.014 using ANOVA test with post-hoc Tukey). Interestingly, the decreased calyx size was also observed in the *Csf1r*$^{-/-}$ mice compared to their littermate controls. While the mean calyx size of the wildtype mice was 48.05 ± 2.645 µm$^2$ (n=11), *Csf1r*$^{-/-}$ mice had significantly smaller calyx area compared to their

wildtype littermates (Figure 3.3C; 30.46±4.36 μm$^2$; *p*=0.007 using t-test with Bonferroni correction; n=4).

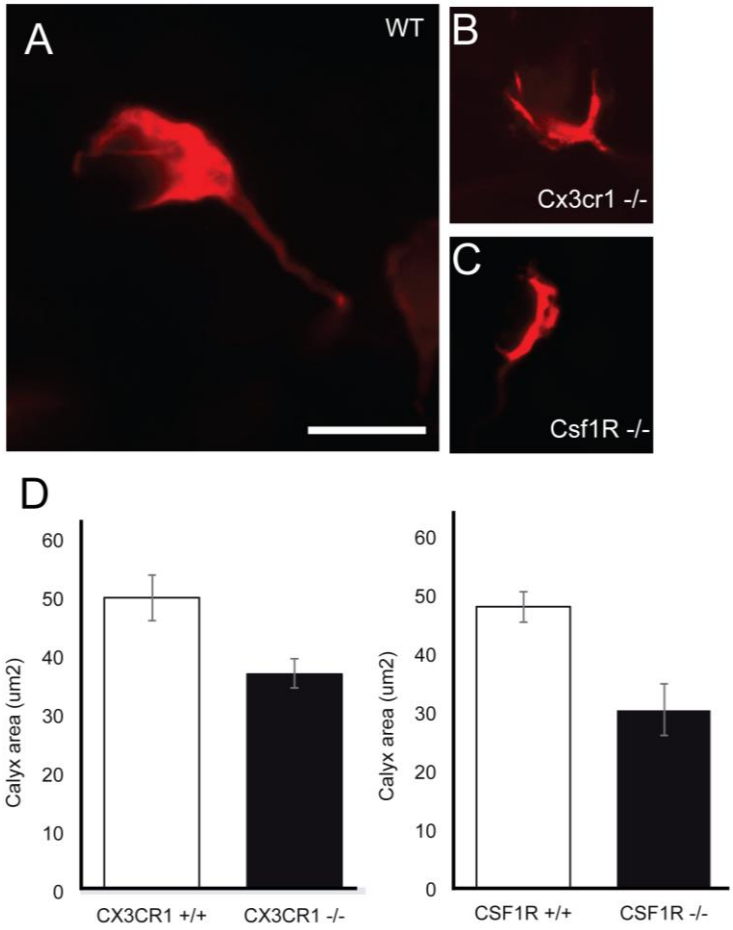


**Figure 3.3 Calyx morphology in *Cx3cr1* $^{-/-}$ and *Csf1R* $^{-/-}$ mutant mice.** Compared to wildtype mice (A), *Cx3cr1* $^{-/-}$ and *Csf1R* $^{-/-}$ mice have significantly smaller calyces (B, C). Scale bar, 10μm. Quantifications of calyceal area in both mouse lines shown in panel (D). For the *Cx3cr1* study, 13 wildtype and 9 mutant mice were used. For the *Csf1R* study, 11 wildtype and 4 mutants were used.

We next measured the size of MNTB principal neurons. We found that *Cx3cr1*$^{-/-}$ mice had a smaller mean cell size in MNTB compared to control mice in which wildtype mice had a mean cell size of 107.07 ± 1.85 μm$^2$ (Figure 3.4A, n=8). The mean cell size of *Cx3cr1*$^{-/-}$ mice was 119.85 ± 3.67 μm$^2$ (Figure 3.4B, n = 13; *p*=0.021; ANOVA test

with post-hoc Tukey analysis). To determine whether the decreased MNTB cell area was attributable to a delay in development, we also measured MNTB cell size in adult *Cx3cr1*$^{-/-}$ mice and found the decrease in cell size persisted through to adulthood. Compared to *Cx3cr1*$^{+/-}$ which had an average MNTB cell size of 84.53 ± 2.36 µm$^2$, the average cell size in mutants was 102.78 ± 7.04 µm$^2$ (data not shown, $p$=0.008, t-test with Bonferroni correction). We also measured cell size in *Csf1R* mice and found no differences between control and mutant mice ($p=0.55$, n = 3 per group).

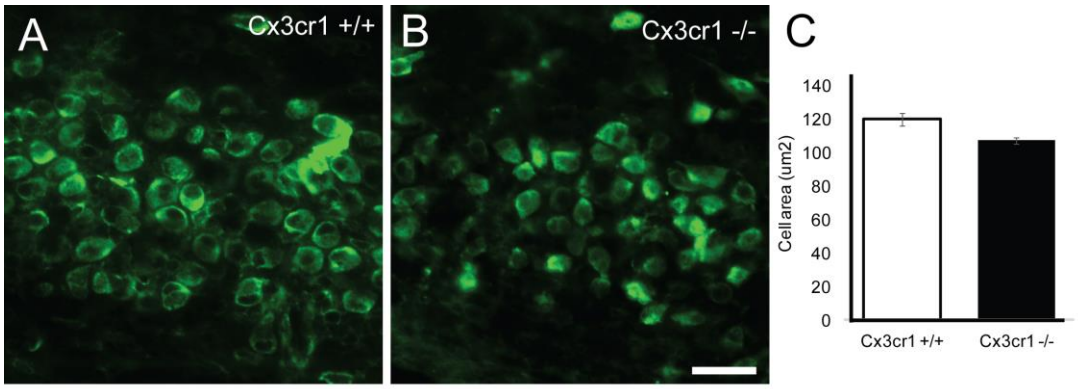


**Figure 3.4. Cell area in *Cx3cr1*$^{-/-}$ mice. (**A) NeuN immunofluorescence in wild type mice. (B) Compared to heterozygote control mice, mutant mice have smaller MNTB cell area. (C) Quantifications of cell area are depicted ($p$ = 0.021, n = 8 wildtype and 13 mutant mice). Scale bar, 50 µm.

### 3.4.3 *Cx3cr1*$^{-/-}$ *and Csf1r*$^{-/-}$ *mice have impaired pruning*

While we observed a decrease in both calyceal size and MNTB cell area, we were interested in determining if impaired microglial signaling would affect synaptic pruning. We assessed pruning by comparing the VGLUT associated with the labelled RDA presynaptic input ($VGLUT_{RDA}$), against the overall VGLUT levels of the total cell ($VGLUT_{total}$). By calculating the ratio of $VGLUT_{RDA}$ / $VGLUT_{total,}$ we could differentiate between single versus multiple inputs onto a single MNTB neuron. Using this ratio, we quantified the number of pruned synapses by using ratio values that were above 0.8 as

indicative of complete pruning, in which a single calyx innervates one MNTB neuron. Values smaller than 0.8 would suggest incomplete pruning, with multiple cells providing synaptic input to an MNTB neuron. We hypothesized that compared to wildtype mice, both *Cx3cr1*$^{-/-}$ and *Csf1R*$^{-/-}$ mice would exhibit either delayed pruning or no pruning (Figure 3.5).

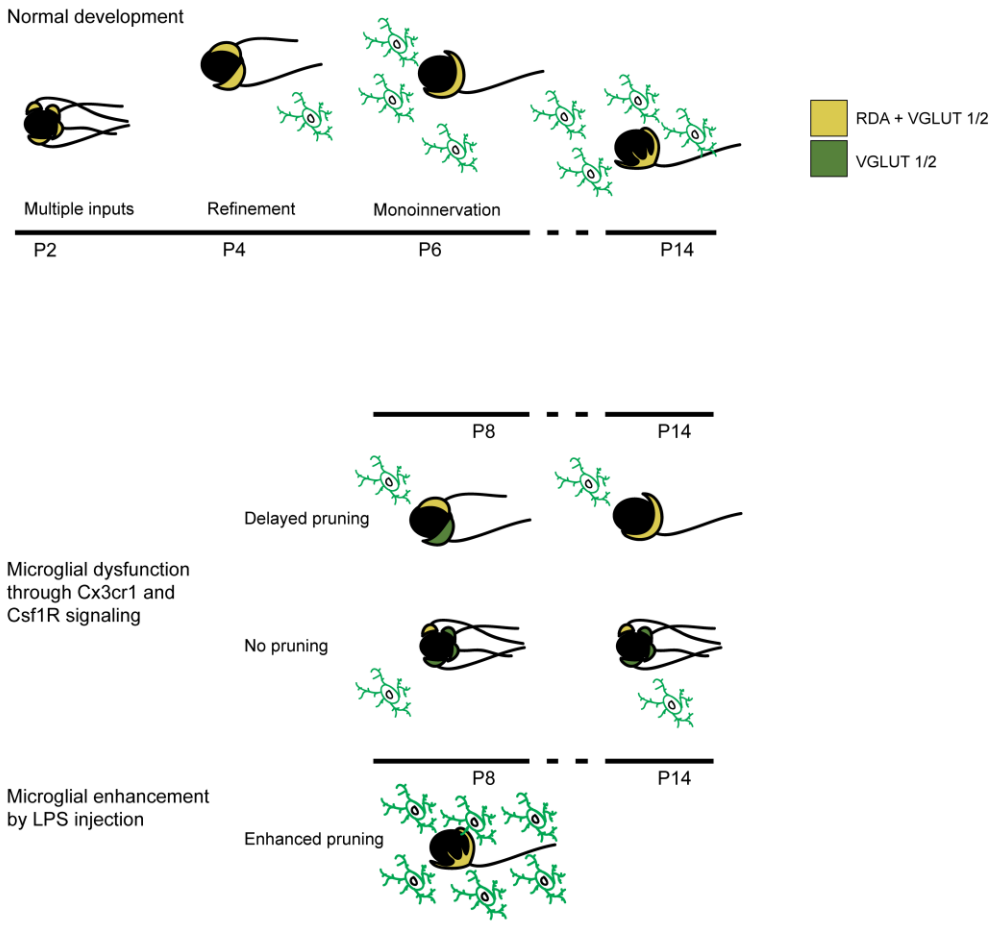


**Figure 3.5 Schematic of microglial signaling on VCN-MNTB pathway.** (Top row) In normal development, several calyces terminate onto a single MNTB neuron and actively compete until a dominant input is established. (Middle row) We hypothesize that with reduced microglial numbers or impaired signaling, pruning would either be delayed or prevented altogether. Delayed pruning would be observed by comparing VGLUT1/2 expression coinciding with RDA labelled calyx against overall VGLUT1/2 levels. (Bottom row) With enhancement of microglial signaling, we hypothesize that the mechanisms underlying pruning would be enhanced.

We first investigated the *Cx3cr1*$^{-/-}$ mice for pruning deficits by staining for VGLUT1/2 (Figure 3.6). We examined the proportion of VGLUT1/2 immunolabel associated with individual labeled calyces to identify monoinnervated versus polyinnervated MNTB neurons (Figure 3.6A-B; see Methods). In control mice (Figure 3.6A'-B'), we found that 66.67 ± 7.89% of MNTB neurons studied were determined to be monoinnvervated (Figure 3.6E). In contrast, immunolabel for VGLUT1/2 in the *Cx3cr1*$^{-/-}$ showed many areas of VGLUT1/2 labeling that did not coincide with the labeled calyx (Figure 3.6C'-D'), suggesting additional calyceal inputs were present (Figure 3.6C''-D'', 3.6F). Using our criteria, we found that on average 34.32 ± 8.48% of MNTB neurons studied were monoinnervated. This value was significantly less than that obtained in control mice (Figure 3.6E; $p = 0.01$ using t-test with Bonferroni correction, n = 9 wildtypes and 10 mutants).

Additionally, we investigated if there were any pruning deficits in the *Csf1R*$^{-/-}$ mutant mice (Figure 3.7). We found that control mice had high overlap of VGLUT1/2 expression localized with the labeled calyx (Figure 3.7 A -A'') with a mean of 83.33 ± 6.86% of MNTB neurons monoinnervated (n=8). Similar to the *Cx3cr1*$^{-/-}$ mice, the *Csf1R*$^{-/-}$ mutants had significantly fewer monoinnervated MNTB neurons (Figure 3.7B-B''; 33.33 ± 13.61, $p = 0.004$ using t-test with Bonferroni correction, n = 4).

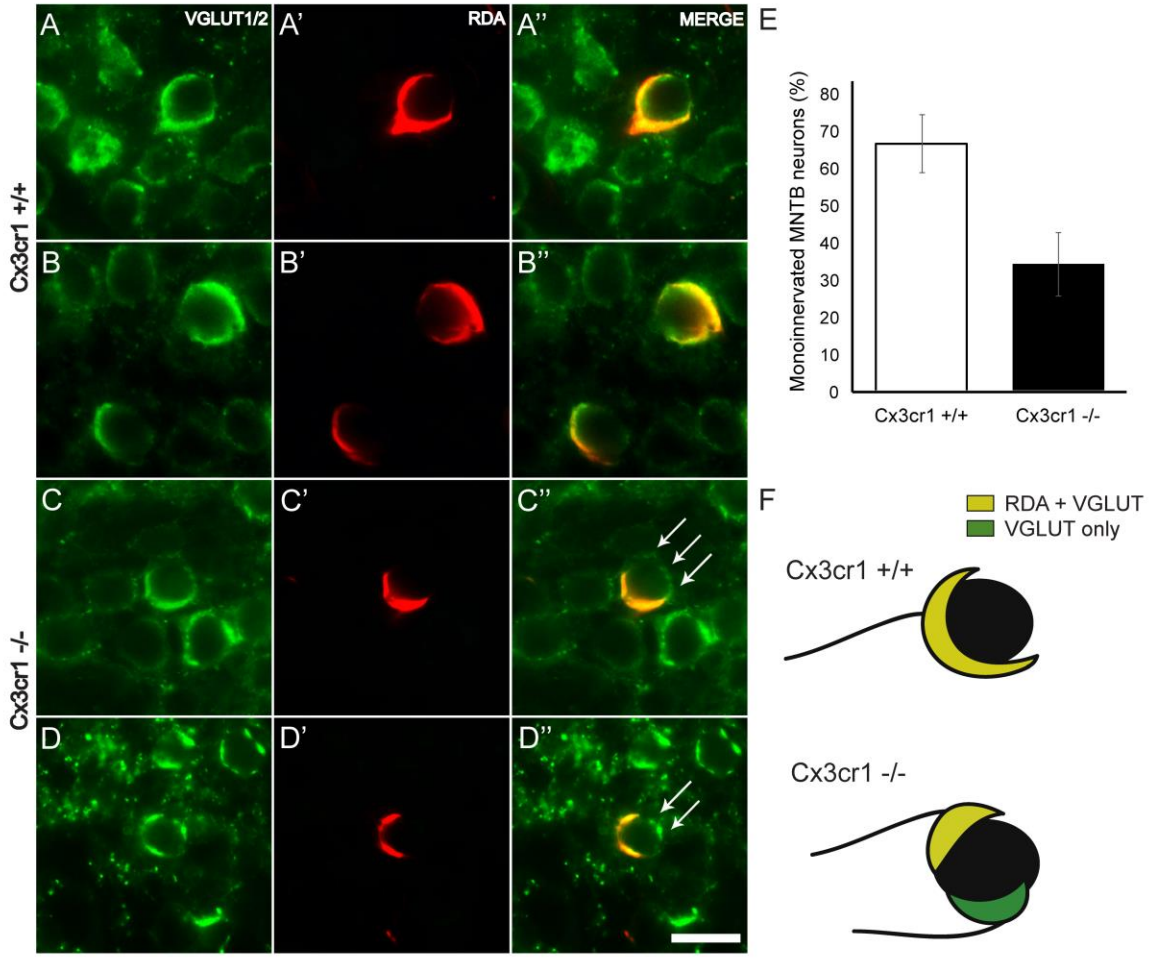


**Figure 3.6. *Cx3cr1*$^{-/-}$ mice exhibit pruning deficits.** (A -B) Representative images from wildtype *Cx3cr1* mice showing VGLUT immunolabel (A, B); RDA-labeled calyces (A', B'); and merged images (A", B"). (C - D) represent *Cx3cr1*$^{-/-}$ mice of RDA labeled calyces (C' and D') and VGLUT staining showing areas of VGLUT labeling that may be competing inputs (indicated by white arrows). Merged images of both VGLUT and RDA shown in (A'' – D''). (E) Compared to wildtype mice, *Cx3cr1*$^{-/-}$ had significantly less pruned synapses ($p$ = 0.01; n = 9 wildtype and 10 mutant). (F) shows a schematic comparing pruning efficiency between wildtype and mutant mice. Scale bar, 10 µm.

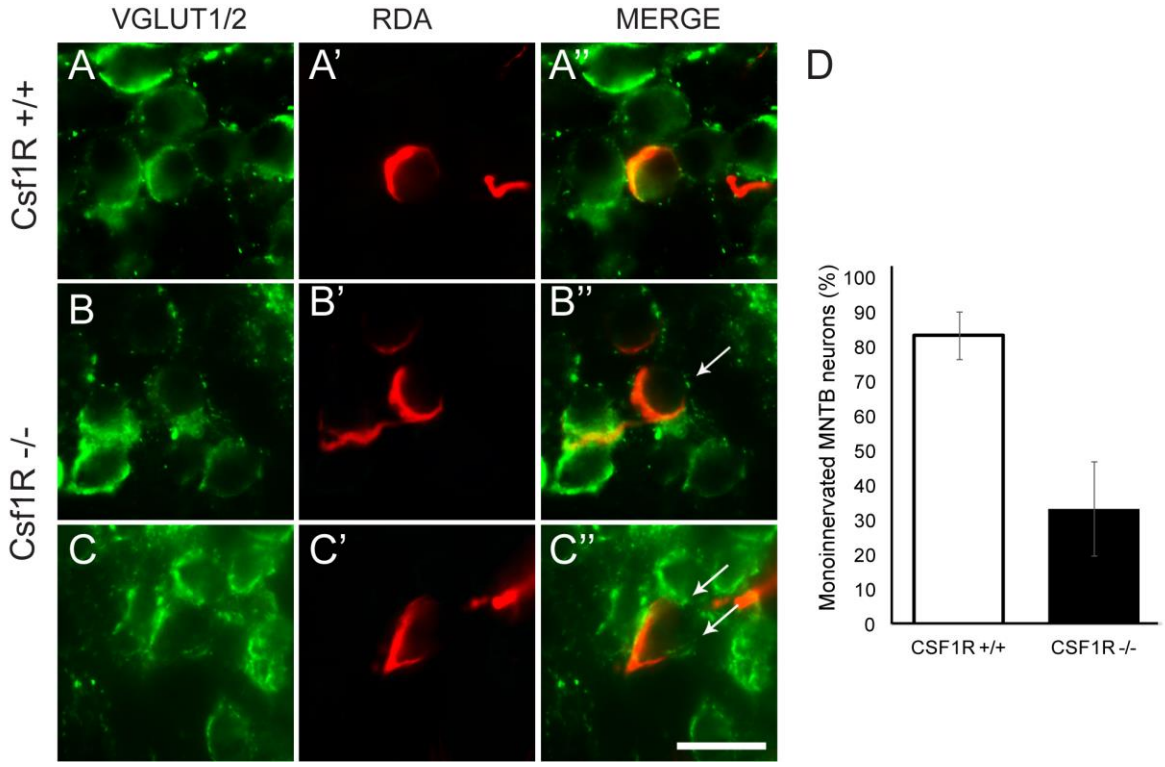


**Figure 3.7 *Csf1R*$^{-/-}$ mutant mice exhibit pruning deficits.** (A) Representative images from wildtype *Csf1R* mice of VGLUT expression (A and B); RDA-labeled calyces (A' and B'); and merged images (A" and B"). (B - C) VLUT expression, RDA labeled calyces (B', C"), and merged images (B", C") in *Csf1R*$^{-/-}$ mutant mice. White arrows denote areas immunolabeled for VGLUT that are do not coincide with calyx labeling. (D) *Csf1R1*$^{-/-}$ mice exhibited fewer pruned synapses compared to control mice ($p < 0.005$; n = 8 wildtype and 4 mutant), suggesting an impairment in pruning. Scale bar, 10 µm.

### 3.4.4 *High resolution imaging reveals decrease in synaptic VGLUT1/2 protein in Cx3cr1*$^{-/-}$ *mice*

After observing a reduction in size of both the calx and postsynaptic MNTB neuron, we then quantified the synaptic proteins in mutants compared to control mice using super resolution STORM imaging. The use of STORM imaging allows the advantage of measuring individual VGLUT molecules within a given calyx. We were able to acquire high magnification images of calyces of both the wildtype and mutant

mice (Figure 3.8A and B, respectively) in relation to the expression of VGLUT1/2 (Figure 3.8A' and B', respectively). We found that compared to the wildtype mice, *Cx3cr1*$^{-/-}$ mutants had significantly less VGLUT1/2 molecules within the calyx (Figure 3.8 B-B'). The control mice had 10463.80 ± 3798.78 VGLUT1/2 molecules, whereas mutant mice had 3079.41 ± 631.32 (Figure 3.8, $p$=0.03, n = 4 wildtype and 4 mutants; Mann-Whitney rank sum test).

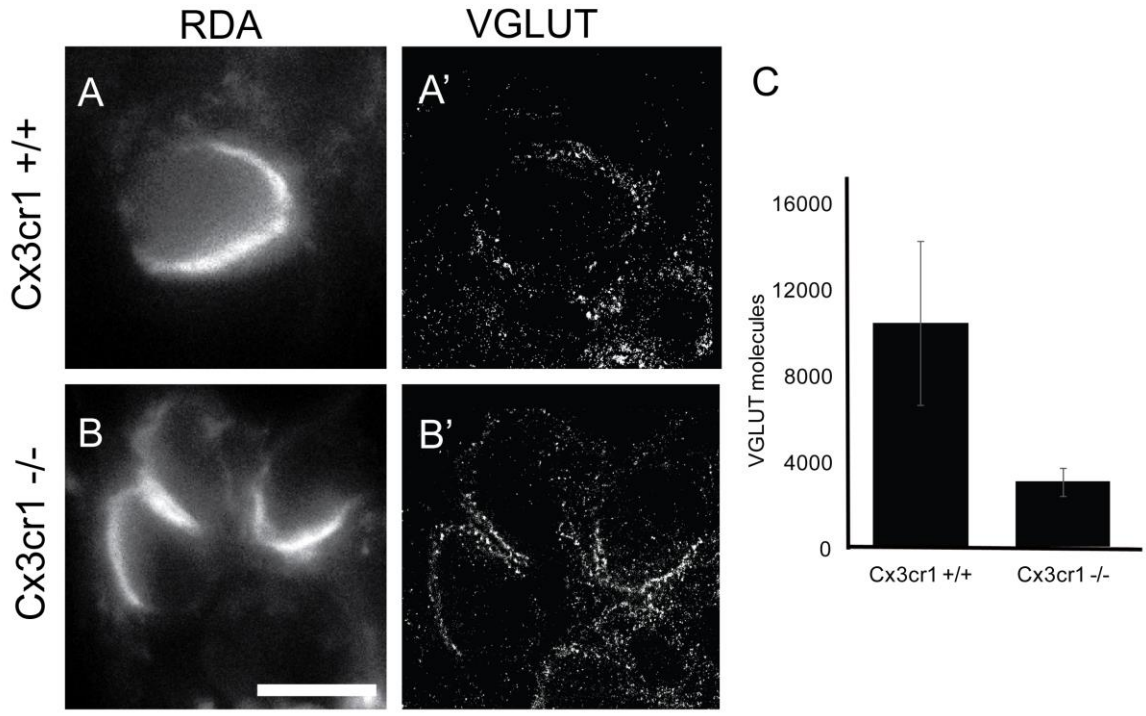


**Figure 3.8 STORM analysis of *Cx3cr1*$^{-/-}$ mice.** (A) represents RDA labeled calyx from wildtype mouse with VGLUT STORM imaging (A'). (B) represents RDA labelled calyces from *Cx3cr1*$^{-/-}$ mouse with VGLUT STORM imaging (B'). (C) Quantification of single VGLUT molecule activation between wildtype and *Cx3cr1*$^{-/-}$ show fewer VGLUT molecules within calyx in mutant mice ($p$=0.03; n = 4 wildtype and 4 mutants). Scale bar, 10 µm.

### 3.4.5 *LPS-induced microglial activation results in increased VGLUT1/2 levels*

While the previous experiments investigated effects on brainstem development using mutations with decreased microglial signaling and activity, we also explored synaptic changes associated with activation of microglia. Specifically, we used lipopolysaccharide (LPS) injections. We hypothesized that compared to controls, LPS injected animals would exhibit an increase in synaptic proteins, suggesting enhanced pruning (Figure 3.5). Compared to saline treated mice, LPS injected mice had significantly more IBA1-positive microglia (Figure 3.9A-B).

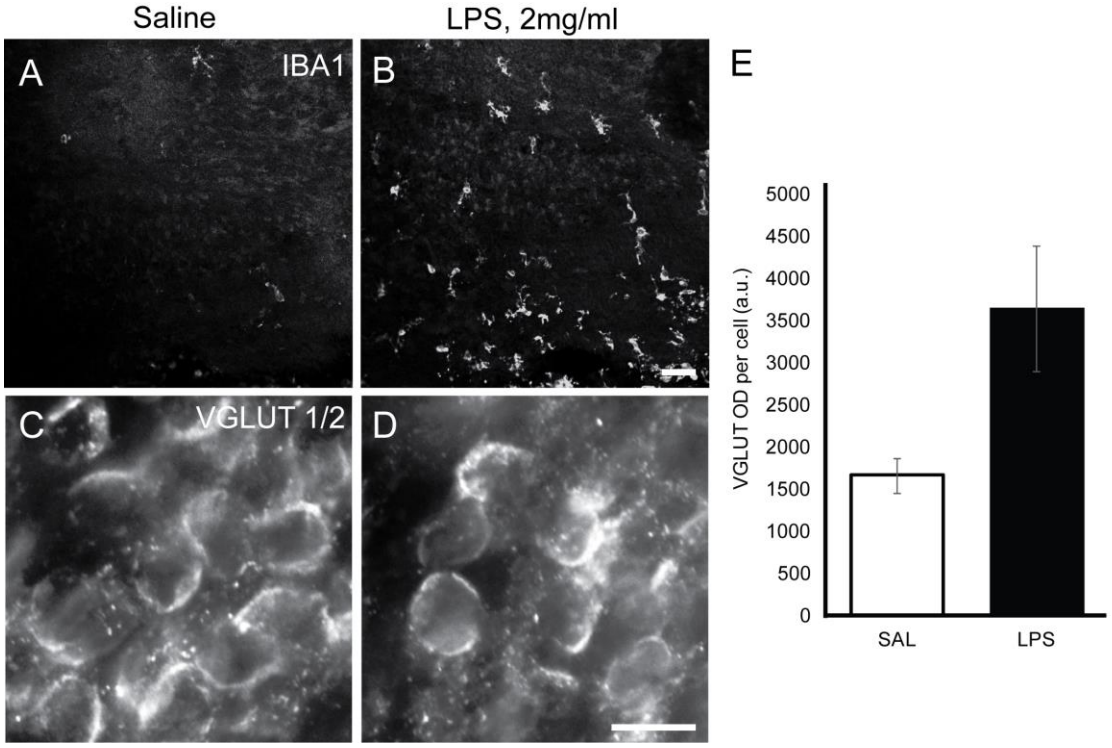


**Figure 3.9 LPS injected mice exhibit more microglia and increased VGLUT expression.** (A and B) represents IBA1 staining of microglial cells in LPS versus Saline injected mice. (C and D) shows VGLUT1/2 suggests an increase in VGLUT levels in LPS injected mice (quantifications in panel E) ($p$=0.06, n=3 wildtype and 3 mutants). Scale bar represents 100 µm in panel (B) and 50 µm in panel (D).

Following LPS treatment, brainstems were collected and immunolabelled with VGLUT1/2 (Figure 3.9C-D). We found that compared to their control, saline injected littermates, mice injected with saline had an increased VGLUT1/2 expression (Figure 3.9, $p$=0.06, student t-test). Whereas LPS injected mice had 3639.20±748.84 optical density, their saline injected cohort had 1657.80±210.68 (n = 3 wildtype and 3 mutants).

## 3.5 DISCUSSION

### 3.5.1 *Decreased presynaptic and postsynaptic targets*

Our data investigated the microglial influences on VCN-MNTB development. Using both the fractalkine and Csf1R signaling pathways, we found that mutant mice had impaired calyx growth and decreased MNTB cell size compared to their control littermates. While previous work in the lab has shown the presence of IBA-1 positive microglia in the brainstem as early as postnatal day 0 (P0), microglia appear in the cortex as early as E11.5 (Verney et al., 2010, Swinnen et al., 2013, Dinh et al., 2014). During this embryonic period, microglia may be poised to influence development of VCN axons that have already made weak contacts onto MNTB. In postnatal development however, microglia may provide critical information for determining the synaptic strength of the calyx, and in turn, influence the overall neural input onto MNTB neurons. In the cortex, microglia are important for mediating synaptic development of thalamocortical synapses (Hoshiko et al., 2012). In this study, impaired *Cx3cr1* signaling led to the reduced migration of microglia into the barrel cortex and as a result, a decrease in postsynaptic glutamate receptor expression (Hoshiko et al., 2012). In the hippocampus,

*Cx3cr1*$^{-/-}$ mice exhibited decreased excitatory postsynaptic potentials (EPSPs), further demonstrating the role of microglia in synapse maturation (Paolicelli et al., 2011). Despite the neural region, it seems that microglial signaling is important for mediating synaptic maturation. In order to determine if the microglia are important for promoting synaptic maturation, we could look at in adult mice to determine if the smaller calyces actually develop into a mature, fully fenestrated structure. If microglia determine calyceal maturation, then impaired microglial signaling would result in poor synaptic maturation of the calyx. Preliminary work in the lab has shown that adult *Cx3cr1*$^{-/-}$ mice have a delay in auditory brainstem responses (unpublished work from S. Rotschafer).

While we observed synaptic deficits in our *Cx3cr1*$^{-/-}$ and *Csf1R*$^{-/-}$ mutant mice, we did not investigate any influences microglia may have on other glial cells, such as astrocytes. As part of the quad-partite synapse (presynaptic, postsynaptic, astrocyte and microglial cell), microglia can work alongside astrocytes to mediate excitatory neurotransmission. Specifically, microglia can secrete adenosine triphosphate (ATP) to bind onto the astrocytic purinergic receptor, P2Y1R, which in turn leads to astrocytic release of glutamate to upregulate mGLUR expression (Pascual et al., 2012). As astrocytic populations such as ALDH1L1 or S100β are expressed as early as P0, microglia and astrocytes may be communicating together in order to mediate maturation of the calyx (Dinh et al., 2014). In our studies, astrocytes are more closely positioned to the developing calyx than microglia. While we looked at ALDH1L1-positive cells within the Cx3cr1 wildtypes and mutant mice and observed no difference in expression pattern (Figure 3.10), deficient microglial signaling may result in astrocyte secretion of fewer

trophic molecules. Future work would look at the expression of glial secreted factors in the wildtype and microglial deficient mice.

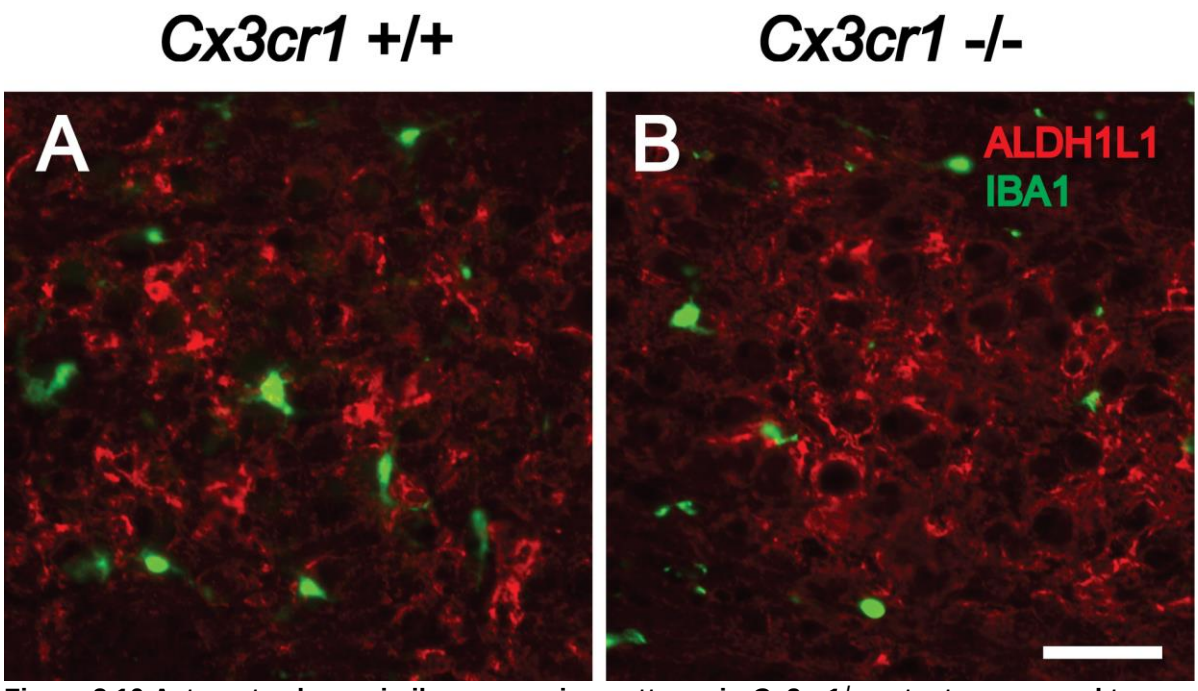


**Figure 3.10 Astrocytes have similar expression patterns in *Cx3cr1*$^{-/-}$ mutants compared to control mice.** (A) shows ALDH1L1 expression in wildtype mice, which is similar to expression pattern observed in *Cx3cr1*$^{-/-}$ mutants (B). Scale bar represents 20 µm.

In addition to ATP, microglia may secrete other trophic factors. In other systems microglial secretion of glutamate and chemokines such as interleukin-10 mediate synaptic transmission through upregulation of dendritic spines (Lim et al., 2013). Unlike cortical neurons, MNTB neurons are aspiny; however, microglia may be regulating other synaptic conditions such as calyx growth or levels of synaptic proteins. If microglia are secreting trophic growth molecules, then having a reduced number or lack of microglia such as seen in the *Cx3cr1* and *Csf1R* mutant mice would result in an overall decrease in synaptic growth factors, affecting presynaptic and postsynaptic targets (Erblich et al., 2011, Paolicelli et al., 2011). In the cortex for instance, *Cx3cr1* signaling mediates

neuronal survival, as mutant mice exhibited increased cell death in layer V neurons (Ueno et al., 2013). In our studies, we observed a decrease in MNTB cell size – as the first postnatal week of brainstem development consists of an increase in MNTB neurogenesis, an interesting follow up study would look at if *Cx3cr1*$^{-/-}$ mice exhibit neuronal loss in MNTB.

### 3.5.2 *Microglia mediate pruning the calyx of Held*

In our studies, we have demonstrated that deficits in fractalkine and *Csf1R* receptor signaling result in pruning deficits of the calyx of Held. Aside from fractalkine signaling, complement-dependent pathways have also been mediated in synaptic pruning (Paolicelli et al., 2011, Schafer et al., 2012). It has been shown that the microglia MerTK and P2Y6 receptors trigger microglia to phagocytose synaptic material (Koizumi et al., 2007, Caberoy et al., 2012).

Both mutant mouse lines have impairments in microglial signaling or number. If microglia are actively surveying the environment and making contacts onto several synapses, an impairment in microglia would result in fewer neurons receiving the appropriate signals to mature or prune. Previous work by Holcomb and colleagues have suggested the idea of glial cells as additionally controlling the boundary for calyx formation. In early development, calyces terminate onto open regions of MNTB that are uninhabited by glial cells (Holcomb et al., 2013). If microglia are necessary for determining boundaries for calyceal formation, then having impairments in this glial populations would result in more potential areas for calyces to terminate. Additionally,

the lack of growth factors being secreted by microglia would further promote an immature calyx phenotype.

### 3.5.3 *Impaired or enhanced microglial signaling*

Our results point to parallel functions between the fractalkine and *Csf1R* dependent signaling pathways. In particular, our results show that impaired microglial signaling and lack of microglia result in a similar immature developmental phenotype that results in smaller presynaptic and postsynaptic targets. When we compare overall calyx growth between both mutants, the *Csf1R*$^{-/-}$ mice seem to have smaller calyces. While both mutant mouse models are a form of impaired microglial signaling, it is important to note that only the *Csf1R*$^{-/-}$ mice completely lack microglia (Li et al., 2006, Erblich et al., 2011). In contrast, the *Cx3cr1*$^{-/-}$ mice impaired microglial signaling, but still show similar phenotypic deficits, albeit not as large (Paolicelli et al., 2011).

Interestingly, our study of microglial activation using LPS suggests an enhancement of glutamatergic innervation. Our data show a trend for an increase in overall VGLUT1/2 levels in the LPS injected mice compared to the control mice. In a state with activated microglia, these glial cells may be secreting trophic factors that either could directly influence their neural targets, or indirectly influence neurotransmission by working with another glial cell. Other neural regions have shown a potentiation in synaptic activity following LPS injection. For instance, in the CA1, LPS injections led to enhanced astrocytic release of glutamate (Pascual et al., 2012). A future study would look at if LPS injected mice have an enhanced rate of synaptic maturation, such as faster pruning and quicker calyx development. Additionally, we

could investigate whether LPS mediated effects on synapses are through microglia directly communicating with neurons, or if microglia affect neuronal function through other glial cells.

### 3.5.4 *Concluding remarks*

Collectively, our results point to an importance of microglial signaling in mediating several synaptic properties occurring during normal VCN-MNTB circuitry development. Our results show that *Cx3cr1* mutant mice exhibited immature calyx morphology, smaller MNTB cell size, and pruning deficits. The *Csf1R* mutant mice also had smaller calyces and pruning deficits. Additionally, our results suggest that microglia may be mediating synaptic development by regulating synaptic molecules such as VGLUT1/2 to the synapse.

## 3.6 ACKNOWLEDGEMENTS

I would like to thank Veronica Veksler and Thao Pham for their technical assistance with the tissue preparation, immunohistochemistry, and analysis. Additionally, I would like to thank Allison Haskell and Dr. Kim Green for their assistance with confocal imaging. Lastly, the STORM data would not be possible without the help of Dr. Ian Smith and Brett Settle, who assisted in STORM image acquisition and designing software to analyze VGLUT molecules, respectively.

## CHAPTER 4: Microglial contributions to lesion-induced plasticity

### 4.1 SUMMARY

A fundamental question in neuroscience is how synapses can be maintained and modified throughout life. Early development marks a unique time during which synapses are highly plastic and susceptible to extensive reorganization. In this study, we investigated the mechanisms that contribute to lesion-induced reorganization of synapses in the mammalian auditory brainstem. We focused on the pathway from the ventral cochlear nucleus (VCN) to the medial nucleus of the trapezoid body (MNTB), part of a brainstem circuit that contributes to sound localization. VCN axons project to contralateral MNTB where they terminate in a highly specialized synapse known as the calyx of Held. While the projection is normally strictly contralateral, it can branch and make additional ipsilateral terminations following early removal of the cochlea on the opposite side. As microglia have been shown to mediate synaptic plasticity in other neural circuits, we investigated if microglia could also contribute towards regulating synaptic induction within the brainstem. Our previous work investigated the distribution of glial cells following early (P2) unilateral cochlear removal. We found that following perturbation, astrocytic and microglial markers showed expression near the ectopic ipsilateral calyx. In this study, we used the *Cx3cr1*$^{-/-}$ mouse line in order to assess microglial contributions to synaptic plasticity. We observed that microglia were observed around the normal contralateral calyces as well as the lesion-induced ipsilateral calyces in both control and mutant mice. In addition, we found that compared to control mice, *Cx3cr1*$^{-/-}$ mutant mice had significantly fewer induced ipsilateral connections to the denervated MNTB compared to their littermate controls. These

studies show that microglia are localized near lesion-induced calyces, where they contribute to synapse formation following injury through Cx3cr1 mediated signaling.

## 4.2 INTRODUCTION

During development, synapses are dynamically established, modified, and strengthened. Large scale structural reorganization of connections in response to denervation is in some instances limited to a developmental time window, or critical period. An example of this type of plasticity is found in the mammalian auditory brainstem. Globular bushy cells from the ventral cochlear nucleus (VCN) project to the contralateral medial nucleus of the trapezoid body (MNTB). The VCN axon ending forms one of the largest synaptic terminations in the brain, the calyx of Held (Tolbert et al., 1982, Kuwabara et al., 1991). The calyx of Held is a highly reticulated structure, providing a single encapsulating input onto the MNTB neuron, and plays an integral role in sound localization (reviewed in (Borst and Soria van Hoeve, 2012). Whereas the calyx of Held normally terminates onto the contralateral MNTB neuron, the VCN-MNTB circuitry exhibits remarkable plasticity during development. After early postnatal unilateral cochlear removal, VCN cells on the lesioned side undergo cell death and in turn result in denervation of the contralateral MNTB. Axons from the VCN on the intact side rapidly branch and form a new, ipsilateral calyceal input in the MNTB denervated by the lesion (Moore and Kowalchuk, 1988, Hashisaki and Rubel, 1989, Kitzes et al., 1995, Russell and Moore, 1995, Mostafapour et al., 2000).

Previous work has looked at the role of several axon guidance molecules in determining the mechanism behind lesion-induced ipsilateral calyces (Hsieh et al., 2007, Nakamura et al., 2012, Nakamura and Cramer, 2013). An additional mechanism

involves glial cells. Astrocytes and microglia are found near developing calyces and may play a role in mediating communication between pre- and postsynaptic neurons during lesion-induced synaptogenesis (Dinh et al., 2014). Glial signaling pathways have been implicated in synaptic plasticity (reviewed in (Bacci et al., 1999, Allen and Barres, 2005, Schafer and Stevens, 2015)). The focus of this study was on microglia, immune responsive cells within the brain that rapidly survey the environment and are found in dynamic contact with synapses (Nimmerjahn et al., 2005).

Microglial cells are unique in their origin, as they derive from the yolk sac and migrate into the brain during development (Alliot et al., 1999). Microglia are implicated in several aspects of synapse development and refinement. For example, following cochlear perturbation, microglia become reactive and are localized near excitatory synapses within VCN (Campos Torres et al., 1999, Janz and Illing, 2014). Moreover, microglia are important for neuron survival, as mutations in the fractalkine – chemokine receptor signaling pathway have resulted in decreased survival of neurons (Ueno et al., 2013). In addition to a neuroprotective role, microglia survey the synaptic environment and are also responsible for removing damaged synapses (Kettenmann et al., 2013). Lastly, through either a complement-dependent or fractalkine-chemokine receptor mediated pathway, microglia are able to phagocytose synaptic material in development and mediate synaptic reorganization and overall connectivity (Schafer et al., 2012, Zhan et al., 2014).

In this study, we investigated whether lesion-induced VCN-MNTB synaptic reorganization is influenced by microglial cells. Our hypothesis was that microglial cells have similar roles in synapse development as in lesion-induced synaptic reorganization.

As described in Chapter 3, microglia promote synapse maturation and may contribute to refinement, which relies on activity-mediated competition (Holcomb et al., 2013). Lesion-induced calyx growth similarly requires assembly of synaptic proteins, elaboration of the synaptic termination, and cues arising from denervation. Specifically, we hypothesized that if microglia are important for mediating synaptic development, then these cells would be in communication with normal developing calyces as well as with ectopically induced calyces. Furthermore, if glial cells are important for controlling the number of newly formed calyces following lesion, then perturbing microglial signaling would result in a decreased number of new synapses formed. We first examined the presence of microglial cells in denervated versus intact MNTB seven days following cochlear removal. We found that microglial cells were observed in close proximity to the emerging ipsilateral calyces, similar to our developmental studies. We investigated whether microglial signaling was needed for synaptic plasticity following cochlear removal. We found that fractalkine receptor deficient mice (*Cx3cr1*$^{-/-}$) displayed fewer induced calyceal terminations than their littermate controls. Our data suggest that microglial cells play a critical role both in early postnatal plasticity of the mammalian auditory circuit.

## 4.3 MATERIALS AND METHODS

### 4.3.1 *Animals*

All procedures were approved by the University of California, Irvine Institutional Animal Care and Use Committee. To observe plasticity effects following impaired microglial signaling, we used the Cx3c chemokine receptor 1 (*Cx3cr1*) mutant mice on the *C57BL/6* from Jackson Laboratory. This strain has enhanced green fluorescent

protein (EGFP) inserted into exon 2, resulting in impaired communication between neurons and microglial cells, which are GFP-positive (Jung et al., 2000). *Cx3cr1*$^{-/-}$ mutant mice were compared to their littermate heterozygote controls (denoted as *Cx3cr1*$^{+/-}$).

Mice were perfused initially with 0.5% saline followed by 4% paraformaldehyde (PFA). The brainstem was extracted and fixed in 4% PFA for 2 hours at 4ºC and submerged in 30% sucrose in phosphate buffer saline (PBS; 137mM NaCl, 2.7mM KCl, 10mM $Na_2HPO_4$, and1.8mM $KH_2PO_4$) overnight. Samples were sectioned in the coronal plane at 18 µm thickness and thawed onto chrome-alum subbed slides.

### 4.3.2 *Cochlear removal*

Unilateral cochlear removal was performed at P2 using previously published methods (Hsieh and Cramer, 2006, Hsieh et al., 2007, Nakamura et al., 2012, Nakamura and Cramer, 2013, Dinh et al., 2014). Surgery was performed under a dissecting microscope using heat sterilized instruments (Germinator 500, Cell Point Scientific). Briefly, animals were anesthetized under hypothermic conditions and a small incision was made ventral to the pinna to expose the tympanic membrane. A sterilized glass pipette was used to aspirate the cochlea. After surgery, pups were placed on a heated pad to recover and were returned to their mother. Pups were allowed 7 days to recover prior to tissue collection. Pups were given a local analgesic (Flunixin, Western Medical Supply) at a dosage of 2.5mg/kg for two days including the day of surgery. For sham-operated animals, all procedures were performed except aspiration of the cochlea. Following perfusion, animals were used for neuroanatomical tracing of induced and normally developing calyces. The VCN was examined upon

careful dissection. Cochlea removal was ascertained when VCN on the lesioned side was less than half of the volume of the intact VCN.

### 4.3.3 *Neuroanatomical labeling*

Two methods were used to trace VCN axons projecting to MNTB. Rhodamine dextran amine (RDA; Invitrogen) served the purpose of visualizing expression of microglia in relation to calyces. The RDA (MW: 3000) dye injection solution included 6.35% RDA with 0.4% Triton-X100 in PBS. Brainstems were isolated and submerged in artificial cerebrospinal fluid (aCSF; 130mM NaCl, 3mM KCl, 1.2mM $KH_2PO_4$, 20mM $NaHCO_3$, 3mM HEPES, 10mM glucose, 2mM $CaCl_2$, 1.3mM $MgSO_4$ perfused with 95% $O_2$ and 5% $CO_2$). A pulled glass micropipette was filled with RDA and pulses of RDA were injected medial to the cochlear nucleus using a Picospritzer at 25 msec. The region surrounding the injection site was electroporated at a rate of 5 pulses per second (pps) at 40 volts (V) for 50 msec. The tissue was immersed in aCSF for 2 hours under continuous oxygenation to allow axonal transport of the dye, then fixed for two hours in 4% PFA, rinsed, and incubated in 30% sucrose overnight. Brainstem samples were placed in OCT solution in cryomolds and coronally sectioned on the cryostat (Leica) at 18 µm thickness. Samples were collected on chrome-alum subbed slides and used for histology purposes.

In another set of tracing experiments we used NeuroVue (PTI Research, Inc.), a lipophilic dye that can be used for bulk label of the majority of VCN axons, thus allowing quantification of ipsilateral and contralateral calyces following cochlear removal as previously reported (Fritzsch et al., 2005, Hsieh and Cramer, 2006, Hsieh et al., 2007, Nakamura et al., 2012, Nakamura and Cramer, 2013). A small piece of dye was placed

in the intact VCN (on the non-lesioned side) and brainstems were incubated in 4% PFA for 2 weeks in a 37ºC incubator. Samples were sectioned at 100 µm thickness on a Vibratome (Leica) and coverslipped with Glycergel (Dako).

### 4.3.4 *Imaging*

Fluorescent images were taken using a Zeiss Axioskop microscope, Axiocam camera, and Axiovision software. Confocal microscopy was used to capture high magnification images of microglial apposition in relation to the calyx. Images were adjusted for brightness and contrast accordingly using Adobe Photoshop and edited using Adobe Illustrator.

### 4.3.5 *Image Analysis*

In our initial studies, we calculated microglial density by counting the number of microglia in at least 3 randomly selected images per animal. Microglia were counted in MNTB, VCN and LSO brain regions in both *Cx3cr1*$^{+/+}$ and *Cx3cr1*$^{-/-}$ mice. Statistical comparisons in microglial density within different brainstem regions was performed using ANOVA analysis.

To determine if microglial signaling influences lesion-induced plasticity, we quantified the number of calyceal projections terminating onto the ipsilateral MNTB (ipsilateral to NeuroVue dye placement) or contralateral MNTB (contralateral to NeuroVue dye placement), as previously described (Fritzsch et al., 2005, Hsieh and Cramer, 2006). A ratio of total calyces from the ipsilateral side to the total calyces on the contralateral MNTB (I/C ratio) was used to normalize for variations in the numbers of labeled fibers. Values were then compared between *Cx3cr1*$^{-/-}$ mutant mice and *Cx3cr1*$^{+/-}$ littermate controls. Because the projection is normally contralateral, an I/C

ration close to zero signifies little or no lesion-induced plasticity. In contrast, larger numbers signify a greater extent of plasticity. Statistical comparisons across the cochlear removal groups were made using student t-tests using the SigmaStat software.

## 4.4 RESULTS

### 4.4.1 *Microglial density within brainstem nuclei in Cx3cr1 mice*

Aside from impaired microglial-neuronal communication, the *Cx3cr1*$^{-/-}$ mice also exhibit a decrease in microglial number within the hippocampus (Paolicelli et al., 2011). We first investigated microglia morphology and calculated microglial density within MNTB, VCN and LSO nuclei regions of the *Cx3cr1*$^{-/-}$ mice. We observed that microglia within the *Cx3cr1*$^{+/-}$ mice exhibited highly complex processes that radiated out from the cell body (Figure 4.1 A – B). In addition, microglia from the mutant mice also had highly ramified processes (Figure 4.1 C). We then quantified the number of microglia in these mice (Figure 4.1 D). In MNTB, the *Cx3cr1*$^{+/+}$ littermate controls had a mean of 20.09 ± 3.24 cells. The *Cx3cr1*$^{-/-}$ mice had a mean microglia number of 17.06 ± 3.24 cells and was not significantly different (Figure 4.1; $p = 0.15$, n = 3 controls and 17 mutants). We also measured microglial density within VCN and LSO and found no significant difference in microglial number when comparing littermate controls to mutant mice ($p$=0.75 and 0.34, respectively). Within VCN, while *Cx3cr1*$^{+/+}$ littermate controls had a mean microglial number of 24.03 ± 5.86 cells, the *Cx3cr1*$^{-/-}$ mice had a mean microglial number of 25.6 ± 8.05 cells. The microglial density in LSO from the *Cx3cr1*$^{+/+}$ littermate controls had a mean microglial number of 21.62 ± 2.86 cells. The *Cx3cr1*$^{-/-}$ mice had a mean LSO microglial number of 19.30 ± 3.92 cells (data not shown).

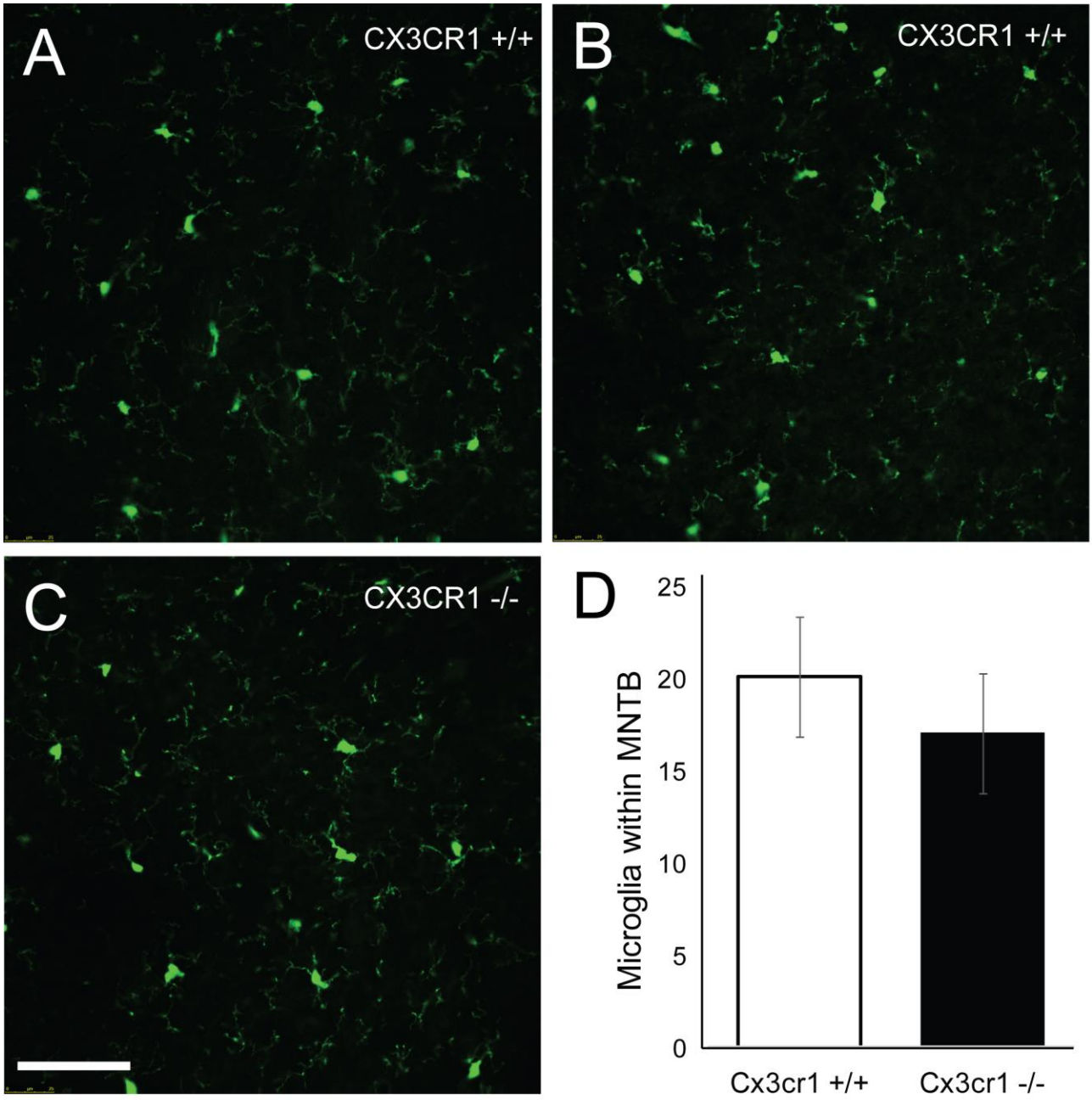


**Figure 4.1**. **Microglia morphology and density in the *Cx3cr1*$^{-/-}$ mice.** (A-B) Microglia within MNTB in wildtype mice exhibit complex processes. (C) In *Cx3cr1*$^{-/-}$ mice, microglia exhibit ramified, intricate processes. (D) Quantification of microglia within MNTB was not different between wildtype and mutant mice ($p$=0.9; n = 3 wildtype and 17 mutants). Scale bar = 50 µm.

### 4.4.2 *Microglia are found in apposition with lesion-induced calyces*

We then performed cochlear removal at P2 in *Cx3cr1*$^{+/-}$ and *Cx3cr1*$^{-/-}$ mice and examined the distribution of microglia in MNTB both ipsilateral and contralateral to the lesion. We found that in heterozygote control mice, microglia were apposed near the induced and normally developing calyces (Figure 4.2A – B). The *Cx3cr1*$^{-/-}$ mutant mice also had microglia nearby the ipsilateral and contralateral developing calyces (Figure 4.2 C – D).

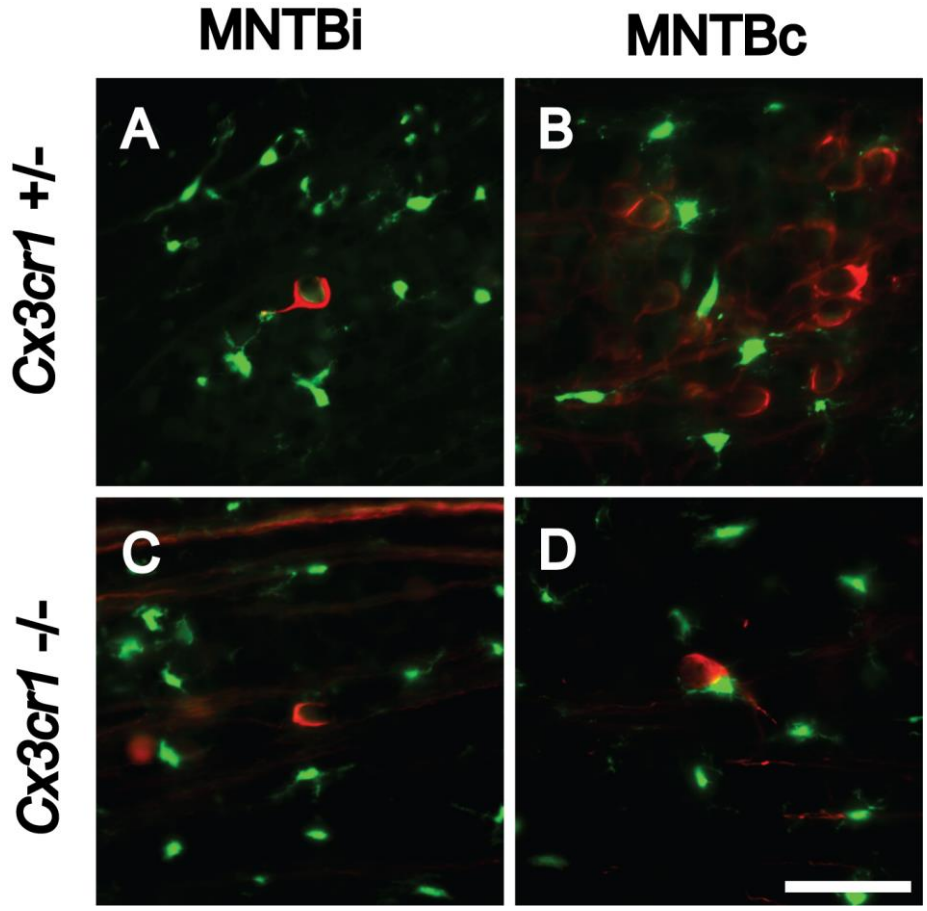


**Figure 4.2**. **Microglia are associated with contralateral and ipsilateral calyces.** (A – B) In heterozygote mice, microglia establish contacts onto ipsilaterally induced (A) and contralateral calyces (B). Like control mice, *Cx3cr1*$^{-/-}$ microglia are near ipsilateral calyces (C) and apposed near contralateral calyces (D). Scale bar = 50 µm

When we viewed the lesion-induced calyces arising from the intact VCN at a higher magnification, we were able to identify microglial processes in close proximity to the induced calyces (Figure 4.3). In the littermate controls, the microglial cells were in close proximity to the induced calyx (Figure 4.3A – C). These results were similar to our previous work showing microglial cells in close proximity to both normally developing and lesion-induced calyces (see Figure 2.10, (Dinh et al., 2014). While microglia were apposed near the induced calyces in heterozygotes, we also observed that the microglia from the *Cx3cr1*$^{-/-}$ mice also had microglial processes that contacted the calyx (Figure 4.3D, arrow).

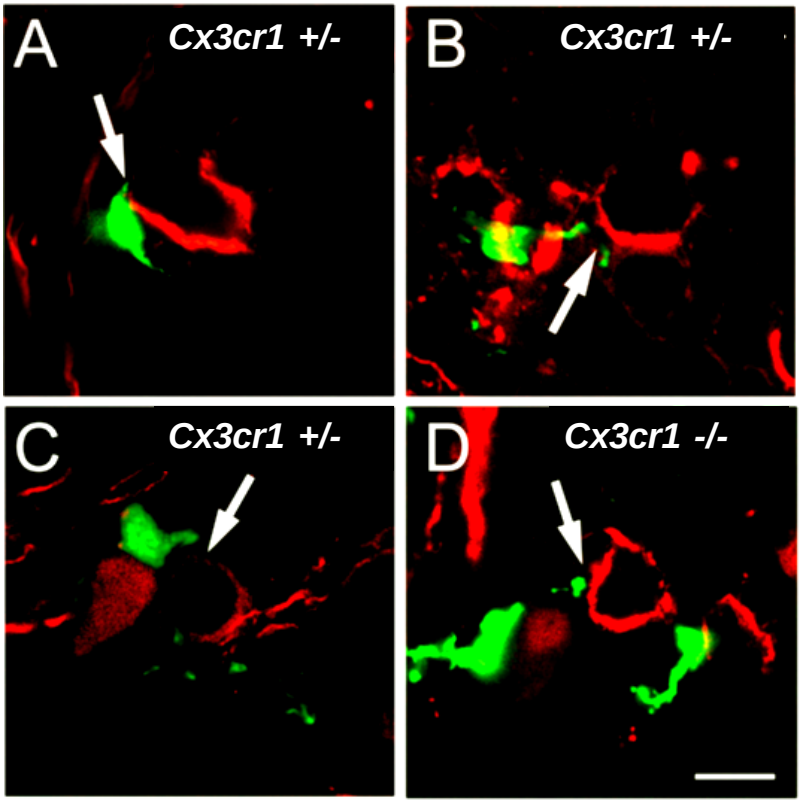


**Figure 4.3**. **Following cochlear removal, microglia are localized near ipsilaterally induced calyces.** (A – C) In *Cx3cr1*$^{+/-}$ control mice, microglia are directly apposed to newly formed calyces (indicated by white arrows). (D) *Cx3cr1*$^{-/-}$ microglia are also localized near induced calyces. Scale bar, 25 µm.

From our observations and previous work demonstrating the neuroprotective role of microglia, we investigated how impairments in the microglial-dependent *Cx3cr1* signaling pathway would affect synaptic plasticity. In normal development, many new calyces are formed from the ipsilateral, innervated VCN following unilateral cochlear removal (Figure 4.4, panels A and B; (Kitzes et al., 1995, Hsieh and Cramer, 2006).

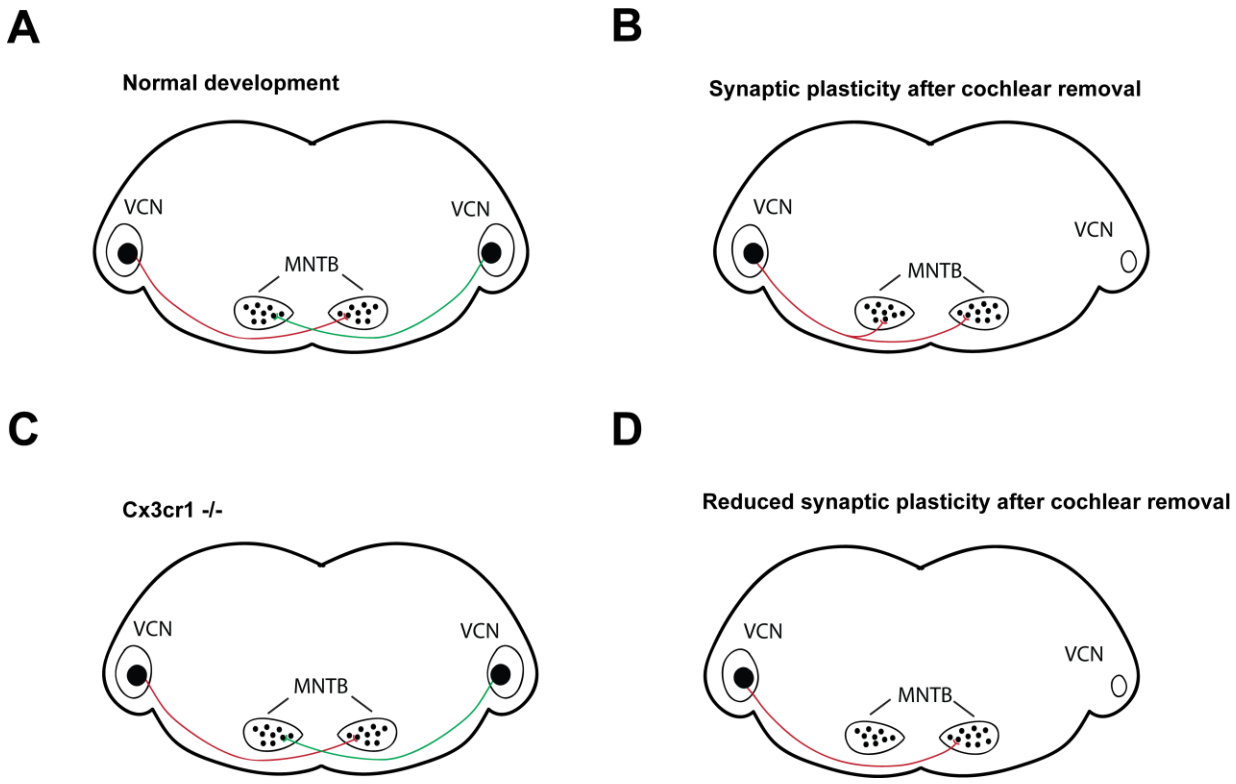


**Figure 4.4**. **Schematic depicting expected outcomes from unilateral cochlea removal experiments.** (A) In normal development, VCN axons terminate onto contralateral MNTB neurons and form the calyces of Held. (B) Following a unilateral cochlea removal, the denervated VCN (right side) loses neurons and decreases in size. New calyceal projections arise from the intact VCN (left side) forming ectopic calyces. We propose that the *Cx3cr1*$^{-/-}$ mice would have normal contralateral calyceal terminations during development (C), but exhibit reduced plasticity following unilateral cochlea removal. Mutant mice would have a reduced number of ipsilaterally induced calyces forming from the intact, innervated VCN (D).

In contrast, we hypothesized that impairments in microglial signaling would result in an overall decrease in plasticity, resulting in fewer ipsilateral calyces being formed following cochlea deafferentation (Figure 4.4, panels C and D).

### 4.4.3 *Decreased plasticity observed in Cx3cr1 mutant mice following cochlear removal*

To investigate if microglia are important for determining plasticity following cochlear removal, we counted calyceal terminations from the ipsilateral and contralateral MNTB. In order to normalize the amount of dye labeling, we calculated a ratio of the total number of calyces from the ipsilateral MNTB in comparison to the total number of calyces in the contralateral MNTB (I/C ratio). The mean I/C ratio of *Cx3cr1*$^{+/-}$ was 0.35 ± 0.04 (n = 5; Figure 4.5A-B). The *Cx3cr1*$^{+/-}$ mice mean total ipsilateral and contralateral calyces labelled was 22.4 ± 3.42 and 70 ± 13.52, respectively. In contrast, the mean I/C ratio for *Cx3cr1*$^{-/-}$ mutant mice was significantly less with a value of 0.14 ± 0.02 (n = 4; $p < 0.005$, Student's *t*-test; Figure 4.5C-F). The mean total ipsilateral and contralateral calyces labelled for the *Cx3cr1*$^{-/-}$ was 17.75 ± 3.5 and 130.5 ± 23.68, respectively.

## 4.5 DISCUSSION

### 4.5.1 *Cx3cr1*$^{-/-}$ *microglia localization near ipsilateral calyces after cochlear lesion*

To investigate potential mechanisms that promote novel synaptogenesis in tissue denervated following a lesion, we focused on the impact of microglial cells on the VCN-MNTB pathway. Our studies used the *Cx3cr1* mouse line that has previously been

shown to have reduced microglia and impaired microglial signaling the hippocampal and cortical region of the brain (Paolicelli et al., 2011, Pagani et al., 2015).

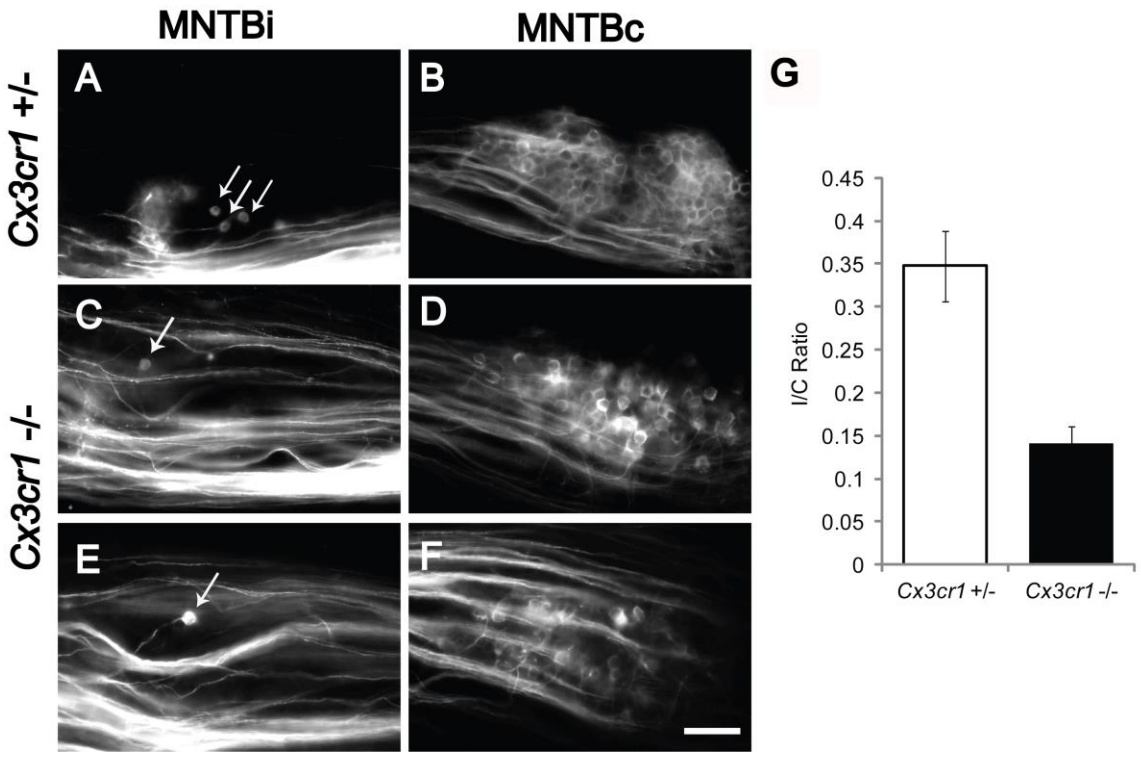


**Figure 4.5**. ***Cx3cr1*$^{-/-}$ mice exhibit reduced plasticity compared to littermate controls.** Cochlear removal was performed on *Cx3cr1r*$^{+/-}$ and *Cx3cr1*$^{-/-}$ mice. After a recovery of 7 days, calyces were labeled using NeuroVue dye to label induced calyces terminating in denervated MNTB (MNTBd shown in panel A, arrows indicate calyces), and normally developing calyces terminating in the innervated MNTB (MNTBi, panel B). Compared to their littermate controls, *Cx3cr1*$^{-/-}$ mice had significantly fewer induced calyces (panel C/E and D/F showing induced and normally developing calyces, respectively). Quantifications for the total number of calyces in the denervated compared to innervated MNTB is are shown in panel G ($p < 0.005$). Scale bar, 50 µm.

Following unilateral cochlear removal, we observed that both control and mutant mice had microglial cells that were situated near the ipsilaterally induced calyces. While both the heterozygotes and mutant mice had microglia near the new synapses, it is possible that the impaired microglia-neuronal signaling in the mutant mice would hinder calyceal growth following cochlear removal. Electron microscopy work has shown that calyx formation during normal development occurs on regions of the MNTB neuron that

are uninhabited by glial cells (Holcomb et al., 2013). If the mutant microglia have impaired microglial-neuron communication, deficient signaling may result in a lack of growth or inhibition of calyceal formation at the ipsilateral MNTB. Furthermore, the *Cx3cr1*$^{-/-}$ microglia may be ineffective at promoting synapse growth. The *Cx3cr1*$^{-/-}$ mice may also have smaller points of contact on the calyx compared to littermate controls. As microglia are constantly surveying their environment for synaptic damage or clearing, having fewer points of microglial contact onto neurons would prevent synapses from becoming strengthened. Microglia can affect synapse formation through the secretion of neurotrophic factors (Parkhurst et al., 2013). It would be interesting to investigate if the actual number of contacts made by microglia was reduced in *Cx3cr1*$^{-/-}$ mice compared to controls.

### 4.5.2 *Reduced plasticity in Cx3cr1*$^{-/-}$ *mutant mice following cochlear lesion*

Our studies demonstrated a reduction in plasticity in the *Cx3cr1*$^{-/-}$ mice. Following cochlear removal, *Cx3cr1*$^{-/-}$ mice exhibited a smaller I/C ratio compared to littermate controls. Microglial involvement in synaptic plasticity has also been demonstrated in the visual system by acting through a purinergic receptor P2Y12 (Sipe et al., 2016). Our results investigated microglial mechanisms at a time when the critical period for synaptic plasticity is still open. Following cochlear ablation, ipsilateral calyces form within 24 hours (Kitzes et al., 1995). Ectopic calyceal formation following cochlear removal only occurs if lesions are done prior to postnatal day 10. In addition, synaptic plasticity decreases with age of cochlear removal with the number of ectopic calyces decreasing (P10, (Hsieh and Cramer, 2006)). In normal development however, microglia predominantly enter MNTB beginning at P6, a time when synapses are

becoming refined (see Figure 3.4). As microglia are more abundant at a time period near the end of the critical period for lesion-induced reorganization, microglia may have dual roles in synapse formation during development, and synapse strengthening once normal calyces have developed. If this is the case, we would expect that impaired microglial signaling would result in weaker induced calyces formed after cochlear removal. A future study would look at if lesion-induced calyces are weaker in the mutant mice. In our studies, we looked at lesion-induced synapses 7 days after cochlear removal. If microglia are important for strengthening of synapses, then the number of ipsilaterally induced calyces formed initially after cochlear removal should be the same in both control mice and mutant mice. Additionally, it would be interesting to look at the stability of induced calyces and see if the *Cx3cr1*$^{-/-}$ induced calyces are stabilized enough to be maintained through adulthood.

### 4.5.3 *Potential microglial mechanism of lesion-induced plasticity*

Several studies have pointed to microglia as important for synaptic connectivity and wiring (Zhan et al., 2014). Microglial reactivity has been observed at VCN following cochlear ablation (Janz and Illing, 2014), but interestingly, we did not observe changes in microglial number in MNTB after cochlear lesion (Dinh et al., 2014). These data suggest that microglia play a role through their signaling pathways and not through modulating their numbers *per se*. Our finding of reduced lesion-induced plasticity in *Cx3cr1*$^{-/-}$ mice suggests that signaling from neurons to microglia through the *Cx3cr1* receptor provides one means of microglial response to changes in innervation. The downstream events effecting changes in plasticity are yet to be characterized.

One potential target of microglial signals is the formation of branching in contralaterally projecting VCN axons toward the ipsilateral MNTB targets. Several microglial mutants aside from the *Cx3cr1*$^{-/-}$ have reduced outgrowth of dopaminergic axons (Squarzoni et al., 2014). Additionally, microglia can act as "synaptic strippers" in clearing damaged or dysfunctional synapses (Kettenmann et al., 2013). During lesion-induced synaptic reorganization, microglia may be important for mediating synaptic clearance of degenerating axons originating from the denervated VCN. In the *Cx3cr1*$^{-/-}$ mutants however, impaired microglial signaling would result in a decrease in synaptic clearing, resulting in less area for new, ectopic calyces to form.

We have previously examined microglial influences on normal development of calyceal formation. In these studies, we found that *Cx3cr1*$^{-/-}$ and *Csf1R*$^{-/-}$ mice exhibit smaller calyx size and pruning deficits (Chapter 3). Our present results suggest a similar role for microglia in lesion-induced plasticity, a time when normal developing calyces have already been established. Collectively, our studies point microglia as being diverse with variable roles in synapse development and synapse maintenance.

### 4.5.4 *Concluding remarks*

This study aimed to identify how microglial mechanisms may coordinate proper brainstem circuitry during a lesion-induced plastic event. We used the *Cx3cr1* mutant mouse line in order to investigate microglial influences on lesion-induced synapse formation and found that deficient microglial signaling reduces the number of new calyces formed. These results point to a role for microglia in affecting synaptic plasticity.

**Acknowledgements**

We would like to thank A. Haskell and Dr. Kim Green for assistance with confocal imaging. We would also like to thank V. Veksler, K. Martinez, T. Phan, and H. Nguyen for their technical assistance.

## CHAPTER 5: SUMMARY AND CONCLUSIONS

A significant challenge in neuroscience is to understand how vast arrays of networks and synapses are correctly assembled and precisely wired. In development, synaptic formation relies on a myriad of molecular cues that can originate from neurons, glial cells, or other cues in the local environment. Understanding the processes that mediate synapse formation during normal development and in lesion-induced plasticity can uncover additional mechanisms underlying neurodevelopmental disorders and may suggest strategies for brain repair.

The focus of this dissertation has been to identify how synapses are properly wired and formed in the auditory brainstem, a region that enables an organism to determine a sound source. This well-characterized brainstem circuitry provides a unique model to study several parameters of synapse development, such as network connectivity, pruning, and strengthening. In this pathway, VCN axons terminate onto the contralateral MNTB principal neuron. Initially in development, several VCN axons terminate onto MNTB – these synapses actively compete until a dominant input remains and forms the Calyx of Held. The Calyx of Held is a highly reticulated, specialized termination that is one of the largest mammalian synapses (Spirou et al., 1990, Kuwabara et al., 1991, Kandler and Friauf, 1993, Kil et al., 1995, Holcomb et al., 2013). This dissertation focuses on the role of glial cells in the VCN-MNTB circuit.

Prior literature has suggested a growing importance for glial cells and their trophic secreted factors in the function and maintenance of synapses both in the developing systems, as well as in repair following injury. This dissertation provides evidence in support of a role for glial cells, in particular, microglia, as being important for

mediating several synaptic events such as pruning, calyx growth, and plasticity following injury. In addition, this dissertation offers support in the coordinated cross-talk between neurons and glial cells in assembling complex circuitry within the brainstem.

In Chapter 2, we first characterized glial development in the mammalian auditory brainstem and identified a spatiotemporal pattern of glial marker expression for astrocytes, oligodendrocytes, and microglia. We tested the hypothesis that if glial cells were important for mediating synapse formation in the brainstem, then different glial markers would be present within the VCN and MNTB region during periods of synaptic development. We found that two populations of astrocytes (protoplasmic and fibrous) emerge within the brainstem during birth in addition to following hearing onset. Microglial cells were also present in the brainstem at birth, with many microglial processes entering MNTB between P6 to P14. The microglia observed at P0 displayed an immature, amoeboid phenotype in comparison to microglia at the older developmental ages examined. At the time of hearing onset, for example, microglia displayed highly ramified, intricate processes that were interspersed throughout MNTB, potentially interacting with the developing calyces or postsynaptic neurons. Oligodendrocytes were present throughout the brainstem from all ages we surveyed. We performed axon tracing in order to visualize the calyx at different ages in addition to following unilateral cochlear removal. Astrocytic and microglial cells were observed in close apposition to the developing calyx, in addition to calyces that were induced following unilateral cochlear removal. Collectively, the expression data suggest that the close proximity of glial cells to the developing calyx can provide molecular cues necessary for calyceal growth in normal development in addition to lesion-induced

reorganization. The results from Chapter 2 served as the foundation for the subsequent experiments outlined in Chapters 3 and 4.

In our second study (Chapter 3), we investigated microglial influences on normal development of the VCN-MNTB circuitry, with a focus on calyx of Held development. During postnatal development, the calyx of Held undergoes synaptic refinement such that only one calyx innervates a single MNTB neuron (Holcomb et al., 2013). Our hypothesis that microglia are necessary for calyx maturation was supported by our findings that mutant mice with impairments in microglial function displayed an immature calyceal phenotype. Our results used both the *Cx3cr1*$^{-/-}$ and *Csf1R*$^{-/-}$ mutant mice in order to assess the effects of impaired microglial signaling and loss of microglia phenotype, respectively. These mice have several connectivity and pruning impairments in the hippocampus and other cortical regions (Erblich et al., 2011, Paolicelli et al., 2011, Squarzoni et al., 2014, Zhan et al., 2014). We found that the mutant mice exhibited a decreased calyx size, decreased postsynaptic MNTB cell size, and pruning deficits. Upon further investigation, we performed high-resolution imaging in order to quantify synaptic proteins and found that *Cx3cr1*$^{-/-}$ mutants had a decrease in VGLUT1/2 levels compared to control. Interestingly, we performed LPS injections on wildtype mice and observed that microglial activation resulted in an increase in VGLUT1/2 levels, further supporting the idea that microglia mediate excitatory synapse formation by potentially regulating the number of synaptic proteins localized to the calyx. While we focused on excitatory synaptic proteins, an informative future study would be to investigate the role of microglial signaling in inhibitory synapse formation. MNTB provides glycinergic inhibition to the LSO and MSO region, which has a major influence

on the calculation of interaural level and timing differences, respectively. The mechanisms by which microglia influence synapse growth remain to be determined. Studies have pointed to microglial secretion of neurotrophic factors in addition to phagocytosis – future directions could entail parsing out the mechanisms using microarray analysis and high-resolution live-cell imaging, respectively.

An important issue regarding calyx phenotype in the microglial mutant mice is whether it leads to hearing or communication problems in adulthood. A future study would entail looking at adult mice and seeing if the developmental problems are still present, and if this synaptic deficit results in behavioral impairments in sound localization. Ongoing research in the laboratory is currently addressing these questions. Our results from Chapter 3 demonstrate the effects of impaired microglial signaling on calyceal development. Other glial populations, such as astrocytes, may also play a role. As we have shown ALDH1L1- and S100β- positive astrocytes to be localized to the developing calyx, microglia and astrocytes may be interacting together in order to construct and stabilize the calyx. Use of astrocyte- and microglial-specific double mutants would be helpful in determining the collective contributions of these two glial populations in brainstem development.

Collectively, our results from Chapter 2 and 3 offer a potential role for both microglia and astrocytes in mediating calyx formation (Figure 5.1). In early development, multiple inputs innervate a MNTB neuron – this age coincides with astrocyte-specific markers expressed within MNTB. During the first postnatal week, a dominant input innervates the MNTB neuron, and begins to mature. At this age, microglia were found within MNTB and could serve to secrete trophic factors supporting

growth of the calyx. After hearing onset, the calyx becomes a reticulated structure, with astrocytes found directly apposed to the calyx.

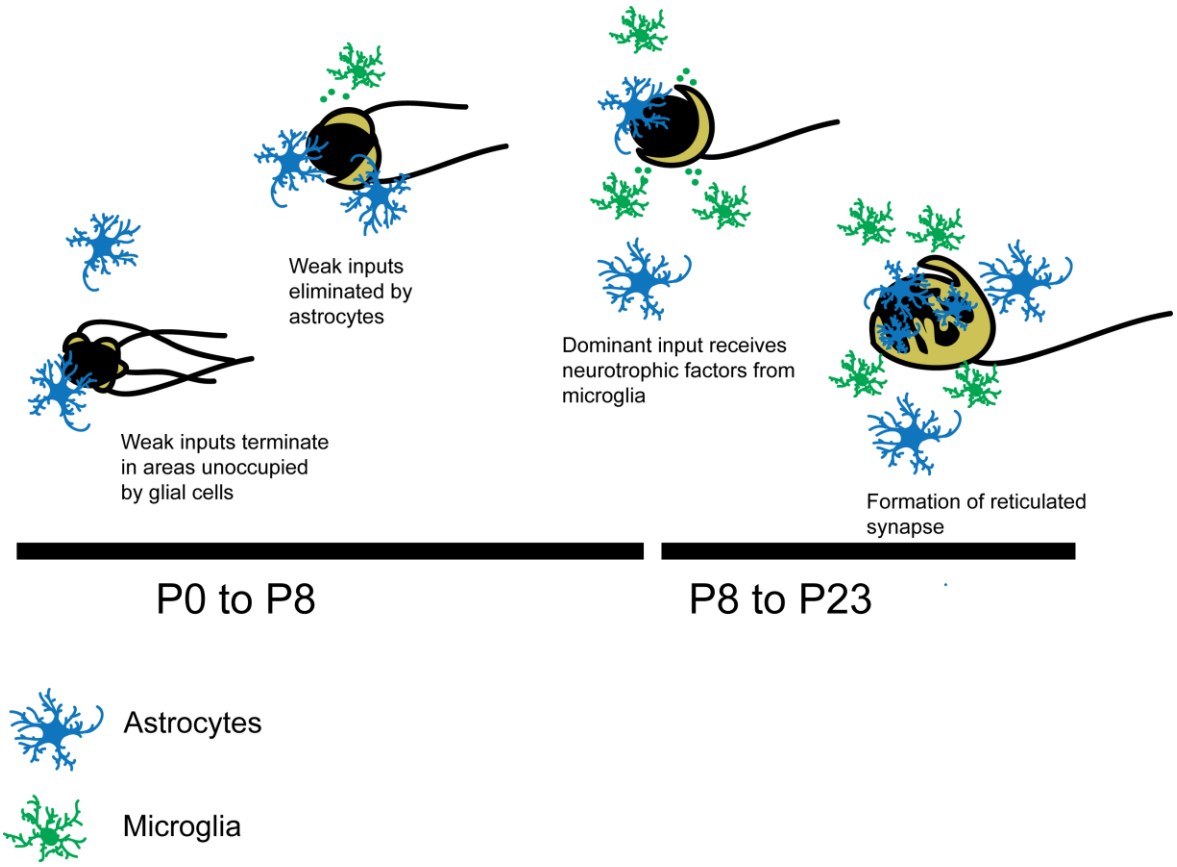


**Figure 5.1. Schematic depicting microglia and astrocyte role during calyx development.** During early development, astrocytes are present in MNTB at a time when multiple, immature calyceal inputs innervate a single MNTB neuron. By the first postnatal week, the weak inputs are eliminated and a dominant calyx innervates the MNTB neuron. Microglia may potentially promote calyx growth by secretion of trophic molecules. After hearing onset, the calyx becomes reticulated, with many processes innervating the MNTB neuron – areas on the MNTB neuron that are not occupied by the calyx have astrocytic processes.

Lastly, Chapter 4 investigated whether microglia contribute to synaptic plasticity following a lesion-induced reorganization event. Following cochlear removal, calyces from the intact VCN ectopically branch and terminate onto the denervated MNTB. We observed that microglia are apposed to both normally developing and lesion-induced

calyces in both control and mutant mice. Furthermore, the *Cx3cr1*$^{-/-}$ mutant mice had a decreased I/C ratio compared to their control littermates. It is important to note that several coordinated processes are occurring following a cochlear removal – there is cell death due to deafferentation, axonal degeneration, stabilization of normally developing calyces, and induction of new, ipsilateral calyces. While our data showed a decrease in plasticity, in the form of the total number of new calyces, it is unclear what role microglia may actually have in injury-induced plasticity. For instance, microglia may be phagocytosing damaged synaptic material or providing trophic support to signal new calyces to form (Figure 5.2). In the *Cx3cr1*$^{-/-}$ mutants however, impaired microglial signaling would result in a decrease in synaptic clearing, resulting in less area for new, ectopic calyces to form. One potential way to investigate this theory would be to image axons from the intact VCN and see if there is a change in the number of ipsilateral branches between mutant and control mice. If impaired microglial signaling prevents new calyces from forming after cochlear removal, then we would see the same number of ipsilateral branches occurring in both groups, but fewer calyces actually forming on the ipsilateral MNTB.

Alternatively, microglia may be regulating the critical period of lesion-induced reorganization. In Chapter 3, we observed that microglial activation by LPS resulted in an increase in VGLUT1/2 levels. If microglia serve to stabilize synapses by the assembly of synaptic proteins, then increasing microglia activity within the brain would serve to extend the critical period allowed for lesion-induced calyces to form, or allow the lesion-induced calyces to mature faster.

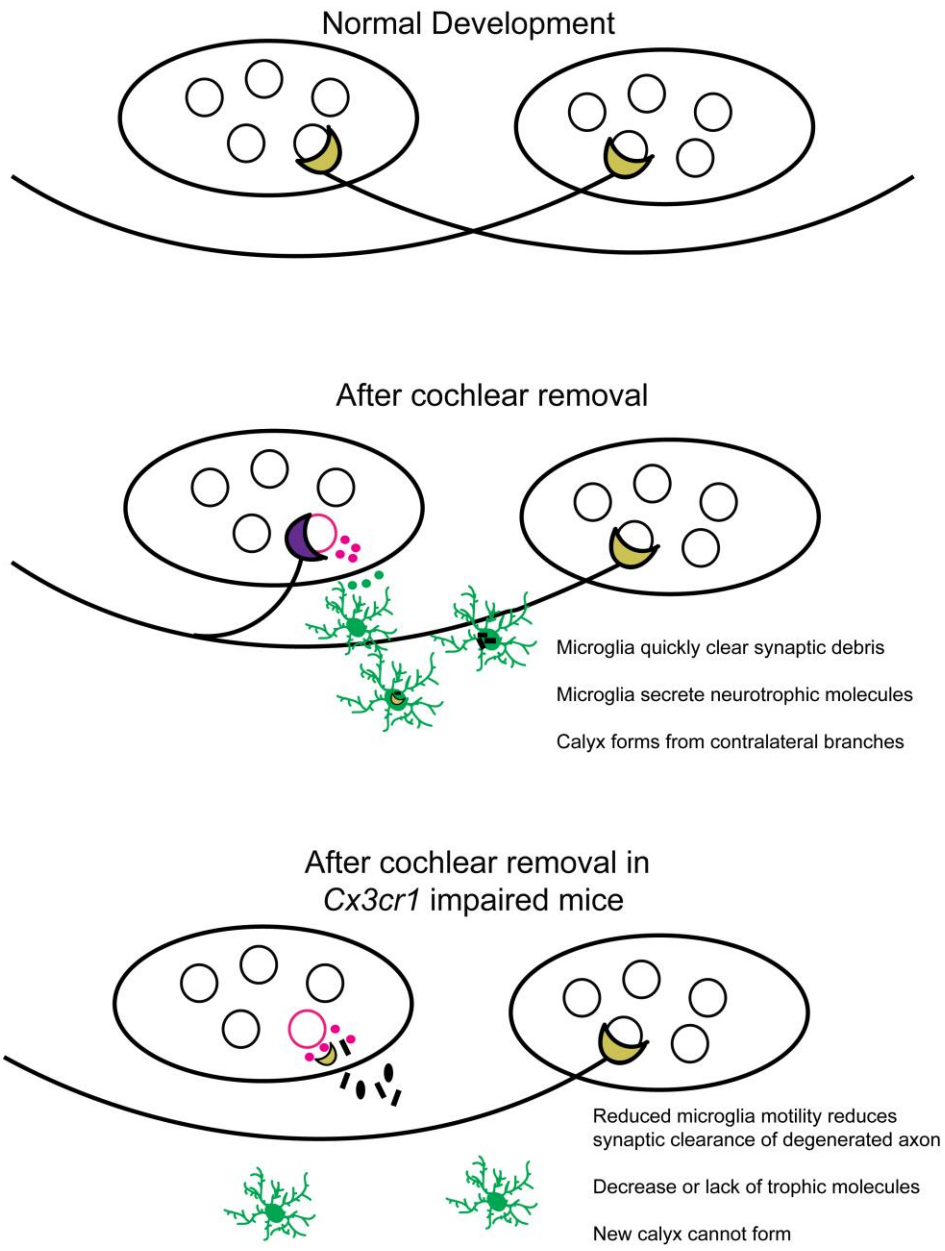


**Figure 5.2. Microglia may act to clear synaptic debris following cochlear removal.** (Top panel) In normal development, calyces terminate strictly onto contralateral MNTB neurons. (Middle panel) Following cochlear removal, neurons secrete molecules that signal for microglia to clear degenerating synaptic material. Microglia may also secrete trophic molecules that support new calyx formation from the ipsilateral target. (Bottom row) In the Cx3cr1$^{-/-}$ mice, microglia have reduced motility and may not clear synaptic debris as efficiently. In addition, lack of trophic molecules may prevent new calyx formation, leading to reduced plasticity.

## REFERENCES


Abdul-Latif ML, Salazar JA, Marshak S, Dinh ML, Cramer KS (2015) Ephrin-A2 and ephrin-A5 guide contralateral targeting but not topographic mapping of ventral cochlear nucleus axons. Neural development 10:27.

Allen NJ, Barres BA (2005) Signaling between glia and neurons: focus on synaptic plasticity. Curr Opin Neurobiol 15:542-548.

Allen NJ, Bennett ML, Foo LC, Wang GX, Chakraborty C, Smith SJ, Barres BA (2012) Astrocyte glypicans 4 and 6 promote formation of excitatory synapses via GluA1 AMPA receptors. Nature 486:410-414.

Alliot F, Godin I, Pessac B (1999) Microglia derive from progenitors, originating from the yolk sac, and which proliferate in the brain. Brain Res Dev Brain Res 117:145-152.

Ashida G, Carr CE (2011) Sound localization: Jeffress and beyond. Curr Opin Neurobiol 21:745-751.

Bacci A, Verderio C, Pravettoni E, Matteoli M (1999) The role of glial cells in synaptic function. Philos Trans R Soc Lond B Biol Sci 354:403-409.

Banks MI, Smith PH (1992) Intracellular recordings from neurobiotin-labeled cells in brain slices of the rat medial nucleus of the trapezoid body. The Journal of neuroscience : the official journal of the Society for Neuroscience 12:2819-2837.

Barres BA (2008) The mystery and magic of glia: a perspective on their roles in health and disease. Neuron 60:430-440.

Beattie EC, Stellwagen D, Morishita W, Bresnahan JC, Ha BK, Von Zastrow M, Beattie MS, Malenka RC (2002) Control of synaptic strength by glial TNFalpha. Science (New York, NY) 295:2282-2285.

Borst JG, Soria van Hoeve J (2012) The calyx of held synapse: from model synapse to auditory relay. Annu Rev Physiol 74:199-224.

Bushong EA, Martone ME, Jones YZ, Ellisman MH (2002) Protoplasmic astrocytes in CA1 stratum radiatum occupy separate anatomical domains. The Journal of neuroscience : the official journal of the Society for Neuroscience 22:183-192.

Caberoy NB, Alvarado G, Li W (2012) Tubby regulates microglial phagocytosis through MerTK. Journal of neuroimmunology 252:40-48.

Cahoy JD, Emery B, Kaushal A, Foo LC, Zamanian JL, Christopherson KS, Xing Y, Lubischer JL, Krieg PA, Krupenko SA, Thompson WJ, Barres BA (2008) A transcriptome database for astrocytes, neurons, and oligodendrocytes: a new resource for understanding brain development and function. The Journal of neuroscience : the official journal of the Society for Neuroscience 28:264-278.

Campos-Torres A, Touret M, Vidal PP, Barnum S, de Waele C (2005) The differential response of astrocytes within the vestibular and cochlear nuclei following unilateral labyrinthectomy or vestibular afferent activity blockade by transtympanic tetrodotoxin injection in the rat. Neuroscience 130:853-865.

Campos Torres A, Vidal PP, de Waele C (1999) Evidence for a microglial reaction within the vestibular and cochlear nuclei following inner ear lesion in the rat. Neuroscience 92:1475-1490.

Cant NB (1984) The fine structure of the lateral superior olivary nucleus of the cat. The Journal of comparative neurology 227:63-77.

Christopherson KS, Ullian EM, Stokes CC, Mullowney CE, Hell JW, Agah A, Lawler J, Mosher DF, Bornstein P, Barres BA (2005) Thrombospondins are astrocyte-secreted proteins that promote CNS synaptogenesis. Cell 120:421-433.

Chung WS, Barres BA (2012) The role of glial cells in synapse elimination. Curr Opin Neurobiol 22:438-445.

Chung WS, Clarke LE, Wang GX, Stafford BK, Sher A, Chakraborty C, Joung J, Foo LC, Thompson A, Chen C, Smith SJ, Barres BA (2013) Astrocytes mediate synapse elimination through MEGF10 and MERTK pathways. Nature 504:394-400.

Dalmau I, Finsen B, Tonder N, Zimmer J, Gonzalez B, Castellano B (1997) Development of microglia in the prenatal rat hippocampus. The Journal of comparative neurology 377:70-84.

Dalmau I, Finsen B, Zimmer J, Gonzalez B, Castellano B (1998) Development of microglia in the postnatal rat hippocampus. Hippocampus 8:458-474.

de Waele C, Campos Torres A, Josset P, Vidal PP (1996) Evidence for reactive astrocytes in rat vestibular and cochlear nuclei following unilateral inner ear lesion. Eur J Neurosci 8:2006-2018.

Delassalle A, Zalc B, Lachapelle F, Raoul M, Collier P, Jacque C (1981) Regional distribution of myelin basic protein in the central nervous system of quaking, jimpy, and normal mice during development and aging. Journal of neuroscience research 6:303-313.

Delpech JC, Saucisse N, Parkes SL, Lacabanne C, Aubert A, Casenave F, Coutureau E, Sans N, Laye S, Ferreira G, Nadjar A (2015) Microglial activation enhances associative taste memory through purinergic modulation of glutamatergic neurotransmission. The Journal of neuroscience : the official journal of the Society for Neuroscience 35:3022-3033.

Dinh ML, Koppel SJ, Korn MJ, Cramer KS (2014) Distribution of glial cells in the auditory brainstem: normal development and effects of unilateral lesion. Neuroscience 278:237-252.

Elezgarai I, Bilbao A, Mateos JM, Azkue JJ, Benitez R, Osorio A, Diez J, Puente N, Donate-Oliver F, Grandes P (2001) Group II metabotropic glutamate receptors are differentially expressed in the medial nucleus of the trapezoid body in the developing and adult rat. Neuroscience 104:487-498.

Elmariah SB, Oh EJ, Hughes EG, Balice-Gordon RJ (2005) Astrocytes regulate inhibitory synapse formation via Trk-mediated modulation of postsynaptic GABAA receptors. The Journal of neuroscience : the official journal of the Society for Neuroscience 25:3638-3650.

Elmore MR, Najafi AR, Koike MA, Dagher NN, Spangenberg EE, Rice RA, Kitazawa M, Matusow B, Nguyen H, West BL, Green KN (2014) Colony-stimulating factor 1 receptor signaling is necessary for microglia viability, unmasking a microglia progenitor cell in the adult brain. Neuron 82:380-397.

Erblich B, Zhu L, Etgen AM, Dobrenis K, Pollard JW (2011) Absence of colony stimulation factor-1 receptor results in loss of microglia, disrupted brain development and olfactory deficits. PloS one 6:e26317.

Fekete DM, Rouiller EM, Liberman MC, Ryugo DK (1984) The central projections of intracellularly labeled auditory nerve fibers in cats. The Journal of comparative neurology 229:432-450.

Foran DR, Peterson AC (1992) Myelin acquisition in the central nervous system of the mouse revealed by an MBP-Lac Z transgene. The Journal of neuroscience : the official journal of the Society for Neuroscience 12:4890-4897.

Ford MC, Grothe B, Klug A (2009) Fenestration of the calyx of Held occurs sequentially along the tonotopic axis, is influenced by afferent activity, and facilitates glutamate clearance. The Journal of comparative neurology 514:92-106.

Freeman MR (2010) Specification and morphogenesis of astrocytes. Science (New York, NY) 330:774-778.

Friauf E, Ostwald J (1988) Divergent projections of physiologically characterized rat ventral cochlear nucleus neurons as shown by intra-axonal injection of horseradish peroxidase. Exp Brain Res 73:263-284.

Fritzsch B, Muirhead KA, Feng F, Gray BD, Ohlsson-Wilhelm BM (2005) Diffusion and imaging properties of three new lipophilic tracers, NeuroVue Maroon, NeuroVue Red and NeuroVue Green and their use for double and triple labeling of neuronal profile. Brain research bulletin 66:249-258.

Fuentes-Santamaria V, Alvarado JC, Juiz JM (2012) Long-term interaction between microglial cells and cochlear nucleus neurons after bilateral cochlear ablation. The Journal of comparative neurology 520:2974-2990.

Garcia O, Torres M, Helguera P, Coskun P, Busciglio J (2010) A role for thrombospondin-1 deficits in astrocyte-mediated spine and synaptic pathology in Down's syndrome. PloS one 5:e14200.

Ghandour MS, Vincendon G, Gombos G (1980) Astrocyte and oligodendrocyte distribution in adult rat cerebellum: an immunohistological study. J Neurocytol 9:637-646.

Grothe B, Pecka M, McAlpine D (2010) Mechanisms of sound localization in mammals. Physiological reviews 90:983-1012.

Hajos F, Kalman M (1989) Distribution of glial fibrillary acidic protein (GFAP)-immunoreactive astrocytes in the rat brain. II. Mesencephalon, rhombencephalon and spinal cord. Exp Brain Res 78:164-173.

Hakim Y, Yaniv SP, Schuldiner O (2014) Astrocytes play a key role in Drosophila mushroom body axon pruning. PloS one 9:e86178.

Halassa MM, Fellin T, Takano H, Dong JH, Haydon PG (2007) Synaptic islands defined by the territory of a single astrocyte. The Journal of neuroscience : the official journal of the Society for Neuroscience 27:6473-6477.

Hama H, Kurokawa H, Kawano H, Ando R, Shimogori T, Noda H, Fukami K, Sakaue-Sawano A, Miyawaki A (2011) Scale: a chemical approach for fluorescence imaging and reconstruction of transparent mouse brain. Nature neuroscience 14:1481-1488.

Hashisaki GT, Rubel EW (1989) Effects of unilateral cochlea removal on anteroventral cochlear nucleus neurons in developing gerbils. The Journal of comparative neurology 283:5-73.

Hirrlinger J, Hulsmann S, Kirchhoff F (2004) Astroglial processes show spontaneous motility at active synaptic terminals in situ. Eur J Neurosci 20:2235-2239.

Hoffpauir BK, Grimes JL, Mathers PH, Spirou GA (2006) Synaptogenesis of the calyx of Held: rapid onset of function and one-to-one morphological innervation. The Journal of neuroscience : the official journal of the Society for Neuroscience 26:5511-5523.

Holcomb PS, Hoffpauir BK, Hoyson MC, Jackson DR, Deerinck TJ, Marrs GS, Dehoff M, Wu J, Ellisman MH, Spirou GA (2013) Synaptic inputs compete during rapid formation of the calyx of Held: a new model system for neural development. The Journal of neuroscience : the official journal of the Society for Neuroscience 33:12954-12969.

Hoshiko M, Arnoux I, Avignone E, Yamamoto N, Audinat E (2012) Deficiency of the microglial receptor CX3CR1 impairs postnatal functional development of thalamocortical synapses in the barrel cortex. The Journal of neuroscience : the official journal of the Society for Neuroscience 32:15106-15111.

Howell DM, Morgan WJ, Jarjour AA, Spirou GA, Berrebi AS, Kennedy TE, Mathers PH (2007) Molecular guidance cues necessary for axon pathfinding from the ventral cochlear nucleus. The Journal of comparative neurology 504:533-549.

Hsieh CY, Cramer KS (2006) Deafferentation induces novel axonal projections in the auditory brainstem after hearing onset. The Journal of comparative neurology 497:589-599.

Hsieh CY, Hong CT, Cramer KS (2007) Deletion of EphA4 enhances deafferentation-induced ipsilateral sprouting in auditory brainstem projections. The Journal of comparative neurology 504:508-518.

Hsieh CY, Nakamura PA, Luk SO, Miko IJ, Henkemeyer M, Cramer KS (2010) Ephrin-B reverse signaling is required for formation of strictly contralateral auditory brainstem pathways. The Journal of neuroscience : the official journal of the Society for Neuroscience 30:9840-9849.

Hughes EG, Elmariah SB, Balice-Gordon RJ (2010) Astrocyte secreted proteins selectively increase hippocampal GABAergic axon length, branching, and synaptogenesis. Mol Cell Neurosci 43:136-145.

Jackson H, Parks TN (1982) Functional synapse elimination in the developing avian cochlear nucleus with simultaneous reduction in cochlear nerve axon branching. The Journal of neuroscience : the official journal of the Society for Neuroscience 2:1736-1743.

Janz P, Illing RB (2014) A role for microglial cells in reshaping neuronal circuitry of the adult rat auditory brainstem after its sensory deafferentation. Journal of neuroscience research 92:432-445.

Jung S, Aliberti J, Graemmel P, Sunshine MJ, Kreutzberg GW, Sher A, Littman DR (2000) Analysis of fractalkine receptor CX(3)CR1 function by targeted deletion and green fluorescent protein reporter gene insertion. Molecular and cellular biology 20:4106-4114.

Kandler K, Clause A, Noh J (2009) Tonotopic reorganization of developing auditory brainstem circuits. Nature neuroscience 12:711-717.

Kandler K, Friauf E (1993) Pre- and postnatal development of efferent connections of the cochlear nucleus in the rat. The Journal of comparative neurology 328:161-184.

Karimi-Abdolrezaee S, Billakanti R (2012) Reactive astrogliosis after spinal cord injury-beneficial and detrimental effects. Mol Neurobiol 46:251-264.

Kettenmann H, Hanisch UK, Noda M, Verkhratsky A (2011) Physiology of microglia. Physiological reviews 91:461-553.

Kettenmann H, Kirchhoff F, Verkhratsky A (2013) Microglia: new roles for the synaptic stripper. Neuron 77:10-18.

Kierdorf K, Erny D, Goldmann T, Sander V, Schulz C, Perdiguero EG, Wieghofer P, Heinrich A, Riemke P, Holscher C, Muller DN, Luckow B, Brocker T, Debowski K, Fritz G, Opdenakker G, Diefenbach A, Biber K, Heikenwalder M, Geissmann F, Rosenbauer F, Prinz M (2013) Microglia emerge from erythromyeloid precursors via Pu.1- and Irf8-dependent pathways. Nature neuroscience 16:273-280.

Kil J, Kageyama GH, Semple MN, Kitzes LM (1995) Development of ventral cochlear nucleus projections to the superior olivary complex in gerbil. The Journal of comparative neurology 353:317-340.

Kitzes LM, Kageyama GH, Semple MN, Kil J (1995) Development of ectopic projections from the ventral cochlear nucleus to the superior olivary complex induced by neonatal ablation of the contralateral cochlea. The Journal of comparative neurology 353:341-363.

Koizumi S, Shigemoto-Mogami Y, Nasu-Tada K, Shinozaki Y, Ohsawa K, Tsuda M, Joshi BV, Jacobson KA, Kohsaka S, Inoue K (2007) UDP acting at P2Y6 receptors is a mediator of microglial phagocytosis. Nature 446:1091-1095.

Korn MJ, Cramer KS (2008) Distribution of glial-associated proteins in the developing chick auditory brainstem. Dev Neurobiol 68:1093-1106.

Korn MJ, Koppel SJ, Cramer KS (2011) Astrocyte-secreted factors modulate a gradient of primary dendritic arbors in nucleus laminaris of the avian auditory brainstem. PloS one 6:e27383.

Korn MJ, Koppel SJ, Li LH, Mehta D, Mehta SB, Seidl AH, Cramer KS (2012) Astrocyte-secreted factors modulate the developmental distribution of inhibitory synapses in nucleus laminaris of the avian auditory brainstem. The Journal of comparative neurology 520:1262-1277.

Kucukdereli H, Allen NJ, Lee AT, Feng A, Ozlu MI, Conatser LM, Chakraborty C, Workman G, Weaver M, Sage EH, Barres BA, Eroglu C (2011) Control of excitatory CNS synaptogenesis by astrocyte-secreted proteins Hevin and SPARC. Proceedings of the National Academy of Sciences of the United States of America 108:E440-449.

Kuwabara N, DiCaprio RA, Zook JM (1991) Afferents to the medial nucleus of the trapezoid body and their collateral projections. The Journal of comparative neurology 314:684-706.

Kuwabara N, Zook JM (1991) Classification of the principal cells of the medial nucleus of the trapezoid body. The Journal of comparative neurology 314:707-720.

Lawson LJ, Perry VH, Dri P, Gordon S (1990) Heterogeneity in the distribution and morphology of microglia in the normal adult mouse brain. Neuroscience 39:151-170.

Leao RM, Kushmerick C, Pinaud R, Renden R, Li GL, Taschenberger H, Spirou G, Levinson SR, von Gersdorff H (2005) Presynaptic Na+ channels: locus, development, and recovery from inactivation at a high-fidelity synapse. The Journal of neuroscience : the official journal of the Society for Neuroscience 25:3724-3738.

Li J, Chen K, Zhu L, Pollard JW (2006) Conditional deletion of the colony stimulating factor-1 receptor (c-fms proto-oncogene) in mice. Genesis (New York, NY : 2000) 44:328-335.

Lim SH, Park E, You B, Jung Y, Park AR, Park SG, Lee JR (2013) Neuronal synapse formation induced by microglia and interleukin 10. PloS one 8:e81218.

Lurie DI, Rubel EW (1994) Astrocyte proliferation in the chick auditory brainstem following cochlea removal. The Journal of comparative neurology 346:276-288.

Maezawa I, Jin LW (2010) Rett syndrome microglia damage dendrites and synapses by the elevated release of glutamate. The Journal of neuroscience : the official journal of the Society for Neuroscience 30:5346-5356.

Maezawa I, Swanberg S, Harvey D, LaSalle JM, Jin LW (2009) Rett syndrome astrocytes are abnormal and spread MeCP2 deficiency through gap junctions. The Journal of neuroscience : the official journal of the Society for Neuroscience 29:5051-5061.

Mauch DH, Nagler K, Schumacher S, Goritz C, Muller EC, Otto A, Pfrieger FW (2001) CNS synaptogenesis promoted by glia-derived cholesterol. Science (New York, NY) 294:1354-1357.

Michalski N, Babai N, Renier N, Perkel DJ, Chedotal A, Schneggenburger R (2013) Robo3-driven axon midline crossing conditions functional maturation of a large commissural synapse. Neuron 78:855-868.

Mikaelian D, Alford BR, Ruben RJ (1965) Cochlear Potentials and 8 Nerve Action Potentials in Normal and Genetically Deaf Mice. Ann Otol Rhinol Laryngol 74:146-157.

Miller RH, Raff MC (1984) Fibrous and protoplasmic astrocytes are biochemically and developmentally distinct. The Journal of neuroscience : the official journal of the Society for Neuroscience 4:585-592.

Moore DR, Kowalchuk NE (1988) Auditory brainstem of the ferret: effects of unilateral cochlear lesions on cochlear nucleus volume and projections to the inferior colliculus. The Journal of comparative neurology 272:503-515.

Morest DK (1968) The growth of synaptic endings in the mammalian brain: a study of the calyces of the trapezoid body. Z Anat Entwicklungsgesch 127:201-220.

Mostafapour SP, Cochran SL, Del Puerto NM, Rubel EW (2000) Patterns of cell death in mouse anteroventral cochlear nucleus neurons after unilateral cochlea removal. The Journal of comparative neurology 426:561-571.

Muller CM (1992) Astrocytes in cat visual cortex studied by GFAP and S-100 immunocytochemistry during postnatal development. The Journal of comparative neurology 317:309-323.

Nakamura PA, Cramer KS (2011) Formation and maturation of the calyx of Held. Hear Res 276:70-78.

Nakamura PA, Cramer KS (2013) EphB2 signaling regulates lesion-induced axon sprouting but not critical period length in the postnatal auditory brainstem. Neural development 8:2.

Nakamura PA, Hsieh CY, Cramer KS (2012) EphB signaling regulates target innervation in the developing and deafferented auditory brainstem. Dev Neurobiol 72:1243-1255.

Nimmerjahn A, Kirchhoff F, Helmchen F (2005) Resting microglial cells are highly dynamic surveillants of brain parenchyma in vivo. Science (New York, NY) 308:1314-1318.

Pagani F, Paolicelli RC, Murana E, Cortese B, Di Angelantonio S, Zurolo E, Guiducci E, Ferreira TA, Garofalo S, Catalano M, D'Alessandro G, Porzia A, Peruzzi G, Mainiero F, Limatola C, Gross CT, Ragozzino D (2015) Defective microglial development in the hippocampus of Cx3cr1 deficient mice. Frontiers in cellular neuroscience 9:111.

Paolicelli RC, Bolasco G, Pagani F, Maggi L, Scianni M, Panzanelli P, Giustetto M, Ferreira TA, Guiducci E, Dumas L, Ragozzino D, Gross CT (2011) Synaptic pruning by microglia is necessary for normal brain development. Science (New York, NY) 333:1456-1458.

Parkhurst CN, Yang G, Ninan I, Savas JN, Yates JR, 3rd, Lafaille JJ, Hempstead BL, Littman DR, Gan WB (2013) Microglia promote learning-dependent synapse formation through brain-derived neurotrophic factor. Cell 155:1596-1609.

Pascual O, Ben Achour S, Rostaing P, Triller A, Bessis A (2012) Microglia activation triggers astrocyte-mediated modulation of excitatory neurotransmission. Proceedings of the National Academy of Sciences of the United States of America 109:E197-205.

Pfrieger FW, Barres BA (1997) Synaptic efficacy enhanced by glial cells in vitro. Science (New York, NY) 277:1684-1687.

Preissler J, Grosche A, Lede V, Le Duc D, Krugel K, Matyash V, Szulzewsky F, Kallendrusch S, Immig K, Kettenmann H, Bechmann I, Schoneberg T, Schulz A (2015) Altered microglial phagocytosis in GPR34-deficient mice. Glia 63:206-215.

Rappert A, Bechmann I, Pivneva T, Mahlo J, Biber K, Nolte C, Kovac AD, Gerard C, Boddeke HW, Nitsch R, Kettenmann H (2004) CXCR3-dependent microglial recruitment is essential for dendrite loss after brain lesion. The Journal of neuroscience : the official journal of the Society for Neuroscience 24:8500-8509.

Renden R, Taschenberger H, Puente N, Rusakov DA, Duvoisin R, Wang LY, Lehre KP, von Gersdorff H (2005) Glutamate transporter studies reveal the pruning of metabotropic glutamate receptors and absence of AMPA receptor desensitization at mature calyx of held synapses. The Journal of neuroscience : the official journal of the Society for Neuroscience 25:8482-8497.

Reyes-Haro D, Muller J, Boresch M, Pivneva T, Benedetti B, Scheller A, Nolte C, Kettenmann H (2010) Neuron-astrocyte interactions in the medial nucleus of the trapezoid body. J Gen Physiol 135:583-594.

Richardson WD, Kessaris N, Pringle N (2006) Oligodendrocyte wars. Nat Rev Neurosci 7:11-18.

Rodriguez-Contreras A, de Lange RP, Lucassen PJ, Borst JG (2006) Branching of calyceal afferents during postnatal development in the rat auditory brainstem. The Journal of comparative neurology 496:214-228.

Rodriguez-Contreras A, van Hoeve JS, Habets RL, Locher H, Borst JG (2008) Dynamic development of the calyx of Held synapse. Proceedings of the National Academy of Sciences of the United States of America 105:5603-5608.

Rubel EW, MacDonald GH (1992) Rapid growth of astrocytic processes in N. magnocellularis following cochlea removal. The Journal of comparative neurology 318:415-425.

Russell FA, Moore DR (1995) Afferent reorganisation within the superior olivary complex of the gerbil: development and induction by neonatal, unilateral cochlear removal. The Journal of comparative neurology 352:607-625.

Rust MJ, Bates M, Zhuang X (2006) Sub-diffraction-limit imaging by stochastic optical reconstruction microscopy (STORM). Nature methods 3:793-795.

Saliu A, Adise S, Xian S, Kudelska K, Rodriguez-Contreras A (2014) Natural and lesion-induced decrease in cell proliferation in the medial nucleus of the trapezoid body during hearing development. The Journal of comparative neurology 522:Spc1.

Saunders JC, Coles RB, Gates GR (1973) The development of auditory evoked responses in the cochlea and cochlear nuclei of the chick. Brain Res 63:59-74.

Schafer DP, Lehrman EK, Kautzman AG, Koyama R, Mardinly AR, Yamasaki R, Ransohoff RM, Greenberg ME, Barres BA, Stevens B (2012) Microglia sculpt postnatal neural circuits in an activity and complement-dependent manner. Neuron 74:691-705.

Schafer DP, Stevens B (2015) Microglia Function in Central Nervous System Development and Plasticity. Cold Spring Harbor perspectives in biology 7:a020545.

Sipe GO, Lowery RL, Tremblay ME, Kelly EA, Lamantia CE, Majewska AK (2016) Microglial P2Y12 is necessary for synaptic plasticity in mouse visual cortex. Nature communications 7:10905.

Smith PH, Joris PX, Yin TC (1998) Anatomy and physiology of principal cells of the medial nucleus of the trapezoid body (MNTB) of the cat. Journal of neurophysiology 79:3127-3142.

Spangler KM, Warr WB, Henkel CK (1985) The projections of principal cells of the medial nucleus of the trapezoid body in the cat. The Journal of comparative neurology 238:249-262.

Spirou GA, Brownell WE, Zidanic M (1990) Recordings from cat trapezoid body and HRP labeling of globular bushy cell axons. Journal of neurophysiology 63:1169-1190.

Squarzoni P, Oller G, Hoeffel G, Pont-Lezica L, Rostaing P, Low D, Bessis A, Ginhoux F, Garel S (2014) Microglia modulate wiring of the embryonic forebrain. Cell reports 8:1271-1279.

Stellwagen D, Malenka RC (2006) Synaptic scaling mediated by glial TNF-alpha. Nature 440:1054-1059.

Swinnen N, Smolders S, Avila A, Notelaers K, Paesen R, Ameloot M, Brone B, Legendre P, Rigo JM (2013) Complex invasion pattern of the cerebral cortex bymicroglial cells during development of the mouse embryo. Glia 61:150-163.

Takebayashi H, Yoshida S, Sugimori M, Kosako H, Kominami R, Nakafuku M, Nabeshima Y (2000) Dynamic expression of basic helix-loop-helix Olig family members: implication of Olig2 in neuron and oligodendrocyte differentiation and identification of a new member, Olig3. Mech Dev 99:143-148.

Taschenberger H, Leao RM, Rowland KC, Spirou GA, von Gersdorff H (2002) Optimizing synaptic architecture and efficiency for high-frequency transmission. Neuron 36:1127-1143.

Tolbert LP, Morest DK, Yurgelun-Todd DA (1982) The neuronal architecture of the anteroventral cochlear nucleus of the cat in the region of the cochlear nerve root: horseradish peroxidase labelling of identified cell types. Neuroscience 7:3031-3052.

Tremblay ME, Lowery RL, Majewska AK (2010) Microglial interactions with synapses are modulated by visual experience. PLoS Biol 8:e1000527.

Trune DR (1982) Influence of neonatal cochlear removal on the development of mouse cochlear nucleus: I. Number, size, and density of its neurons. The Journal of comparative neurology 209:409-424.

Ueno M, Fujita Y, Tanaka T, Nakamura Y, Kikuta J, Ishii M, Yamashita T (2013) Layer V cortical neurons require microglial support for survival during postnatal development. Nature neuroscience 16:543-551.

Ullian EM, Sapperstein SK, Christopherson KS, Barres BA (2001) Control of synapse number by glia. Science (New York, NY) 291:657-661.

Verney C, Monier A, Fallet-Bianco C, Gressens P (2010) Early microglial colonization of the human forebrain and possible involvement in periventricular white-matter injury of preterm infants. Journal of anatomy 217:436-448.

Wake H, Moorhouse AJ, Jinno S, Kohsaka S, Nabekura J (2009) Resting microglia directly monitor the functional state of synapses in vivo and determine the fate of ischemic terminals. The Journal of neuroscience : the official journal of the Society for Neuroscience 29:3974-3980.

Wake H, Moorhouse AJ, Miyamoto A, Nabekura J (2013) Microglia: actively surveying and shaping neuronal circuit structure and function. Trends Neurosci 36:209-217.

Xiao L, Michalski N, Kronander E, Gjoni E, Genoud C, Knott G, Schneggenburger R (2013) BMP signaling specifies the development of a large and fast CNS synapse. Nature neuroscience 16:856-864.

Young SR, Rubel EW (1986) Embryogenesis of arborization pattern and topography of individual axons in N. laminaris of the chicken brain stem. The Journal of comparative neurology 254:425-459.

Zhan Y, Paolicelli RC, Sforazzini F, Weinhard L, Bolasco G, Pagani F, Vyssotski AL, Bifone A, Gozzi A, Ragozzino D, Gross CT (2014) Deficient neuron-microglia signaling results in impaired functional brain connectivity and social behavior. Nature neuroscience 17:400-406.

Zhu YB, Gao W, Zhang Y, Jia F, Zhang HL, Liu YZ, Sun XF, Yin Y, Yin DM (2016) Astrocyte-derived phosphatidic acid promotes dendritic branching. Scientific reports 6:21096.

Ziegenfuss JS, Doherty J, Freeman MR (2012) Distinct molecular pathways mediate glial activation and engulfment of axonal debris after axotomy. Nature neuroscience 15:979-987.

Abdul-latif et al. Neural Development (2015) 10:27
DOI 10.1186/s13064-015-0054-6

Neural Development

RESEARCH ARTICLE Open Access

# Ephrin-A2 and ephrin-A5 guide contralateral targeting but not topographic mapping of ventral cochlear nucleus axons

Mariam L. Abdul-latif[1], Jesus A. Ayala Salazar[2], Sonya Marshak[2], Minhan L. Dinh[2] and Karina S. Cramer[2*]

## Abstract

**Background:** In the auditory brainstem, ventral cochlear nucleus (VCN) axons project to the contralateral, but not ipsilateral, medial nucleus of trapezoid body (MNTB), terminating in the calyx of Held. Dorsal VCN neurons, representing high frequencies, synapse with medial MNTB neurons, while low frequency-coding ventral VCN neurons synapse with lateral MNTB neurons, reflecting tonotopic organization. The mechanisms that ensure strictly contralateral targeting and topographic ordering are incompletely understood. Here we examined the roles of ephrin-A signaling in both types of targeting.

**Results:** Ephrin-A2 and ephrin-A5 are expressed in VCN cells during late embryonic and early postnatal development. At these ages ephrin-A2 is expressed in axons surrounding MNTB and ephrin-A5 is expressed in MNTB principal neurons. *Ephrin-A2/A5* double knockout mice displayed axon targeting errors in which VCN axons project to MNTB on both sides of the brainstem, where they terminate in calyceal endings. *Ephrin-A2* and *ephrin-A5* single knockout mice showed a similar phenotype. In contrast to effects on contralateral targeting, *ephrin-A2/A5* double knockout mice showed no defects in formation of tonotopically ordered projections from VCN to MNTB.

**Conclusions:** These findings demonstrate that distinct mechanisms regulate targeting of VCN axons to the contralateral MNTB and targeting to appropriate tonotopic locations. Ephrin-A signaling plays a similar role to ephrin-B signaling in the VCN-MNTB pathway, where both classes normally prevent formation of calyceal projections to ipsilateral MNTB. These classes may rely in part on common signaling pathways.

**Keywords:** Axon guidance, Medial nucleus of the trapezoid body (MNTB), Calyx of Held, Auditory, Brainstem, Tonotopy

## Background

Specialized neural circuits in the auditory brainstem underlie the computation of interaural time and intensity differences used in sound localization. In mammals, ventral cochlear nucleus (VCN) neurons receive input from central projections of spiral ganglion cells. VCN globular bushy cell axons cross the midline and terminate in the contralateral medial nucleus of the trapezoid body (MNTB) with large specialized endings known as calyces of Held [1]. MNTB neurons send inhibitory projections to ipsilateral LSO, where the balance of excitation and inhibition is used to determine interaural intensity differences. Central auditory pathways display tonotopic maps reflecting the ordered frequency selectivity of the sensory epithelium [2]. In VCN the dorsoventral axis represents high-to-low best frequencies. Neurons along this axis project topographically to the mediolateral axis of the contralateral MNTB. The VCN-MNTB projection to the appropriate side and tonotopic location reflects specificity that arises initially during axon outgrowth.

During development VCN axons initially reach the midline by embryonic day 13 (E13) and extend to the contralateral MNTB by E17 [3, 4]. The synaptic termination forms at postnatal day 0 (P0) and displays a calyceal morphology at P4-P5 [5–8]. The protracted and orderly growth of these axons reflects the coordinated activity of several families of axon guidance molecules.

* Correspondence: cramerk@uci.edu
[2]Department of Neurobiology and Behavior, University of California, Irvine, 2205 McGaugh Hall, Irvine, CA 92697-4550, USA
Full list of author information is available at the end of the article

Guidance cues include the Eph family proteins, which comprise the Eph receptor tyrosine kinases and their ephrin ligands. These cell surface proteins facilitate cell-cell interactions that play significant roles in axon guidance, cell migration, and other processes [2, 9–11]. This large family of proteins is subdivided into A and B classes based on sequence homology and binding affinity [12]. Ephrin-A ligands bind to EphA receptors and ephrin-B ligands bind to EphB receptors. Crosstalk between the classes emerges from exceptions to this specificity in that ephrin-B ligands bind to EphA4 and ephrin-A5 binds to EphB2 [12–14].

Studies in mutant mouse models have revealed roles for Eph proteins in establishing VCN-MNTB projections and tonotopy. VCN axon projections to MNTB are almost entirely contralateral in the auditory brainstem of wild type mice, but in *ephrin-B2*$^{lacZ/+}$ and *EphB2*$^{-/-}$;*EphB3*$^{-/-}$ mice, which have diminished EphB signaling, a significant number of ipsilateral calyceal projections to MNTB were found [8, 15]. Ipsilateral projections in these mice form at the same time as the normal contralateral projection and do not appear to be eliminated in later maturation. In spite of these significant numbers of aberrant ipsilateral projections, the majority of inputs to MNTB arise as branches from contralaterally projecting VCN axons. Evidence establishing a role for EphB proteins in central tonotopic map formation comes from a study in which mutant mice were exposed to pure tones and patterns of neuronal activation in the auditory brainstem nuclei were examined. Results suggest that ephrin-B2 is needed to form appropriately restricted tonotopic maps in the dorsal cochlear nucleus [16].

Auditory brainstem phenotypes associated with EphB mutations thus show significant effects but suggest that other molecules contribute to specificity in circuit formation. The goal of this study was to evaluate the contributions of EphA signaling. Ephrin-A2 and ephrin-A5 display graded expression levels in retinal axons, and mutations in Ephrin-A2 and ephrin-A5 have been shown to disrupt topographic ordering of projections in the developing visual system [17–20]. In the peripheral auditory system ephrin-A2 and ephrin-A5 are expressed in the cochlea where they regulate afferent axon targeting [21, 22]. Null mutations in *ephrin-A2* and *ephrin-A5* result in frequency-specific abnormalities in auditory brainstem responses that show central as well as peripheral effects [23]. Within the auditory brainstem, ephrin-A5 is expressed in the developing cochlear nucleus and MNTB neurons during embryonic and postnatal ages [8]. Here we examined the function of ephrin-A2 and ephrin-A5 in contralateral target specificity and topographic mapping of VCN projections to MNTB.

## Results

### Developmental expression patterns

#### *Ephrin-A2 expression*

We examined expression of ephrin-A2 in the auditory brainstem during the development of the VCN-MNTB pathway. At E17 ephrin-A2 immunolabeling showed patchy expression in MNTB at low levels, particularly in comparison to the regions surrounding MNTB (Fig. 1a). In VCN ephrin-A2 expression was seen diffusely throughout in a fibrous pattern that did not appear to correlate with cell bodies (Fig. 1b). Similar expression patterns were seen at P0 (Fig. 1c, d). At P4 this pattern continued, with greater expression in the region dorsal to MNTB (Fig. 1e) and similar expression in VCN (Fig. 1f). At P12 very little expression was seen in MNTB (Fig. 1g) and expression in VCN had diminished in comparison to younger ages (Fig. 1h).

#### *Ephrin-A5 expression*

Similar to results reported in CD-1/129 mice [8], ephrin-A5 expression was observed in C57BL/6 J mice within MNTB and VCN at E17, P0, and P4 (Fig. 2a-f). At E17 (Fig. 2a-b) and P0 (Fig. 2c-d) expression was sparse and diffuse. At P4, expression appeared most concentrated around cell bodies of MNTB (Fig. 2e). The morphology of labeled regions (Fig. 2e, inset) corresponds with either calyceal terminations on MNTB cells or with MNTB cell surfaces. Expression of ephrin-A5 in both nuclei at P12 was lighter compared to earlier ages.

### *Ephrin-A2* and *ephrin-A5* regulate axon targeting to contralateral MNTB

To evaluate the role of *ephrin-A2* and *ephrin-A5* in the formation of contralateral axon projections from VCN to MNTB, we performed neuroanatomical tracing in wild type mice and in mice with mutations in *ephrin-A2* and *ephrin-A5*. Lipophilic fluorescent dye was placed in the VCN on one side. After the dye was transported into the VCN axon projections, coronal sections were cut and calyceal terminations could be readily identified in MNTB. Brainstems with adequate label and at least 50 calyces were included in the analysis. The presence of calyces in MNTB both ipsilateral (MNTBi) and contralateral (MNTBc) to the dye placement was evaluated (Fig. 3a). In wild type mice, the majority of axonal terminations from VCN were found in MNTBc and few or no calyces were present in MNTBi (Fig. 3b,c). In brainstem sections of *ephrin-A2*/*ephrin-A5* double knockout (DKO) mice, we observed normal contralateral calyces (Fig. 3d), but in addition we found numerous aberrant ipsilateral projections (Fig. 3e), indicating significant errors in axon targeting. Projections from VCN to MNTBi terminated in a calyceal structure similar to that seen in the normal, contralateral projection. To evaluate

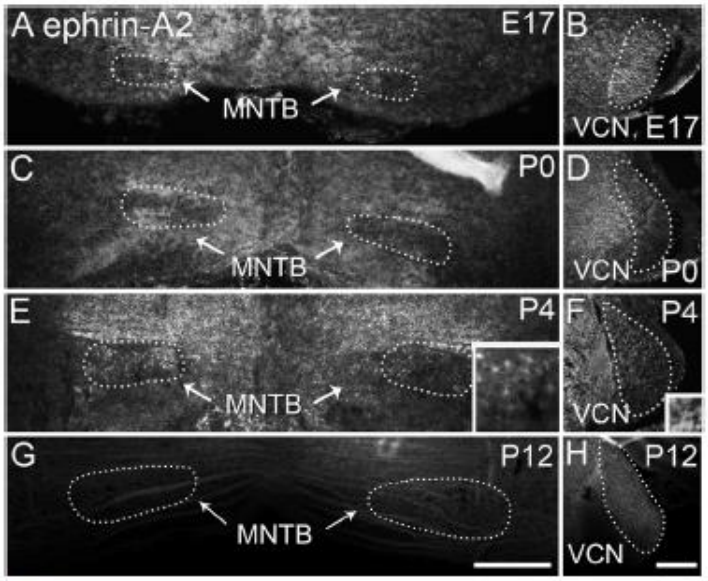


**Fig. 1** Ephrin-A2 expression in the developing auditory brainstem shown in coronal sections. **a** At E17 ephrin-A2 is expressed in regions surrounding MNTB, with relatively lighter, patchy label within MNTB. **b** At E17 light, fibrous expression of ephrin-A2 is seen throughout VCN. **c** At P0 expression is seen just outside MNTB with sparse expression inside the nucleus. **d** Expression remains in VCN. **e** At P4 expression outside MNTB has increased. Inset shows light label within MNTB. **f** Expression remains in VCN; inset shows fibrous label. **g** Expression of ephrin-A2 is greatly diminished in MNTB at P12. **h** At P12 ephrin-A2 expression is relatively decreased in VCN compared to earlier ages. Scale bar in G, 200 μm, applies to A, C, E, G. Scale bar in H, 200 μm, applies to B, D, F, H. Scale bar in insets, 20 μm

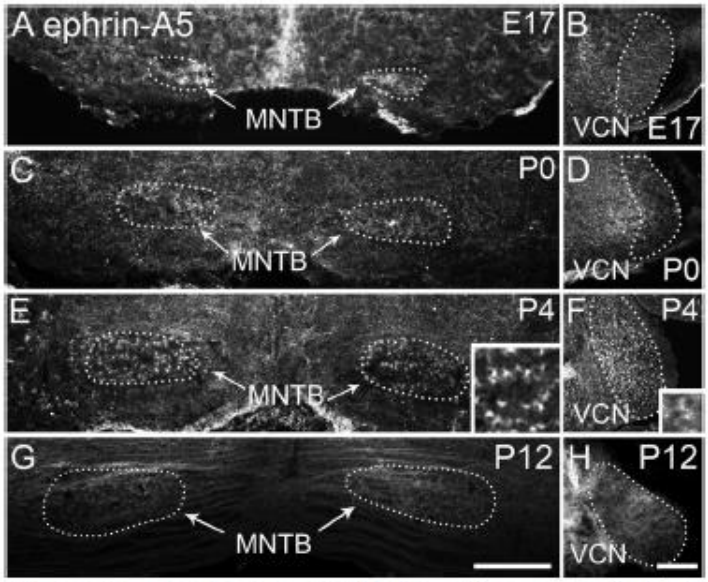


**Fig. 2** Ephrin-A5 expression in the developing auditory brainstem. **a** At E17 MNTB shows diffuse expression of ephrin-A5. **b** Low expression levels are seen in VCN at E17. **c** At P0 ephrin-A5 is expressed in MNTB. **d** VCN expression has slightly increased at P0. **e** At P4 ephrin-A5 surrounds cell bodies in MNTB (inset) and expression levels have increased. **f** Expression is seen throughout VCN with a diffuse pattern (inset). **g** By P12 immunolabeling shows little expression in MNTB. **h** VCN shows low expression levels at P12. Scale bar in G, 200 μm, applies to A, C, E, G. Scale bar in H, 200 μm, applies to B, D, F, H. Scale bar in insets, 20 μm

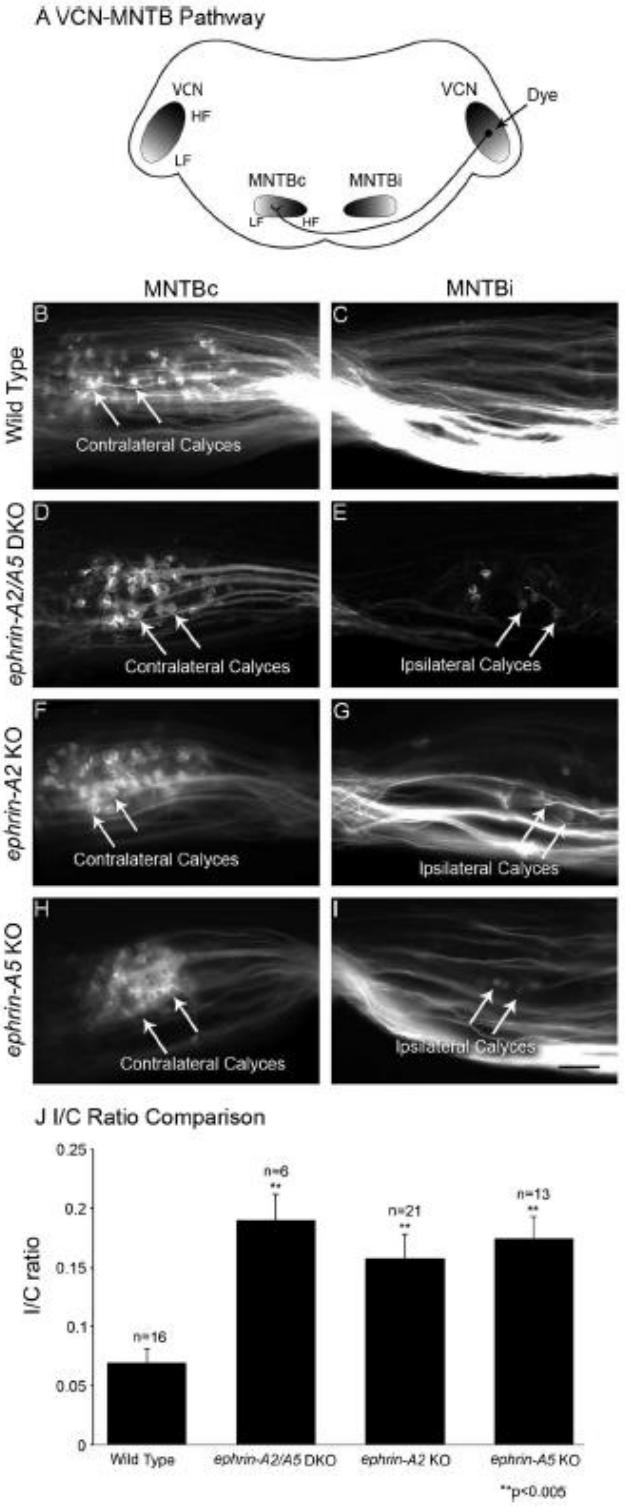


**Fig. 3** (See legend on next page.)

(See figure on previous page.)
**Fig. 3** Ephrin-A2 and ephrin-A5 regulate contralateral targeting of VCN axons. **a** Schematic diagram illustrating circuitry in the VCN pathway. Dye placement in VCN on one side normally results in labeled calyces in contralateral MNTB (MNTBc) but not in ipsilateral MNTB (MNTBi). **b** In wild type mice numerous calyces are labeled in MNTBc. **c** Labeled terminations were not formed in MNTBi in wild type mice. **d** In *ephrin-A2/A5* double knockout mice, VCN axons terminated in MNTBc. **e** In addition to the normal projection, *ephrin-A2/A5* double knockout mice also displayed numerous terminations in MNTBi, indicating significant errors in axon targeting. These projections ended in large terminations with morphology similar to the calyx of Held found in contralateral projections. **f, g** *Ephrin-A2* single knockout mice showed a similar phenotype to *ephrin-A2/A5* double knockout mice, with normal contralateral calyces as well as terminations in MNTBi. **h, i** Similarly, *Ephrin-A5* single knockout mice showed both contralateral and ipsilateral calyceal terminations. **j** To compare axon targeting errors between groups we used the ratio of calyces in MNTBi to MNTBc, the I/C ratio. Using ANOVA with *post hoc* analysis, we found a significant increase in I/C ratio for all three mutant mouse groups compared to wild type mice. I/C ratios for mutant mice did not differ significantly from each other. Scale bar in I indicates 100 μm for B-I

the function of each protein individually, mice with single null mutations in *ephrin-A2* and *ephrin-A5* were analyzed. Similar to the *ephrin-A2*/*ephrin-A5* DKO mice, *ephrin-A2* (Fig. 3f, g) and *ephrin-A5* (Fig. 3h, i) knockout (KO) mice both displayed mistargeting of VCN axons with calyces forming in MNTBi as well as in MNTBc.

To quantify the effects of mutations on axon targeting, we counted all the labeled calyces throughout MNTB on both sides of the brain and obtained a ratio of ipsilateral to contralateral calyces (I/C ratio) for each animal (Fig. 3j). For wild type mice ($n = 16$, mean total calyces labeled = 167 ± 56; s.e.m.) the mean I/C ratio was 0.069 ± 0.012, indicating that, as expected, the majority of inputs were seen on the contralateral side. For *ephrin-A2/A5* DKO mice ($n = 6$; mean total calyces labeled = 162 ± 81) the mean I/C ratio was 0.19 ± 0.021. For *ephrin-A2* KO mice ($n = 21$, mean total calyces labeled = 193 ± 97) the I/C ratio was 0.158 ± 0.019, and for *ephrin-A5* KO mice ($n = 13$, mean total calyces labeled = 191 ± 148) the I/C ratio was 0.175 ± 0.018 (Fig. 2j). The total number of calyces measured in each brainstem did not differ among groups (one-way ANOVA; $p = 0.82$). Values for I/C ratios were normally distributed. A one-way ANOVA with Tukey-Kramer *post-hoc* analysis was used to compare the I/C ratios. We found significant differences between the mean I/C ratio of wild type mice compared to *ephrin-A2/A5* DKO mice ($p < 0.004$); *ephrin-A2* KO mice ($p < 0.002$); and

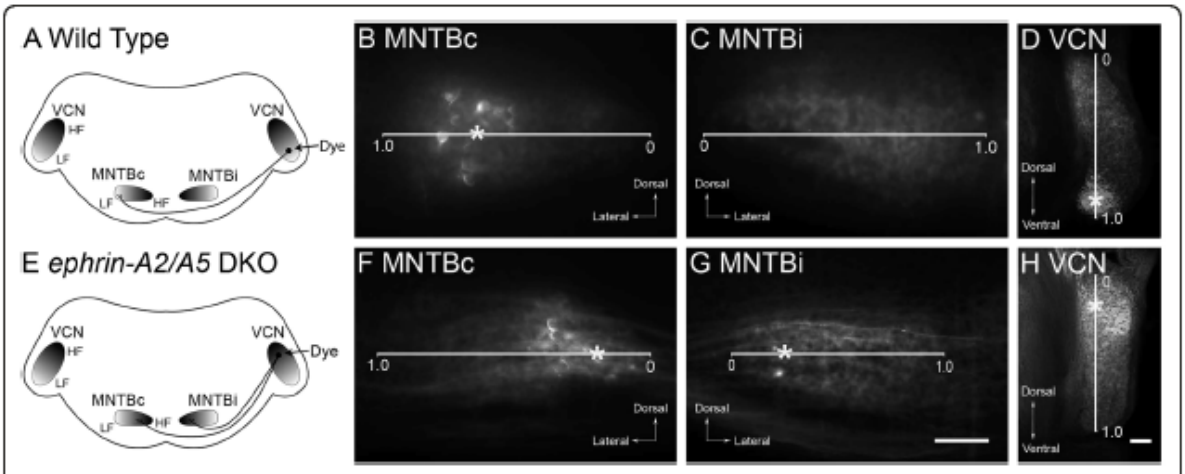


**Fig. 4** Topographic mapping in wild type and *ephrin-A2/A5* double knockout mice. **a** Schematic diagram showing the expected outcome of ventral dye placements in wild type mice, with labeled calyces seen in the lateral portion of the contralateral MNTB. **b** Labeled calyces in MNTBc after a ventral dye placement in VCN in a wild type animal. The normalized location of a calyx along the mediolateral axis is denoted with an asterisk; normalized positions were averaged to obtain values for each animal. As expected, the calyces are clustered in the lateral portion of MNTBc. **c** No calyces are seen in the MNTBi. **d** Section through the VCN of this animal shows the dye placement in the ventral region, with the center indicated (asterisk). **e** Schematic diagram depicting dye labeling in an *ephrin-A2/A5* double knockout mouse. Dorsal dye placement into the high frequency region of VCN results in labeled terminations in the medial regions of both MNTBc and MNTBi. **f** Labeled calyces in MNTBc after a dorsal dye placement in VCN in an *ephrin-A2/A5* double knockout mouse. Calyces appear clustered in the medial region. **g** Ipsilateral calyces are found in medial MNTB regions after dorsal dye placement in *ephrin-A2/A5* double knockout mice. **h** Section through the VCN of this animal shows the dye placement in the dorsal region, with the center indicated (asterisk). Scale bar in G indicates 100 μm for B, C, F, and G. Scale bar in H indicates 100 μm for D and H

*ephrin-A5* KO mice ($p < 0.001$). The I/C ratios did not differ significantly between any of the mutant mouse groups.

### *Ephrin-A2* and *ephrin-A5* mutations do not affect VCN-MNTB topography

We next tested the role of ephrin-A ligands in the formation of the topographic projection from the dorsoventral VCN axis to the mediolateral MNTB axis, which represent the frequency axes of these nuclei (Fig. 4a). As expected, small deposits of lipophilic dye in the dorsal or ventral VCN of wild type mice ($n = 16$) resulted in labeled calyces in the medial or lateral portion of the contralateral MNTB, respectively. A representative example of a ventral dye placement is shown in Fig. 4b-d.

Focal dye labeling experiments were similarly performed in *ephrin-A2/A5* DKO mice ($n = 7$) and the positions of labeled calyceal terminations in MNTB were evaluated as above. A representative example illustrating dye placement in the dorsal portion of VCN is shown in Fig. 4e-h. Calyceal labeling is seen in the medial portion of both the MNTBc (Fig. 4f) and MNTBi (Fig. 4g).

We used the normalized mean center of the dye placement in VCN across sections to assess the dorsoventral position of the labeled area for each animal. The mean normalized mediolateral position of calyces in MNTB was used as a measure of location of terminations for each animal. We found a strong positive linear correlation between VCN dye position and contralateral MNTB calyx position in wild type animals (regression line $y = 1.33x - 0.11$; $R^2 = 0.78$; Fig. 5a). A scatter plot of the mean dorsoventral VCN dye placement position and resulting mean mediolateral positions of calyces in MNTB showed a strong positive linear correlation for both the ipsilateral ($y = 1.63x - 0.22$; $R^2 = 0.75$) and contralateral ($y = 1.43x - 0.37$; $R^2 = 0.72$) MNTB (Fig. 5b). The slope and correlation coefficients for both MNTBc and MNTBi were similar to results seen in wild type mice, indicating that both ipsilateral and contralateral projections displayed topographic mapping in *ephrin-A2/A5* DKO mice.

We observed a slight lateral shift in the position of ipsilateral calyces compared to contralateral calyces labeled by the same VCN injections. In a two-tailed paired t-test for the comparing mean position of ipsilateral vs. contralateral calyces in *ephrin-A2/A5* DKO mice ($n = 7$), we obtained a p-value of 0.018, indicating that this lateral shift is statistically significant. Together, these observations suggest that *ephrin-A2/A5* DKO mice show normal topographic mapping to contralateral MNTB, and further suggest that aberrant ipsilateral VCN-MNTB projections in these mice follow topographic mapping cues with some differences compared to the contralateral projection.

## Discussion

The projection from VCN to MNTB is almost entirely contralateral, and this precision is disrupted when EphB signaling is inhibited. However, a significant proportion of the projection remains contralateral in mice with loss of EphB signaling [15], indicating that additional mechanisms ensure that VCN axons terminate contralaterally. Here we explored the potential function of EphA signaling. We determined the expression patterns of ephrin-A2 and ephrin-A5 and characterized axon targeting in VCN-MNTB projections of mice lacking one or both proteins. We explored both contralateral targeting and topographic mapping to determine the functions of these proteins.

We found that ephrin-A2 and ephrin-A5 are expressed in the brainstem during embryonic and early postnatal development. Ephrin-A2 is expressed in VCN, where the

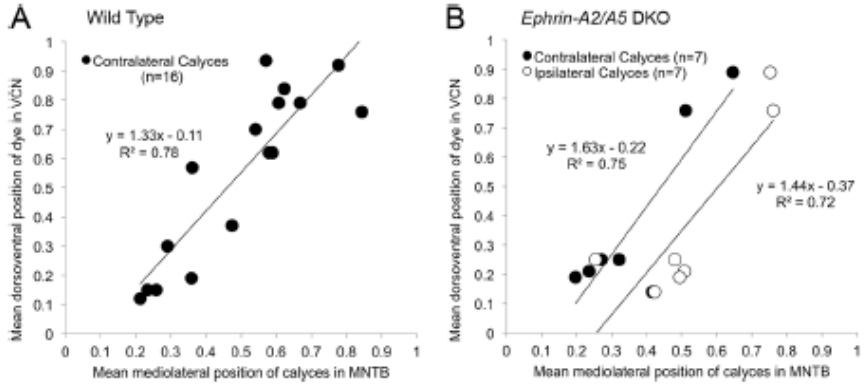


**Fig. 5** Topographic mapping is similar in wild type and *ephrin-A2/A5* double knockout mice. **a** Scatter plot assessing topography using wild type mice ($n = 16$) shows a strong positive correlation between dye position in VCN and mean normalized position of contralateral calyces, with dorsal VCN regions projecting to medial MNTB, and ventral VCN projecting to lateral MNTB. **b** Analysis of topographic mapping in *ephrin-A2/A5* double knockout mice ($n = 7$). The regression line and correlation coefficient is similar to results seen in wild type mice for projections to MNTBc as well as MNTBi. In these mice the ipsilateral calyces were significantly shifted laterally relative to the contralateral calyces

diffuse label is consistent with neuronal and/or glial labeling. It does not appear to be expressed within MNTB but rather in the fibers surrounding the nucleus. This protein may thus act early on VCN axons and may influence their growth *en route* to their targets in MNTB. Ephrin-A5 is expressed in both VCN and MNTB at P4. In MNTB the labeled region is seen around MNTB cells, a pattern consistent with labeling on the MNTB cell surface or in the calyx of Held. Ephrin-A5 immunolabeling is unlikely to represent glial cells given the fibrous morphology of glial markers in MNTB at early ages [24]. Null mutations in *ephrin-A2* and/or *ephrin-A5* both result in the formation of substantial ipsilateral VCN-MNTB projections in addition to the normal contralateral projection. Despite these similar phenotypes between *ephrin-A2* KO and *ephrin-A5* KO mice, the differing expression patterns suggest that ephrin-A2 and ephrin-A5 proteins act at different points in VCN axon growth. In contrast to these effects on contralateral axon targeting, the *ephrin-A2/A5* DKO mice showed normal topographic mapping from VCN to MNTB on both sides.

### Role of *ephrin-A2* and *ephrin-A5* in targeting to contralateral MNTB

Analysis of VCN projections in mutant mice revealed improper targeting to ipsilateral MNTB when *ephrin-A2* and/or *ephrin-A5* are deleted. This observation is similar to that previously reported for mice with reduced signaling through the ephrin-B signaling pathways. Quantitatively, the I/C ratio values are similar to those of *ephrin-B2*$^{lacZ}$ heterozygous mutations and *EphB2/B3* double mutants [15]. This similarity may arise from the two classes of ligands acting on common targets. Ligands are promiscuous within their own class but there is also a degree of crosstalk between classes, and the *EphB2* receptor can bind with *ephrin-A5* ligand [12–14]. Similar phenotypes in mice lacking *ephrin-A5* and *EphB2/B3* suggest that regulation of contralateral targeting relies in part on ephrin-A5-EphB2 binding.

While binding between ephrin-A2 and EphB receptors has not been demonstrated, the similarity in phenotypes in contralateral targeting of the VCN-MNTB pathway suggests that signaling through Eph proteins may converge on a common molecular pathway, possibly through other more complex molecular interactions [2, 25–28]. Additionally, distinct Eph proteins may act at different times, resulting in convergent effects of mutations. Eph proteins influence axon growth and branching at early stages and synaptogenesis at later stages. In the developing MNTB, numerous synapses are formed initially and excess synapses are eliminated during the first postnatal week [29]. It is unclear whether any of the early-eliminated synapses are ipsilateral, but by the time the protocalyx is visible the projection is already nearly entirely contralateral [15]. An interesting possibility is that Eph signaling influences the process of branching in the early MNTB and/or in subsequent synapse elimination. Further evidence for multiple points of regulation lie in the observation that in mutations affecting ephrin-B signaling, ipsilateral projections to MNTB arose either as branches from the contralateral projection of as direct projections from VCN [15]. These effects suggest that some aberrant projections arise from additional proximal branching, whereas others reflect errors in initial axon outgrowth. While the origin of ipsilateral projections is not known for *ephrin-A2* and *ephrin-A5* mutations, the similar phenotype suggests that both trajectories are likely.

### Role of *ephrin-A2* and *ephrin-A5* in topographic targeting

Topographic mapping is seen throughout the central nervous system and represents a fundamental organizing principle of sensory pathways. Topography in a number of pathways has been shown to arise from graded expression of Eph proteins together with varying degrees of activity-dependent refinement [30–32]. In visual system pathways, formation of retinotopy relies extensively on gradients of ephrin-A proteins [33, 34]. In contrast, we found that null mutations in *ephrin-A2* and *ephrin-A5* had no effect on topographic mapping in the VCN-MNTB pathway. Previous studies have suggested that EphB proteins are needed for formation of tonotopy in MNTB [16], the inferior colliculus [32, 35], and the auditory cortex [36]. Our results suggest that ephrin-A2 and ephrin-A5 are not predominant factors in establishment of the VCN-MNTB map in the brainstem. The role of these proteins has not been established in projections from MNTB to its targets, including LSO. The involvement of ephrin-A proteins is not ruled out in other tonotopic projections, as EphA7 modulates tonotopy in the corticothalamic projection from auditory cortex [37]. Moreover, *ephrin-A2/A5* DKO mice show impaired topography in an experimentally induced retinal projection into the medial geniculate nucleus of the thalamus, which normally receives auditory input [38]. These observations suggest a role for EphA signaling in the formation of topography in the auditory thalamus. The roles of other ephrin-A proteins in establishing tonotopy have yet to be identified.

Given that *ephrin-A2/A5* DKO mice have a significant ipsilateral projection, we analyzed this pathway to determine whether the aberrant projection displays topography. We found that topography was similarly strong on the ipsilateral and contralateral sides, indicating that ordering of either projection does not rely critically on ephrin-A2 and ephrin-A5 and instead both rely on other cues. However, a significant lateral shift was noted in the ipsilateral versus contralateral projection in *ephrin-A2/A5* DKO mice. This difference could arise from

differences in expression of receptors for graded cues in the target, which could emerge in crossed versus uncrossed portions of VCN axons. Alternatively, the difference could arise in the timing of growth of VCN axon branches to the two sides. Identification of cues that establish tonotopy in this pathway is needed to characterize differences between the normal contralateral projection and the projection on the ipsilateral side.

## Conclusions

Our data show a role for ephrin-A2 and ephrin-A5 in contralateral vs. ipsilateral targeting but not in topographic map formation, indicating that these cues arise from distinct molecules. Conversely, ephrin-B signaling is needed for topographic mapping of projections to the IC, but not for targeting to discrete modular zones within the IC [32]. In retinocollicular pathways, ephrin-A proteins are necessary for topographic map formation, but not for targeting to specific laminae within the superior colliculus [19]. These observations show that Eph signaling can selectively contribute to several distinct dimensions of targeting. The diversity of Eph proteins may thus permit coordinated guidance to correct regions within each target and accommodate multiple rules for connectivity.

## Methods

### Mice

All procedures were approved by the University of California, Irvine Institutional Animal Care and Use Committee (IACUC). We used wild type, *ephrin-A2* KO mice, *ephrin-A5* KO mice and *ephrin-A2/A5* DKO mice, all on strain C57BL/6 J. Double knockouts were obtained by breeding *Efna2*$^{tm1Rgf}$*Efna5*$^{tm1Ddmo}$/J transgenic mice (Jackson Laboratories), which contained homozygous deletion of *ephrin-A2* and were heterozygous for *ephrin-A5*.

To determine animal genotypes, mice were anesthetized with isoflurane. DNA was then extracted from tail samples as described previously by [15]. Three primers were used for the *ephrin-A2* allele: oIMR8356, 5′-CCG CTT CCT CGT GCT TTA CGG TAT C-3′; oIMR8357, 5′-GGC TAT ACC GTG GAG GTG-3′; and oIMR8358, 5′-CTG CCG GTG GTC ACA GGA-3′. The wild type PCR product is 110 bp while the mutant product is 650 bp as reported by Jackson Laboratory.

The three primers used for the *ephrin-A5* allele: oIMR8359, 5′- ATT CCA GAG GGG TGA CTA CCA CAT T-3′; oIMR8360, 5′- TCC AGC TGT GCA GTT CTC CAA AAC A-3′; and oIMR8361, 5′- AGC CCA GAA AGC GAA GGA GCA AAG C-3′. The wild type PCR product is 397 bp while the mutant product is 513 bp as reported by Jackson Laboratory.

### Immunofluorescence

Wild type mice at ages E17, P0, P4, and P12 mice were used for immunofluorescence. Embryonic tissue was immersion fixed in 4 % paraformaldehyde (PFA) in phosphate-buffered saline (PBS) at 4 °C. P0 and P4 mice were perfused transcardially with 0.9 % saline followed by 4 % PFA in PBS. P0 and P4 brainstems were then dissected and post-fixed for 2 h in 4 % PFA in PBS at 4 °C. Samples were cryoprotected in 30 % sucrose in PBS at 4 °C. Brainstems were sectioned in the coronal plane at 18 μm on a cryostat (Leica Microsystems) and mounted onto chrome-alum-subbed slides. Slides were outlined in PAP pen (Life Technologies) to confine reagents and warmed at 37 °C on a slide warmer for 20 min as described previously [24]. Slides were rinsed in PBS for 30 min and then incubated 1 h in blocking solution consisting of 4 % bovine serum albumin and 0.1 % Triton X-100 in PBS. The primary antibody for ephrin-A2 (5–15 μg/mL in blocking solution) was a goat polyclonal antiserum generated using a recombinant mouse ephrin-A2 protein (aa 1–184, R&D Systems). The primary antibody for ephrin-A5 (5 μg/mL) was a rabbit polyclonal antiserum derived from the C-terminal end of the mouse ephrin-A5 protein (aa 160–250, Invitrogen). Slides were incubated overnight at room temperature with primary antibody, rinsed in PBS for 30 min and then incubated in secondary antibody for 1 h at room temperature. Secondary antibodies used were Alexa Fluor 488 donkey anti-goat for ephrin-A2 and Alexa Fluor 594 goat anti-rabbit for ephrin-A5 (1:300, Life Technologies). Slides were rinsed in PBS for 30 min and coverslipped with Glycergel mounting media (Dako). We confirmed the specificity of the primary antibodies by including control sections derived from *ephrin-A2* KO mice or *ephrin-A5* KO mice for the ephrin-A2 and ephrin-A5 antibodies, respectively; no labeling was seen in these sections.

### Neuroanatomical labeling

Wild type, *ephrin-A2* KO mice, *ephrin-A5* KO mice, and *ephrin-A2/A5* DKO mice were used at P10-P14 for analysis of contralateral targeting. Wild type and *ephrin-A2/A5* DKO mice were used at P10-12 for analysis of topographic mapping. Mice were perfused transcardially with 0.9 % saline then 4 % PFA in PBS. Brainstems and cerebellum were extracted and post-fixed in 4 % PFA in PBS at 4 °C for 24–72 h. The cerebellum was dissected away and a small piece (100–200 μm$^2$) of the lipophilic NeuroVue Red dye (Polysciences) was then placed in VCN on one side as described previously [8, 39]. For studies of topography, a smaller piece of NeuroVue Red dye was placed on one side of either dorsal or ventral portion of VCN. Brainstems were then returned to 4 % PFA in PBS and incubated at 37 °C for 2 weeks to allow for dye to transport along the axon and into the calyces on MNTB.

Brainstems were placed in 4 % low-melting agarose in PBS after incubation and sectioned coronally at 100 μm on a vibratome (Leica Microsystems). Sectioned tissue was then mounted onto chrome-alum-subbed slides and coverslipped.

### Imaging

Immunofluorescence images of brainstem sections were acquired with a Carl Zeiss Axioskop microscope, Axiocam digital camera and Axiovision software (Zeiss). Images were then imported into Adobe Photoshop CS6 v13.0 for brightness and contrast optimization. The boundaries of VCN and MNTB were visualized in green autofluorescence images.

### Analysis of contralateral targeting

The specificity of the VCN-MNTB pathway was analyzed by examining the number of calyceal terminations from the labeled VCN to both contralateral MNTB and ipsilateral MNTB, where the large calyceal terminations can be clearly visualized and counted. Analysis was performed blind to genotype. Samples were included in the study if (1) labeled axons originated from an intact VCN and coursed along the ventral region of the midline; (2) axons terminated at calyces within MNTB; (3) calyceal terminations covered at least one-fourth of the cell surface in MNTB; and (4) at least 50 total labeled calyces were found in the brainstem. To account for variations in dye labeling across animals, we computed an ipsilateral to contralateral ratio (I/C ratio) as described previously [8, 15, 39, 40] by dividing the total number of MNTBi projections by the total number of MNTBc projections to obtain a single value for each animal. A one-way ANOVA with post-hoc analysis was used to compare the I/C ratios.

### Analysis of topographic mapping

Brainstems were included in the analysis of topographic mapping if (1) dye extended 50 % or less than the total dorsoventral length of VCN; (2) dye was transported along the axon from VCN and terminated in calyces; and (3) dye labeled at least 10 calyces total in MNTBi and MNTBc. Brainstems were excluded if dye was located on parts of brainstem other than VCN or if no calyces were labeled in MNTBc. Analysis was performed blind to genotype.

Single 10x magnification green and red fluorescent images of VCN were taken to measure the ventral to dorsal length of VCN and dye mean center using Axiovision software (Zeiss). VCN was identified under green autofluorescence and the most dorsal point of VCN was set as 0 μm per section. The average length for each brainstem was calculated. The borders of dye placement along the ventral to dorsal axis of VCN were determined using the red fluorescence image and the midpoint of the dye extent was used to determine the dye position relative to the 0 μm reference:

$$VCN\ dye\ position = \left(\frac{ventral\ dye\ border - dorsal\ dye\ border 2}{}\right) + dorsal\ dye\ border$$

The VCN dye position was normalized to the dorsoventral length of VCN. This normalized dye position was averaged across all VCN sections containing dye labeling to obtain a single value for each animal.

The average dye extent was calculated to determine inclusion criteria for each brainstem:

$$Avg\ VCN\ dye\ extent = \frac{mean\ ventral\ border - mean\ dorsal\ border}{average\ VCN\ length}\ X\ 100$$

Specimens with values 50 % and lower were included. Z-stack 20x green and red fluorescent images were obtained for MNTBi and MNTBc. The length of the ipsilateral and the contralateral MNTB was measured in each section from the most medial position to the most lateral position using the green fluorescent image. The positions of labeled ipsilateral and contralateral calyces from the medial border MNTB were measured using the z-stack red fluorescent images. For each calyx, the distance from the medial border was normalized to the mediolateral width of MNTB in that section. The average normalized calyx position in MNTBi and MNTBc was calculated for each brainstem.

A scatter plot of the VCN normalized dye position and the MNTB normalized calyx position was constructed to assess topographic mapping in wild type and *ephrin-A2/A5* double knockout mice. Linear regressions were used to assess the correlation between the location of the VCN dye placement and locations of calyces in MNTB.

#### Abbreviations

MNTBc: Contralateral medial nucleus of the trapezoid body; MNTBi: Ipsilateral medial nucleus of the trapezoid body; I/C: Ipsilateral to contralateral; MNTB: Medial nucleus of the trapezoid body; PFA: Paraformaldehyde; PBS: Phosphate-buffered saline; VCN: Ventral cochlear nucleus.

#### Competing interests

None of the authors have any competing interests.

#### Authors' contributions

MLAL carried out immunofluorescence studies and neuroanatomical labeling for contralateral targeting and topography studies. She also performed data analysis and drafted the manuscript. JAAS performed histology and neuroanatomical labeling, and contributed to data analysis and manuscript preparation. SM carried out experiments for contralateral targeting. MLD carried out immunofluorescence and tracing studies and contributed to preparation of the manuscript. KSC conceived of the study and its design and helped with data analysis and manuscript preparation. All authors read and approved the final manuscript.

#### Acknowledgements

This project was supported by funds from the UC Irvine Department of Pediatrics and from the UC Irvine Center for Autism Research and Translation.

**Author details**
[1]Division of Neonatology, Department of Pediatrics, University of California, Irvine, 101 The City Drive, Orange, CA 92868-3298, USA. [2]Department of Neurobiology and Behavior, University of California, Irvine, 2205 McGaugh Hall, Irvine, CA 92697-4550, USA.

**Received: 17 September 2015 Accepted: 10 December 2015**
Published online: 15 December 2015

**References**

1. Kuwabara N, Zook JM. Classification of the principal cells of the medial nucleus of the trapezoid body. J Comp Neurol. 1991;314(4):707–20.
2. Cramer KS, Gabriele ML. Axon guidance in the auditory system: multiple functions of Eph receptors. Neuroscience. 2014;277:152–62.
3. Hoffpauir BK, Kolson DR, Mathers PH, Spirou GA. Maturation of synaptic partners: functional phenotype and synaptic organization tuned in synchrony. J Physiol. 2010;588(Pt 22):4365–85.
4. Howell DM, Morgan WJ, Jarjour AA, Spirou GA, Berrebi AS, Kennedy TE, et al. Molecular guidance cues necessary for axon pathfinding from the ventral cochlear nucleus. J Comp Neurol. 2007;504(5):533–49.
5. Hoffpauir BK, Grimes JL, Mathers PH, Spirou GA. Synaptogenesis of the calyx of Held: rapid onset of function and one-to-one morphological innervation. J Neurosci. 2006;26(20):5511–23.
6. Kil J, Kageyama GH, Semple MN, Kitzes LM. Development of ventral cochlear nucleus projections to the superior olivary complex in gerbil. J Comp Neurol. 1995;353(3):317–40.
7. Nakamura PA, Cramer KS. Formation and maturation of the calyx of Held. Hear Res. 2011;276(1–2):70–8.
8. Nakamura PA, Hsieh CY, Cramer KS. EphB signaling regulates target innervation in the developing and deafferented auditory brainstem. Dev Neurobiol. 2012;72(9):1243–55.
9. Bush JO, Soriano P. Eph/ephrin signaling: genetic, phosphoproteomic, and transcriptomic approaches. Semin Cell Dev Biol. 2012;23(1):26–34.
10. Lai KO, Ip NY. Synapse development and plasticity: roles of ephrin/Eph receptor signaling. Curr Opin Neurobiol. 2009;19(3):275–83.
11. Pasquale EB. Eph receptor signalling casts a wide net on cell behaviour. Nat Rev Mol Cell Biol. 2005;6(6):462–75.
12. Gale NW, Holland SJ, Valenzuela DM, Flenniken A, Pan L, Ryan TE, et al. Eph receptors and ligands comprise two major specificity subclasses and are reciprocally compartmentalized during embryogenesis. Neuron. 1996;17(1):9–19.
13. Himanen JP. Ectodomain structures of Eph receptors. Semin Cell Dev Biol. 2012;23(1):35–42.
14. Himanen JP, Chumley MJ, Lackmann M, Li C, Barton WA, Jeffrey PD, et al. Repelling class discrimination: ephrin-A5 binds to and activates EphB2 receptor signaling. Nat Neurosci. 2004;7(5):501–9.
15. Hsieh CY, Nakamura PA, Luk SO, Miko IJ, Henkemeyer M, Cramer KS. Ephrin-B reverse signaling is required for formation of strictly contralateral auditory brainstem pathways. J Neurosci. 2010;30(29):9840–9.
16. Miko IJ, Nakamura PA, Henkemeyer M, Cramer KS. Auditory brainstem neural activation patterns are altered in EphA4- and ephrin-B2-deficient mice. J Comp Neurol. 2007;505(6):669–81.
17. Feldheim DA, O'Leary DD. Visual map development: bidirectional signaling, bifunctional guidance molecules, and competition. Cold Spring Harb Perspect Biol. 2010;2(11):a001768.
18. Haustead DJ, Lukehurst SS, Clutton GT, Bartlett CA, Dunlop SA, Arrese CA, et al. Functional topography and integration of the contralateral and ipsilateral retinocollicular projections of ephrin-A−/− mice. J Neurosci. 2008;28(29):7376–86.
19. Sweeney NT, James KN, Sales EC, Feldheim DA. Ephrin-As are required for the topographic mapping but not laminar choice of physiologically distinct RGC types. Dev Neurobiol. 2015;75(6):584–93.
20. Cang J, Niell CM, Liu X, Pfeiffenberger C, Feldheim DA, Stryker MP. Selective disruption of one Cartesian axis of cortical maps and receptive fields by deficiency in ephrin-As and structured activity. Neuron. 2008;57(4):511–23.
21. Bianchi LM, Liu H. Comparison of ephrin-A ligand and EphA receptor distribution in the developing inner ear. Anat Rec. 1999;254(1):127–34.
22. Defourny J, Poirier AL, Lallemend F, Mateo Sanchez S, Neef J, Vanderhaeghen P, et al. Ephrin-A5/EphA4 signalling controls specific afferent targeting to cochlear hair cells. Nat Commun. 2013;4:1438.
23. Yates N, Robertson D, Martin-Iverson M, Rodger J. Auditory brainstem responses of ephrin-A2, ephrin-A5(−/−) and ephrin-A2A5(−/−) mice. Audiol Neurootol. 2014;19(2):115–26.
24. Dinh ML, Koppel SJ, Korn MJ, Cramer KS. Distribution of glial cells in the auditory brainstem: normal development and effects of unilateral lesion. Neuroscience. 2014;278:237–52.
25. Arvanitis D, Davy A. Eph/ephrin signaling: networks. Genes Dev. 2008;22(4):416–29.
26. Falivelli G, Lisabeth EM, Rubio de la Torre E, Perez-Tenorio G, Tosato G, Salvucci O, et al. Attenuation of eph receptor kinase activation in cancer cells by coexpressed ephrin ligands. PLoS ONE. 2013;8(11):e81445.
27. Kao TJ, Kania A. Ephrin-mediated cis-attenuation of Eph receptor signaling is essential for spinal motor axon guidance. Neuron. 2011;71(1):76–91.
28. Yaron A, Sprinzak D. The cis side of juxtacrine signaling: a new role in the development of the nervous system. Trends Neurosci. 2012;35(4):230–9.
29. Holcomb PS, Hoffpauir BK, Hoyson MC, Jackson DR, Deerinck TJ, Marrs GS, et al. Synaptic inputs compete during rapid formation of the calyx of Held: a new model system for neural development. J Neurosci. 2013;33(32):12954–69.
30. Cang J, Wang L, Stryker MP, Feldheim DA. Roles of ephrin-as and structured activity in the development of functional maps in the superior colliculus. J Neurosci. 2008;28(43):11015–23.
31. Kandler K, Gillespie DC. Developmental refinement of inhibitory sound-localization circuits. Trends Neurosci. 2005;28(6):290–6.
32. Wallace MM, Kavianpour SM, Gabriele ML. Ephrin-B2 reverse signaling is required for topography but not pattern formation of lateral superior olivary inputs to the inferior colliculus. J Comp Neurol. 2013;521(7):1585–97.
33. Cang J, Kaneko M, Yamada J, Woods G, Stryker MP, Feldheim DA. Ephrin-as guide the formation of functional maps in the visual cortex. Neuron. 2005;48(4):577–89.
34. Cang J, Feldheim DA. Developmental mechanisms of topographic map formation and alignment. Annu Rev Neurosci. 2013;36:51–77.
35. Gabriele ML, Brubaker DQ, Chamberlain KA, Kross KM, Simpson NS, Kavianpour SM. EphA4 and ephrin-B2 expression patterns during inferior colliculus projection shaping prior to experience. Dev Neurobiol. 2011;71(2):182–99.
36. Intskirveli I, Metherate R, Cramer KS. Null mutations in EphB receptors decrease sharpness of frequency tuning in primary auditory cortex. PLoS ONE. 2011;6(10):e26192.
37. Torii M, Hackett TA, Rakic P, Levitt P, Polley DB. EphA signaling impacts development of topographic connectivity in auditory corticofugal systems. Cereb Cortex. 2013;23(4):775–85.
38. Ellsworth CA, Lyckman AW, Feldheim DA, Flanagan JG, Sur M. Ephrin-A2 and -A5 influence patterning of normal and novel retinal projections to the thalamus: conserved mapping mechanisms in visual and auditory thalamic targets. J Comp Neurol. 2005;488(2):140–51.
39. Hsieh CY, Cramer KS. Deafferentation induces novel axonal projections in the auditory brainstem after hearing onset. J Comp Neurol. 2006;497(4):589–99.
40. Hsieh CY, Hong CT, Cramer KS. Deletion of EphA4 enhances deafferentation-induced ipsilateral sprouting in auditory brainstem projections. J Comp Neurol. 2007;504(5):508–18.